AD-A078 443 PURDUE UNIV LAFAYETTE IND DEPT OF ELECTRICAL ENGINEERING F/G 17/1
RANDOM SIGNAL FLAW DETECTION.(U)
JUN 79 V L NEWHOUSE , E S FURGASON F33615-75-C-5252
UNCLASSIFIED AFML-TR-79-4077 NL

1 OF 2
ADA
078443

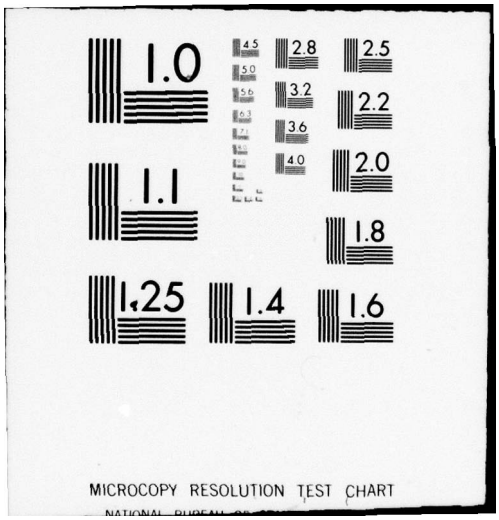
1.0
1.1
1.25
1.4
1.6
1.8
2.0
2.2
2.5
2.8
3.2
3.6
4.0
4.5
5.0
5.6
6.3
7.1
8.0
9.0
MICROCOPY RESOLUTION TEST CHART

AFML-TR-79-4077

RANDOM SIGNAL FLAW DETECTION

V. L. NEWHOUSE
E. S. FURGASON
PURDUE UNIVERSITY
SCHOOL OF ELECTRICAL ENGINEERING
WEST LAFAYETTE, INDIANA 47907

JUNE 1979

TECHNICAL REPORT AFML-TR-79-4077
Final Report for period August 1975 — February 1979

AIR FORCE MATERIALS LABORATORY
AIR FORCE WRIGHT AERONAUTICAL LABORATORIES
AIR FORCE SYSTEMS COMMAND
WRIGHT PATTERSON AIR FORCE BASE, OHIO 45433

NOTICE

When Government drawings, specifications, or other data are used for any purpose other than in connection with a definitely related Government procurement operation, the United States Government thereby incurs no responsibility nor any obligation whatsoever; and the fact that the government may have formulated, furnished, or in any way supplied the said drawings, specifications, or other data, is not to be regarded by implication or otherwise as in any manner licensing the holder or any other person or corporation, or conveying any rights or permission to manufacture, use, or sell any patented invention that may in any way be related thereto.

This report has been reviewed by the Information Office (OI) and is releasable to the National Technical Information Service (NTIS). At NTIS, it will be available to the general public, including foreign nations.

The views and conclusions contained in this document are those of the authors and should not be interpreted as representing the official policies, either expressed or implied, of the Defense Advanced Research Projects Agency or the U.S. Government.

This technical report has been reviewed and is approved for publication.

Roger D. Griswold

ROGER D. GRISWOLD
Project Engineer

FOR THE COMMANDER

D. M. FORNEY, Jr., Chief
Nondestructive Evaluation Branch
Metals and Ceramics Division

"If your address has changed, if you wish to be removed from our mailing list, or if the addressee is no longer employed by your organization please notify AFML/LLP, W-PAFB, OH 45433 to help us maintain a current mailing list".

Copies of this report should not be returned unless return is required by security considerations, contractual obligations, or notice on a specific document.

AIR FORCE/56780/26 November 1979 — 370

SECURITY CLASSIFICATION OF THIS PAGE *(When Data Entered)*

(19) REPORT DOCUMENTATION PAGE

READ INSTRUCTIONS BEFORE COMPLETING FORM

(18) 1. REPORT NUMBER: AFML-TR-79-4077

2. GOVT ACCESSION NO.

3. RECIPIENT'S CATALOG NUMBER

(6) 4. TITLE *(and Subtitle)*: RANDOM SIGNAL FLAW DETECTION •

(9) 5. TYPE OF REPORT & PERIOD COVERED: FINAL REPORT • 2 AUG 75 — 28 FEB 79

6. PERFORMING ORG. REPORT NUMBER

(10) 7. AUTHOR(s): Vernon L. Newhouse, Eric S. Furgason

PE62301E

(15) 8. CONTRACT OR GRANT NUMBER(s): F33615-75-C-5252

9. PERFORMING ORGANIZATION NAME AND ADDRESS
Purdue University
Department of Electrical Engineering
West Lafayette, Indiana 47907

(16) 10. PROGRAM ELEMENT, PROJECT, TASK AREA & WORK UNIT NUMBERS: 23870011 (17) 00

(11) 11. CONTROLLING OFFICE NAME AND ADDRESS
Defense Advanced Research Projects Agency
1400 Wilson Blvd
Arlington, Virginia 22209

12. REPORT DATE: JUN 79

13. NUMBER OF PAGES

14. MONITORING AGENCY NAME & ADDRESS *(if different from Controlling Office)*
Air Force Materials Laboratory (LLP)
Air Force Systems Command
Wright-Patterson Air Force Base, Ohio 45433

15. SECURITY CLASS. *(of this report)*: Unclassified

15a. DECLASSIFICATION/DOWNGRADING SCHEDULE

16. DISTRIBUTION STATEMENT *(of this Report)*

Approved for public release; distribution unlimited.

(12) 99

408 124

17. DISTRIBUTION STATEMENT *(of the abstract entered in Block 20, if different from Report)*

18. SUPPLEMENTARY NOTES

19. KEY WORDS *(Continue on reverse side if necessary and identify by block number)*
ULTRASONICS; FLAW DETECTION; NONDESTRUCTIVE EVALUATION; CONVOLUTION; DECONVOLUTION; RANDOM NOISE; ACOUSTICS; RANDOM SIGNAL SYSTEM

20. ABSTRACT *(Continue on reverse side if necessary and identify by block number)*

This report describes four areas of work. In the first area random signal beam forming techniques are developed which make it possible to transmit several independent beams from a phased array using the same number of incoherent noise sources. Following this ultrasound beam scanning techniques are demonstrated in which random signal correlation systems and RF correlation systems using quadrature phase techniques are used in methods for scanning the intensity profile of ultrasound transducer beams using respectively broadband signals and

DD FORM 1 JAN 73 1473 EDITION OF 1 NOV 65 IS OBSOLETE

i

Unclassified

SECURITY CLASSIFICATION OF THIS PAGE *(When Data Entered)*

408 124

20. (Continued)

narrow band signals. In addition two types of deconvolution procedure are described and demonstrated which have been successful in improving the effective resolution of ultrasound correlation systems when viewing surface features. Finally the design and construction of a random signal correlation system is described which uses an electronic delay line.

FOREWORD

This program was initiated on 21 August 1975 and completed on 28 February 1979. It is entitled "Random Signal Flaw Detection" and was funded under Grant Number F33615-75-C-5252. Its task area number is 23870011. The work was performed by Purdue University Department of Electrical Engineering and was monitored by Mr. R. Griswold of the U. S. Air Force Materials Laboratory, Wright Patterson Air Force Base, Dayton, Ohio.

The work described in this report received substantial contributions from the following Research Assistants, Associates and Engineers whose work is gratefully acknowledged. Gregory Johnson (Beam Scanners), Brian B. Lee (Beam Scanners and Noise Array), Roy E. Twyman (Deconvolution), Martin Mark (Electronic Delay Line).

TABLE OF CONTENTS

LIST OF ILLUSTRATIONS

LIST OF ILLUSTRATIONS (Cont'd)

LIST OF ILLUSTRATIONS (Cont'd)

LIST OF ILLUSTRATIONS (Cont'd)

SECTION I

TECHNICAL OBJECTIVES

During the past few years, we have developed acoustic flaw detection systems of unprecedented sensitivity[1,2] which have considerably increased the range of application of ultrasonic flaw detection and defect structure analysis. The principal objective of our current program has been to develop techniques that will increase the lateral and axial resolution of ultrasonic flaw detection systems. These techniques will then be adapted to our ultra-sensitive random signal flaw detection systems currently under development.

Our original work in this area concentrated on the development of a new type of ultrasonic flaw detection system which utilizes random signal correlation techniques. The use of correlation and time integration techniques in this system has allowed us to achieve a sensitivity which is approximately 10,000 times greater than conventional ultrasonic pulse-echo detection systems. Thus this system greatly extends the size of strongly sound absorbing objects that can be examined using ultrasound.

The enormous sensitivity of this system also enables detection of targets (flaws) that are much smaller than those which can be detected by conventional ultrasonic systems. However, like conventional flaw detection systems, the random signal system is presently limited in its ability to resolve these small defects by both the size of the transmitted ultrasound beam and the limited frequency response of the acoustic transducer. Consequently, one of the goals of this project has been directed toward overcoming the limitations imposed by the acoustic transducer.

Since we do not wish to limit the depth of focus of our system by using focusing lenses, our lateral resolution is determined by the width of the unfocused ultrasound beam. The width of this is determined by the diameter of the acoustic transducer, which is typically between ¼ and ½ inch. Thus the lateral resolution of a 5 MHz. detection system is approximately 50 times less than the resolution along the axis of the ultrasonic beam. The low transverse resolution of the acoustic transducers imposes severe limitations on the usefulness of the advances we have made in developing a high sensitivity detection system. An example of these limitations is seen in the examination of grain structure in metals. Although our system provides ample sensitivity to detect single grain boundaries, which can not be seen by conventional systems, the fact that the width of the ultrasonic beam encompasses many grains precludes the possibility of examining individual grains within the metal. Thus the main objective of this program is to develop techniques to provide a lateral resolution which is of the same order as the present axial resolution of the detection system.

We have also directed our attention to the area of echo processing to improve axial resolution and extract more detailed information about the target structure. Typically, the resolution of an imaging system is determined by the half-power bandwidth of the ultrasonic transducer. Although the transducer can actually pass frequencies over a range much larger than the half-power bandwidth, these additional frequency components exist only at very low power levels. By applying a sophisticated signal processing technique, known as deconvolution, to the echo signal it is possible to recover the information in these low level frequency components, provided that the signal-to-noise ratio of the echo signal is sufficiently high. Since the correlation receiver system we have developed provides extremely high output signal-to-noise

ratios, our system is ideally suited for the application of this additional signal processing step. During the course of this project we have been able to demonstrate that by proper computer processing of the echo signal we can utilize the full bandwidth of the transmitted signal. This processing has allowed us to increase the maximum resolution of standard ultrasonic transducers by a factor of the order of five.

Our original random signal correlation system used a so-called water delay line, made of two acoustic transducers separated by a water path. Since this structure is awkward for mobile systems our last goal in this project was to develop an electronic delay line to replace the water delay line.

SECTION II

Accomplishments

In the first year of this project our efforts centered on overcoming fundamental performance limitations imposed by the acoustic transducers presently in wide use in ultrasonic flaw detection systems. In particular, our work concentrated on two specific aspects of transducer performance, beam pattern and frequency response. Though both parts of our program dealt with transducer performance there is, in fact, little overlap between the two topics. As a result, this work is presented as two separate projects in this report.

Most ultrasonic transducers currently in use for flaw detection consist of a disk of piezoelectric ceramic material on a block of sound absorbing material. For this type of transducer, the lateral resolution is limited by the diameter of the piezoelectric element. Several alternative transducer configurations have been proposed by other workers, principally in the field of medical ultrasound imaging, to deal with this resolution problem. The particular approach we have been considering is based on a new concept which we conceived for using random signals to improve the performance of phased array transducers.

Our initial goal was to verify the underlying principles upon which this technique for enhancing resolution is based. During this contract period we have established that an ultrasonic phased array could simultaneously transmit two different noise signals and that the echoes associated with each of the transmitted signals could be independently recovered, even though echoes due to the two signals may arrive simultaneously at the receiving transducer. The feasibility demonstration of this new principle constitutes a significant step in the development of the proposed transducer system.

The next phase of the proposed work was to have been the construction of a prototype system to demonstrate the use of this technique in controlling the ultrasonic beam pattern of a transducer array. In the course of this work we encountered some unexpected difficulties. We found that the beam pattern of our ultrasonic transducers could not be adequately characterized for the case of transmitting broadband signals. Without an accurate characterization of the existing beam pattern we would be forced to blindly manipulate the beam shape in hopes of obtaining an improved pattern.

Although mathematical models of highly idealized ultrasonic transducers transmitting single frequencies exist in the literature, little useful information could be found about broadband transmission. Taking a more direct approach, we had the beam patterns of some of our transducers analyzed on commercially available beam measuring equipment. Typically, these results lacked sufficient quantitative information to allow us to proceed with this phase of our program. Consequently, a substantial portion of our energies have been directed toward surmounting this obstacle.

Our effort in this area has resulted in the development of two new methods of measuring the intensity distribution of an ultrasonic beam. One of these systems, based on our previous work in the field of ultrasonic doppler flow measurement, is capable of high resolution beam plots for narrow band signals. The second method utilizes a modification of the random signal flaw detection system to examine broadband beam patterns. Preliminary evaluation of these techniques suggest that they represent a significant advance over the existing methods of beam pattern measurement. Although the development of these systems was time consuming and the results important in themselves, these systems are only necessary tools that were required to continue our progress.

The second portion of our program dealt with the application of signal processing to flaw echoes. This work, which was begun during the previous contract period, examined the feasibility of using deconvolution techniques to compensate the frequency response of the acoustic transducer and obtain enhanced resolution along the axis of the ultrasound beam.

Two approaches to the problem of deconvolution have been investigated. Both of these methods apply estimation techniques to the deconvolution procedure and require the echo signals to possess an extremely high signal-to-noise ratio, such as that obtained using the random signal flaw detection system.

The first processing scheme attacked the general problem of deconvolving the response from an unknown target. Experimental results are presented which demonstrate that this procedure could be used to enhance the resolution of the detection system by a factor of 3 to 5 and provide more detailed information about the structure and orientation of the target.

The second technique dealt with the related problem of identifying and accurately locating known targets. By combining deconvolution processing with a pattern recognition procedure, it was experimentally demonstrated that an order of magnitude increase in resolution could be realized.

The final accomplishment reported here is the design of a random signal correlation system in which the original water delay line is replaced by an electronic delay line. It is hoped to evaluate this system and compare it to pseudo-random code versions in future work.

SECTION III

TECHNICAL ACCOMPLISHMENTS

1. INTRODUCTION

Our original efforts in ultrasonic flaw detection concentrated on improving the performance of the receiver and culminated in the development of the random signal flaw detection system. This system has been previously shown to provide a vast improvement in sensitivity compared to conventional ultrasonic pulse-echo systems[1,3]. However, as in most existing pulse-echo systems, the performance of the random signal system is handicapped by the low lateral resolution of the ultrasonic transducers. Thus the main thrust of our current research program has been to develop techniques to increase the lateral resolution of the system to a level comparable to the present axial resolution of the system. This will allow the full potential of the high sensitivity offered by the random signal system to be utilized in detecting and identifying small defects or evaluating grain structure or porosity.

Most ultrasonic flaw detection systems currently use a simple piston type transducer consisting of a piezoelectric ceramic disk mounted on a block of sound absorbing material. The width of the acoustic beam produced by this type of transducer is principally determined by the diameter of the piezoelectric element, which is typically between $\frac{1}{4}$ and $\frac{1}{2}$ inch. Consequently, the lateral resolution of a 5 MHz. detection system will be approximately 50 to 100 times less than the resolution along the axis of the sonic beam. The low transverse resolution of the acoustic transducer generally imposes severe limitations on the performance of detection systems and in particular on the usefulness of the advances we have made in developing a high sensitivity system. Hence there exists a significant need to develop a transducer system with greatly improved lateral

resolution. This improvement in lateral resolution must not, however, compromise the depth of focus, since an effective flaw detection system must produce high resolution images over a large range of depths. This fact precludes the use of focusing lenses to narrow the transmitted sound beam.

Several alternative methods of obtaining improved lateral resolution have been proposed by other workers. These include the use of snythetic aperture techniques,[4] phased array transducers,[5] and holographic systems.[6] Although such systems provide the desired increase in resolution and depth of focus, they require complex mechanics and electronics or computer processing of the signals, which presently makes them unattractive for many flaw detection applications. Our investigation of the lateral resolution problem suggests that of the many possible solutions, phased arrays offer the greatest promise and the widest range of applications.

Phased arrays are usually thought of as a means of electronic beam steering and focusing. However Burckhardt[4] has shown that phased arrays can also be used to improve lateral resolution by beam forming. In this technique sound is transmitted sequentially in two patterns. By storing the echoes from each transmitted pattern and taking their difference it is possible to effectively suppress beam side lobes giving improved lateral resolution.

Some time ago we conceived the idea of implementing phased array beam forming with random signals.[15,16] Instead of transmitting successive beam patterns and storing their echoes, the use of incoherent random signals allows several different beam patterns to be transmitted simultaneously, using one noise source for each beam pattern. The advantage of this procedure is that the echoes can be processed in real time without being digitized and stored. This results in

considerable simplification of the electronics and an increase in operating speed. The concept of random signal beam forming should provide a great improvement over present beam forming techniques and have a broad range of applications.

Random signal beam forming constitutes one of the two major thrusts of the work reported here. Our work in signal processing of flaw echoes to eliminate the effects due to the limited frequency response of the transducer is described in the next section of this report.

SECTION V

Random Signal Beam Forming

1. BASIC PRINCIPLES

One of the principal factors limiting the performance of ultrasonic flaw detection systems is the acoustic transducer. The particular aspect of transducer performance on which we focused the majority of our attention during this work period was the transducer beam pattern and its effect in determining lateral resolution. Before discussing the application of our new technique, random signal beam forming, to the problem of improved lateral resolution, we will examine some of the transducers currently in use or proposed for ultrasonic flaw detection and medical imaging systems.

The most widely used type of ultrasonic transducer employs a single disk of piezoelectric ceramic as the radiating element. If it is assumed that the entire surface of the transducer element moves as a piston, it is possible to analytically derive the transducer beam pattern. In the far field, the sound intensity distribution for this type of transducer can be calculated by simply taking the Fourier transform of the geometry of the radiating element. Consequently the sound distribution for the disk is given by the directivity function[7]

$$D_s = J_1(k \cdot R \cdot r/d)/(k \cdot R \cdot r/d) \qquad (1)$$

where J_1 is the first order Bessel's function of the first kind, R is the transducer radius, k is the wave number of the generated sound, r is the off-axis displacement of the target, and d is the distance to the target. However, in most practical applications the targets are in the near field of the transducer where the beam is confined to a cylindrical region with diameter equal to the

diameter of the piezoelectric element. Within this cylindrical beam however the intensity distribution is nonuniform and a strong function of the distance along the beam as well as the distance off the beam axis. Therefore, this type of transducer generates a broad beam and yields low lateral resolution.

An alternative type of transducer which has received some attention, utilizes an annular piezoelectric element in place of the traditional disk element.[8] For this type of transducer, the directivity function in the far field can be shown to be given by

$$D_s = J_0(k \cdot R \cdot r/d) \qquad (2)$$

where the variables are as defined for Eq. 1. It can be seen from this equation that the annular transducer produces a pattern with a strong, narrow central lobe. Unfortunately, this type of transducer also exhibits large side lobes which limit its lateral resolution.

The principal advantage of the annular transducer is derived from the fact that the distance to the beginning of the far field region is determined by the width of the annulus rather than the radius, as was the case for the disk transducer. Hence this type of transducer can be constructed with the annulus being narrow compared to the radius so that the far field sound pattern actually exists very close to the transducer face. Since the directivity function given in Eq. 2 can be made to apply close to the transducer, this type of transducer provides greater resolution than can be obtained with a traditional disk transducer.

A composite transducer consisting of a small disk element within an annular element has also been reported.[9] By using one element to transmit and the other element to receive, this type of transducer was shown to provide an increase in lateral resolving power of 5 to 10 times greater than that obtained with a

conventional disk transducer. This transducer also displayed the large depth of focus which is characteristic of annular transducers and essential in any practical flaw detection system.

It should be noted that Eq. 2, which gives the directivity function for the annular transducer, applies only for a single transmitted frequency. When a wide band signal is transmitted from a transducer, each frequency component of the signal has its own directivity function. In the case of the annulus, these directivity patterns will tend to add or reinforce each other within the central lobe, whereas interference effects in the side lobes may tend to reduce their significance. This phenomenon may result in the wide band system having greater lateral resolution than a conventional system using an identical transducer.

An annular phased array transducer has been developed by Burckhardt et al. for use in acoustic imaging systems.[10] The motivation for using an annular phased array in place of a single annular transmitting element is to reduce the side lobes of the directivity function, thereby improving the lateral resolution of the transducer.

The directivity function for a simple annular transducer which is used for both transmission and reception is seen from Eq. 2 to be

$$D_s = J_0^2 (k \cdot R \cdot r/d) \qquad (3)$$

As has already been pointed out, the relatively large side lobes of this pattern limit the resolution of the annular transducer. By the use of a segmented annular element, as shown in Fig. 1, it is possible to obtain a good approximation to the following directivity function:

$$D_s = J_2^2 (k \cdot R \cdot r/d) - J_0^2 (k \cdot R \cdot r/d) \qquad (4)$$

The side lobes of this directivity pattern are significantly smaller than the side lobes of the directivity pattern for the simple annulus given in Eq. 3, thus yielding greater lateral resolution.

To achieve this pattern, the annulus is divided into eight segments, as shown in Fig. 1. The segments drawn in black transmit sound whereas the white segments receive sound. Two pulses must be transmitted to produce the lobe reduction and between the two pulses the transducer configuration is electronically rotated by 45 degrees. The partial echo signals from the two pulses are then added to obtain the final echo signal.

Although this system produces the required increase in lateral resolution, the system is quite complex. The entire record of echoes from each pulse must be stored, synchronized, and then processed to produce the final signal. As a result, this system is also slower than a conventional pulse-echo system using either an annular or ordinary disk type transducer.

The new concept that we have conceived uses random signals to improve the performance of phased array systems in general and the annular array system under discussion in particular. The new principle operates as follows.

Instead of transmitting one pulse and then waiting for its echoes to return before transmitting the second pulse and collecting its echoes, it is possible for us to transmit the two pulses simultaneously without confusing their echoes. This can be done by simply drawing the two transmitted pulses from independent random signal sources. Since our system already is designed to store a copy of the transmitted signal and correlate this copy with the received echoes, the echoes from each of the two transmitted signals will automatically be sorted out by the correlation process. Thus we can process the returning echoes in

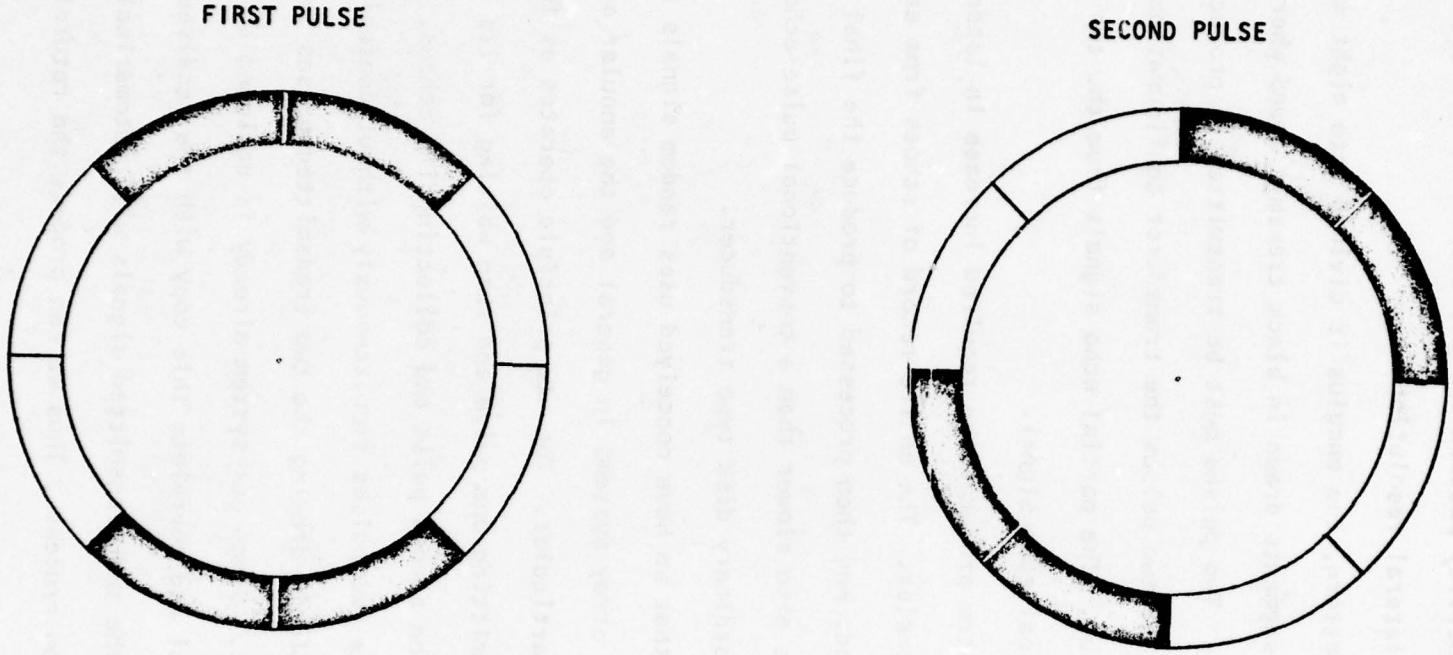

Figure 1. Transmitting and Receiving Segments for the First and Second Pulse. Black: Transmitting, White: Receiving.[8]

real time without the need for electronic storage of the echoes used in the original Burckhardt system. It is important to note that the enormous sensitivity of our present random signal flaw detection system will be preserved in this new system, since the correlators which are used to distinguish the echoes of the two random signals that are being transmitted, still incorporate the time integrators which make this large sensitivity possible.

2. FEASIBILITY DEMONSTRATION

The random signal beam forming technique described in the previous section relies on two basic assumptions. The first underlying assumption is that two or more incoherent random signals can be simultaneously transmitted from common elements of the transducer array. The second assumption is that with several different transmitted signals producing echoes, it is still possible to unscramble the echoes from the various signals even though they may be arriving simultaneously at the receiving elements of the array.

If all the transducer elements were linear in terms of the relationship between the amplitude of the generated acoustic signal and the applied electrical signal and if the noise sources would be connected to a common array element without producing any interaction, then the first assumption can be justified by application of the principle of superposition. If in addition to the required linearity of the transducer, we require that the noise sources be truly incoherent and that the receiver amplifiers and correlator be ideal, the second assumption is also easily justified.

In practice, we find that none of the above conditions on the various elements of the flaw detection system are satisfied. For example, the acoustic transducers are known to possess some non-linearities, the receiver amplifiers have only a limited dynamic range, and the correlators integrate for only a limited amount of time. The deviations from ideality of the various system components initially raised concern about the validity of the assumptions upon which the concept of random signal beam forming was based.

The initial goal of this project was therefore to experimentally verify the underlying principles of this new technique for enhancing resolution. The following experimental results clearly demonstrate the validity of the basic principles and the feasibility of random signal beam forming.

The objective of our first experimental effort was to show that the random signal correlation receiver could distinguish between incoherent noise signals received simultaneously. The test setup used in this demonstration was as shown in Figure 2. Duplicate transmitters were used to supply the two incoherent random signals A and B. The transducer array was simulated by mounting three commercial transducers to form a horizontal linear array as shown in the figure. The center transducer in the array had a one inch diameter and the outer two transducers had a one-half inch diameter. The target used for this experiment consisted of two brass roads, one 5/16 inch diameter and the other 7/16 inch diameter, that were mounted vertically in front of the linear array. The rods

were spaced approximately one inch apart, with the 7/16 rod slightly forward of the 5/16 rod. The transducer array was aligned so that each of the outer transducers illuminated only one of the brass rods while the beam pattern of the center transducer encompassed both of the targets.

Figures 3 and 4 show the results of two of the control tests that were made on this experimental setup. In the first test, transmitter A was used to drive transducer A in the linear array while transmitter B and transducer B were not used. The received signal from the center element of the array was correlated with a copy of the transmitted signal from source A. The output, presented in Figure 3, clearly shows that only echoes from the 5/16 brass rod were received.

A similar control test utilized transmitter B to drive transducer B while transmitter A and transducer A were not in use. In this case, the received signal from the center transducer was correlated with a delayed version of transmitted signal B. Figure 4 shows that the output contains only echoes from the front and back surfaces of the 7/16 rod along with some multiple reflections from within the rod. Thus these results demonstrate that the transmitting array has been properly adjusted so that each of the outer elements of the transducer array only illuminate one of the two rods which compose the target, whereas the center element can receive echoes from both.

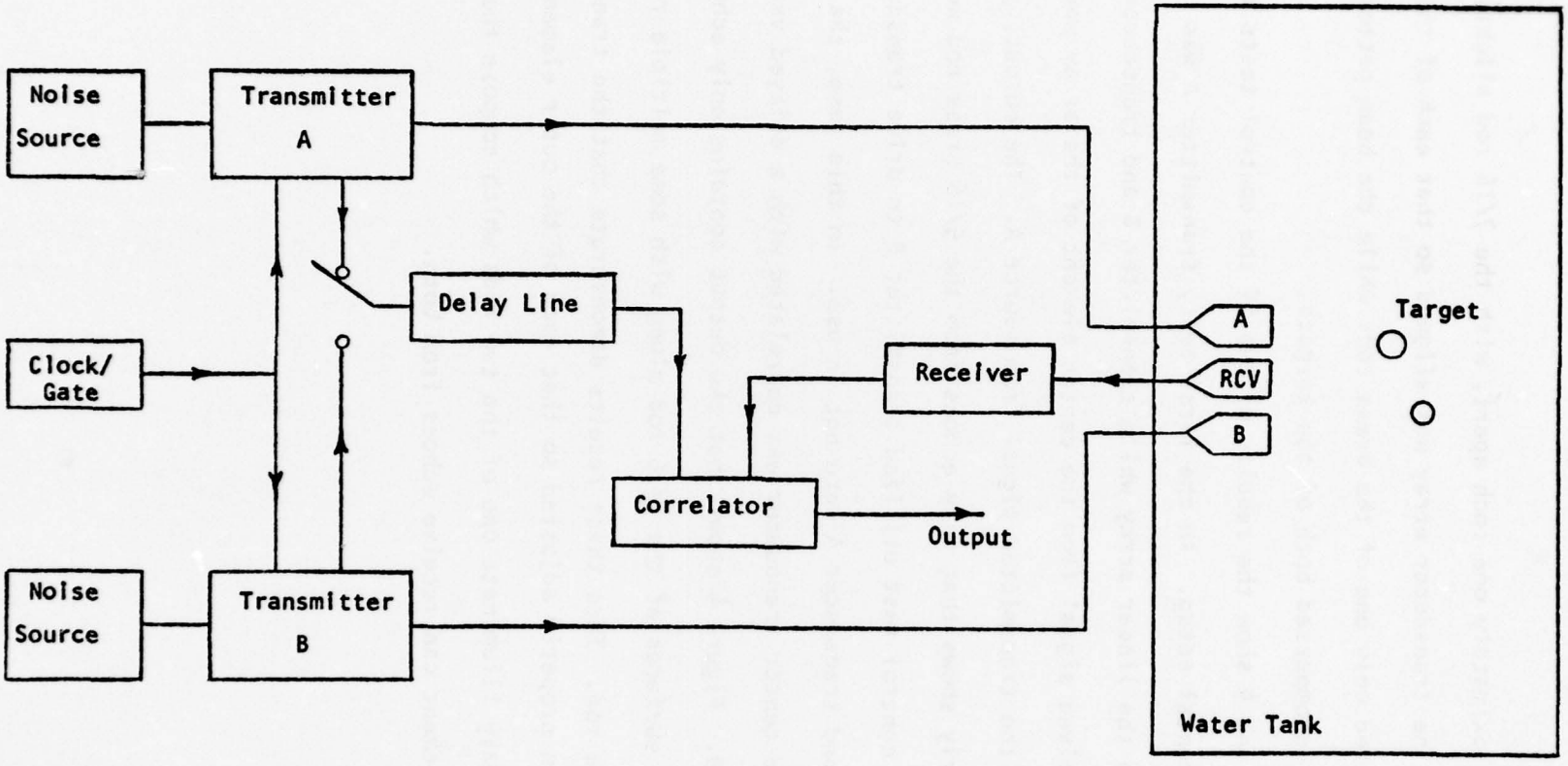

Figure 2. Test Setup for Receiving Two Return Echoes in a Common Transducer.

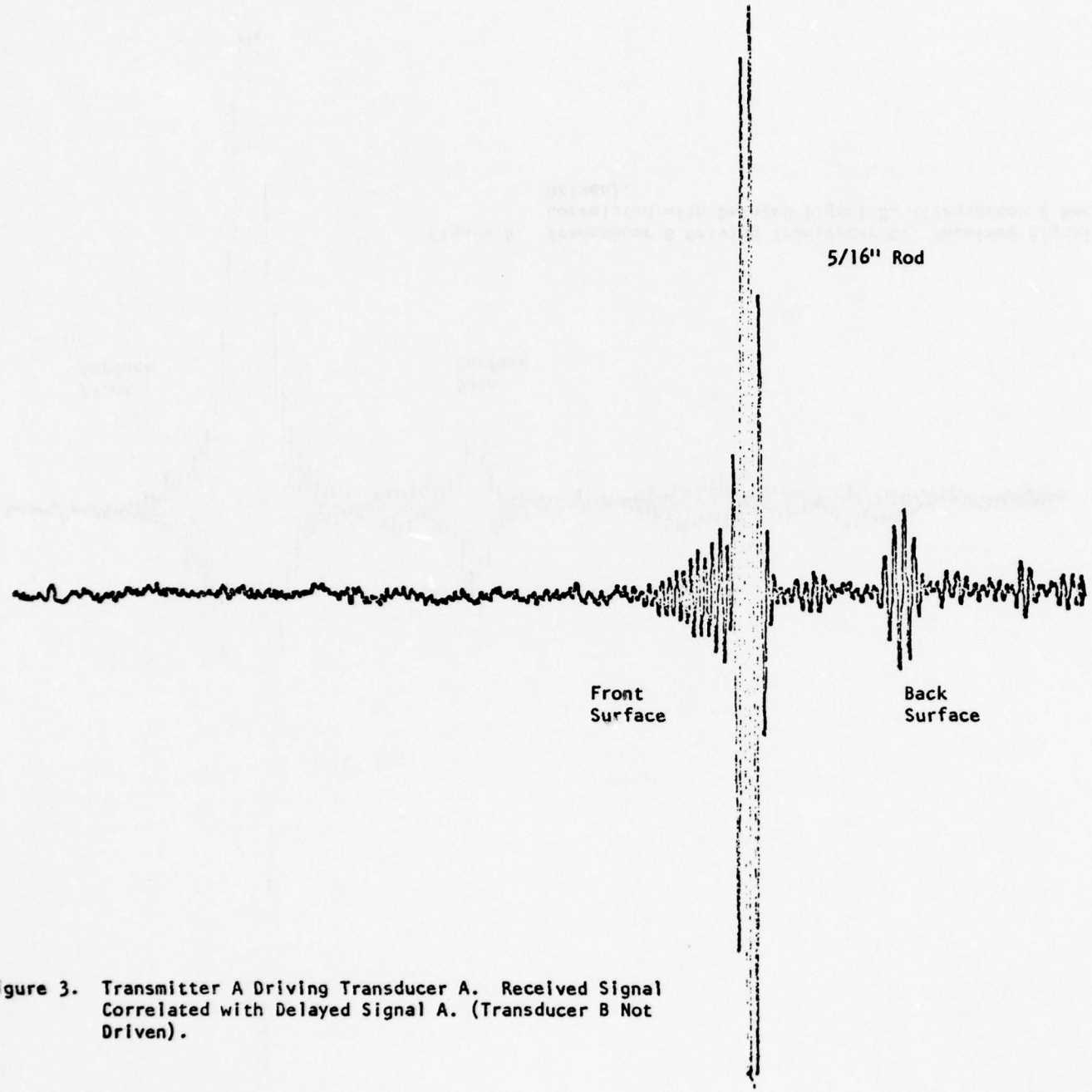

Figure 3. Transmitter A Driving Transducer A. Received Signal Correlated with Delayed Signal A. (Transducer B Not Driven).

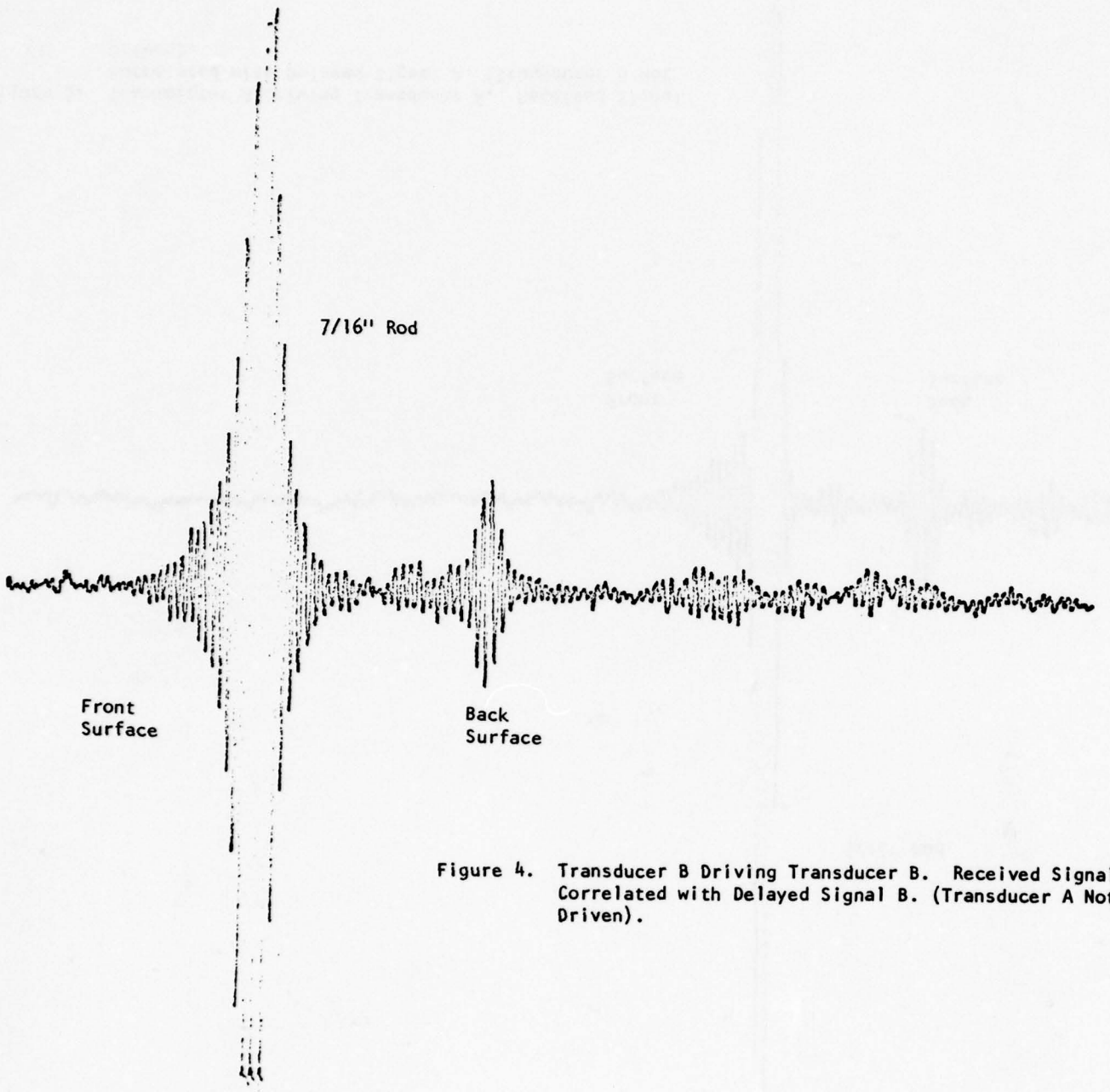

Figure 4. Transducer B Driving Transducer B. Received Signal Correlated with Delayed Signal B. (Transducer A Not Driven).

Several experimental tests were made on this setup to establish the ability of the random signal system to recover echoes associated with a particular transmitter even though echoes from several transmitted signals are present simultaneously. The output displayed in Figure 5 is an excellent example of this capability. In this test, transducer A was driven by transmitter A and transducer B was driven by transmitter B. The timing of the transmitted signals was such that echoes from both rods arrived simultaneously at the receiving element. The received echoes were correlated with a copy of transmitted signal A which was stored in the delay line. Ideally, this arrangement should reproduce the output trace in Figure 3 which shows only echoes from the 5/16 rod. The actual experimental output, presented in Figure 5, shows the echo from the 5/16 rod as expected, however, there also appears a small signal from the other reflector. This additional echo must be attributed to the cross-correlation of echoes due to transmitted signal B with the copy of signal A which was stored in the delay line.

The cross-correlation of two incoherent random signals should, ideally, equal zero. However, this only applies if the integration of the product of the two signals extends over all time. Since the correlator in the random signal flaw detection system integrates for approximately 100 msec, a slight echo from the 7/16 rod survived. It should be noted that in Figure 5 the unwanted echo signal is approximately 40 dB smaller than the corresponding echo shown in Figure 4. This is consistent with the previously quoted signal-to-noise ratio enhancement of 10,000 for the random signal system[1]. Hence the presence of echoes resulting

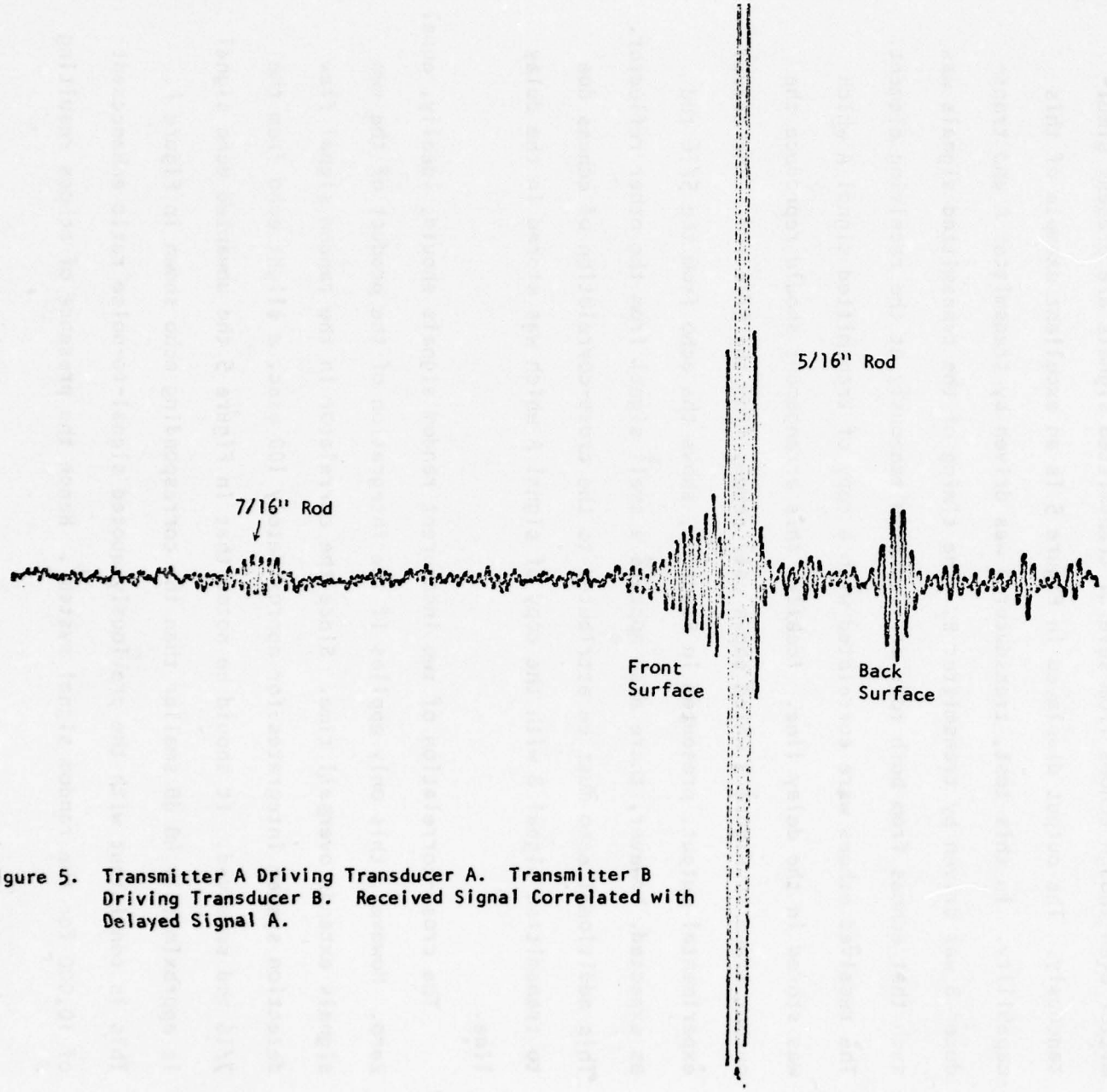

Figure 5. Transmitter A Driving Transducer A. Transmitter B Driving Transducer B. Received Signal Correlated with Delayed Signal A.

from other transmitted signals imposes a limitation on the dynamic range of the system which is inversely proportional to the integration time of the correlator. Since, as can be seen in Figure 5, the unwanted echo is only slightly larger than the noise level, this effect is not expected to be a significant factor in the operation of the beam forming system.

The second phase of the feasibility demonstration consisted of verifying that it is possible to recover the echoes corresponding to a particular transmitted signal even though two incoherent random signals were transmitted simultaneously from a single array element. The test setup for this portion of the experiment is shown in Figure 6. The transducer array and targets are essentially the same as described earlier, with the exception of the spacing between the rods which has been slightly altered. In this case, the transmitted signals are summed and applied to the center transducer whereas the outside elements of the transducer array are connected in parallel and used for reception.

The control test for this experiment used transmitter A only, to drive the center element of the linear array. The echoes received by the outer elements were correlated with a delayed version of signal A to produce the output presented in Figure 7. The output trace shows the echoes from both brass rods since the center element of the array illuminates both targets and each of the outer elements receives echoes from one of the rods.

Figure 8 displays the output which resulted when the sum of transmitted signals A and B was applied to the center transducer and the echoes, received by the outer elements of the array, were correlated with only signal A. This figure shows that the output is essentially the same as that shown in the previous figure. The apparent change in signal-to-noise ratio seen in Figure 8 is due to the reduced amplitude of the transmitted signal resulting from the use of a resistive adder to combine signals A and B.

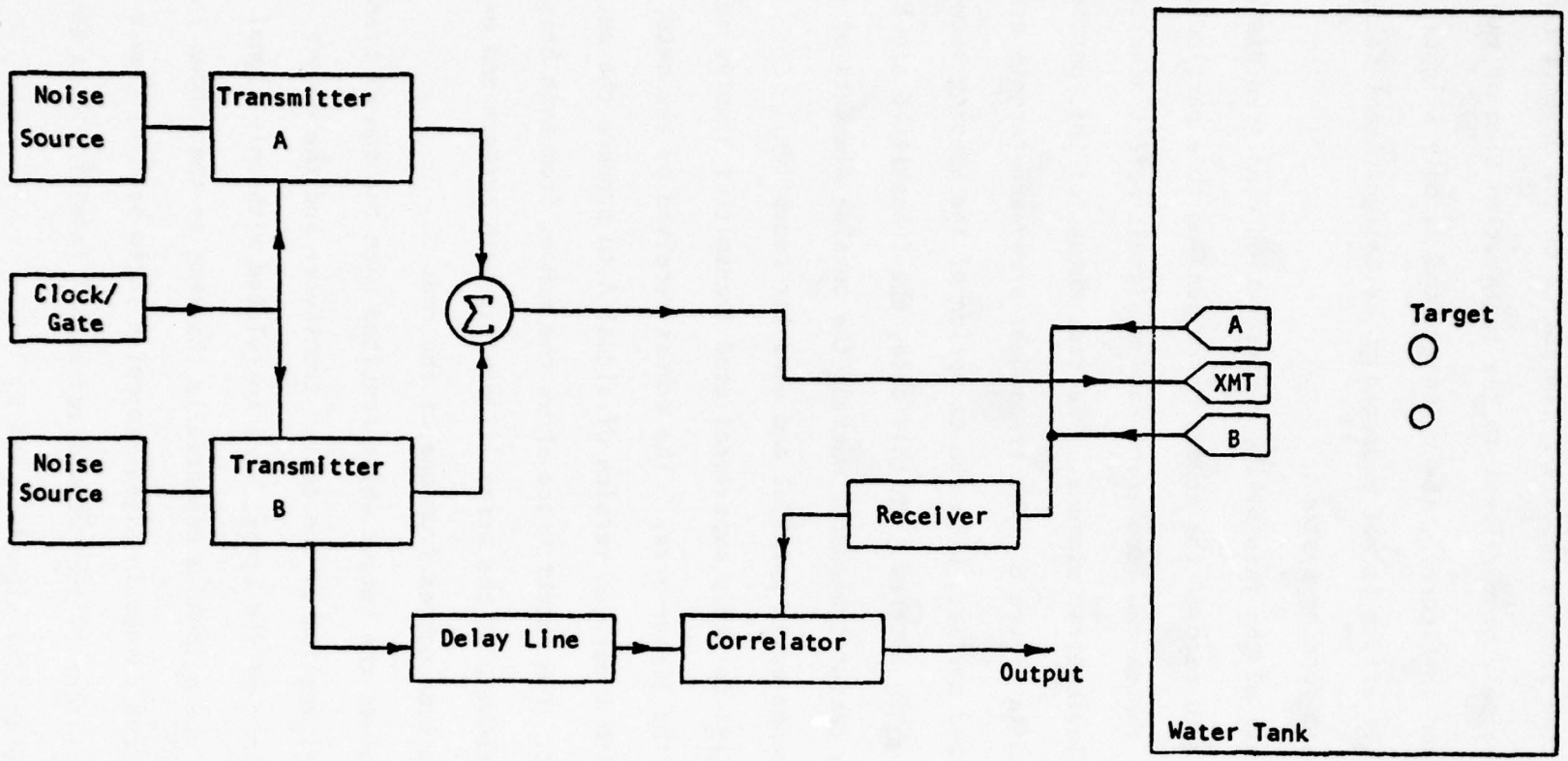

Figure 6. Test Setup for Transmitting the Sum of Signals A and B Through a Common Transducer.

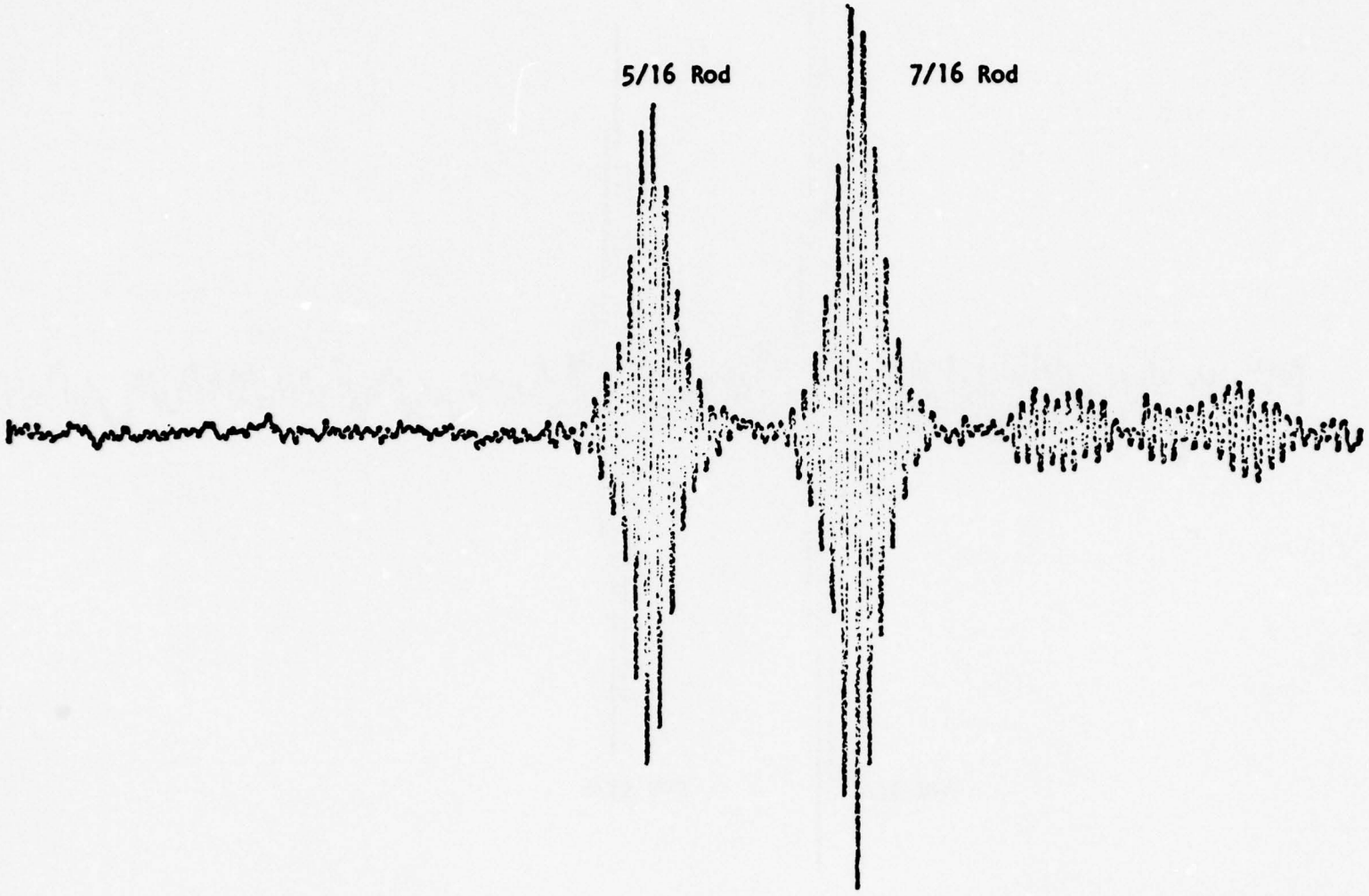

Figure 7. Transmitter A Driving Center Transducer.

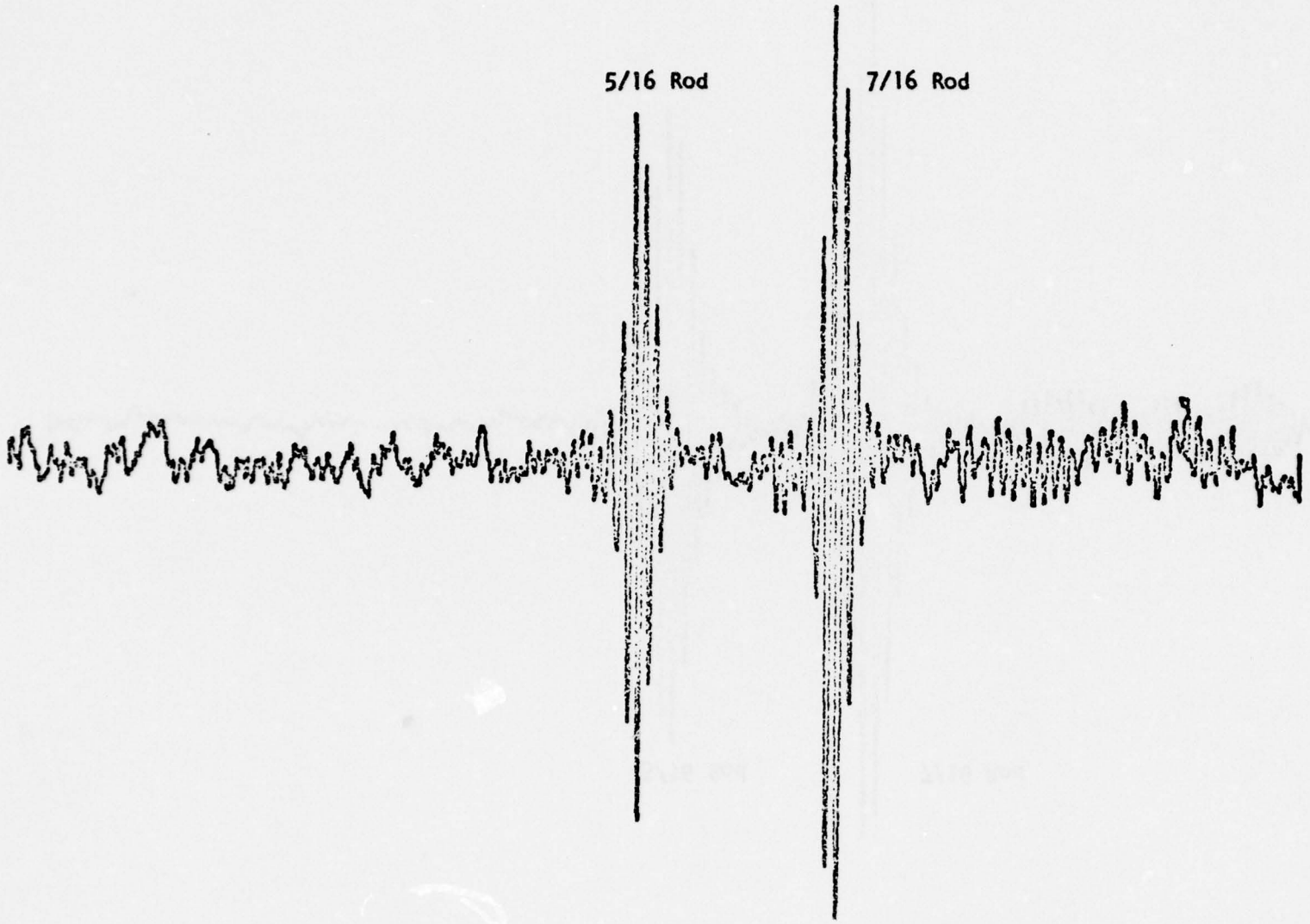

Figure 8. Transmitters A and B Driving Center Transducer.

These two experiments clearly demonstrate that the underlying principles of random signal beam forming are sound. We have explicitly shown by these tests that one random signal can be extracted from others even though a sum of incoherent random signals is transmitted through a single transducer and more than one signal are simultaneously received.

To implement a beam forming system similar to that previously described for the annular array, a prototype system containing two transmitters, receivers, and correlators must be constructed. A new delay line must also be designed to provide two variable delay paths of equal length. Although the transducer array in this system will not require switching, multiplexing circuitry will be needed to isolate segments that are driven by separate transmitters but which must feed into the same receiver. Finally the circuitry must be designed to combine the correlator outputs and provide the final output signal.

3. EXPERIMENTAL BEAM MEASUREMENTS

Having demonstrated the feasibility of random signal beam forming, the next logical step in our program was to construct the prototype system necessary to actually demonstrate this beam forming technique. Therefore the design and construction of the prototype system was begun. Unfortunately, it soon became clear that we were unable to adequately characterize the commercial transducers or linear array that we had secured for the prototype system. The inability to accurately predict the acoustic beam pattern of these transducers made the development of a system, whose purpose was to manipulate the details of the beam pattern, pointless. Consequently, we turned our attention to the ancillary problem of accurately determining the acoustic beam patterns of our transducers.

Although mathematical models of highly idealized ultrasonic transducers exist in the literature, the predicted beam patterns are usually for the case of a single transmitted frequency and apply only in the far field limit. Little useful information seems to have been published about practical acoustic transducers excited by broadband signals.

Taking a more direct approach to the problem, we had the beam patterns of some of our transducers analyzed on commercially available beam measuring equipment. Typically, these results lacked sufficient quantitative information to allow us to proceed with the development of the prototype system. Consequently a substantial portion of our effort during the past year has been directed toward surmounting this obstacle.

Our efforts to fully characterize the performance of the available ultrasonic transducers have resulted in the development of two new methods of measuring the intensity distribution of an acoustic beam. One of these systems, based on our previous work in ultrasonic doppler flow meters, is capable of high resolution beam plots for narrow band signals. The second scheme utilizes a modification of the random signal flaw detection system to examine broadband beam patterns. The remainder of this section reviews the basic operating principles of these two systems and presents results of the preliminary evaluation.

Consider any beam plotting system that is transmitting a signal of the form $\cos(\omega_o t)$. The echo expected from a point reflector, due to this transmitted signal, can be described as

$$A(x,y;z)\ \cos[\omega_o t + \phi(x,y;z)] \qquad (5)$$

where $A(x,y;z)$ is proportional to the square of the amplitude distribution of the ultrasonic field in the plane perpendicular to the axis (z-direction) of the acoustic beam and $\phi(x,y;z)$ is a phase factor dependent on the distance, in wavelengths, between the transducer and the point of measurement. The objective of the measurement process is to accurately extract the amplitude function $A(x,y;z)$ from the above expression.

The most straightforward approach to the determination of $A(x,y;z)$ is to simply measure the envelope of the echo signal as a function of target position. Although straightforward, this method of attack suffers from two serious drawbacks. Since it is necessary to pulse the transmitted signal to eliminate multiple reflections, the transmitted signal is not a single frequency but an entire spectrum whose bandwidth is inversely proportional to the pulse length. As a result the envelope of the echo signal actually contains contributions from many frequency components, making interpretation of the measurement difficult. The second problem is that direct measurement of the echo envelope provides no signal-to-noise ratio enhancement. Therefore, such a system has very limited sensitivity and dynamic range. This is an extremely important shortcoming since accurate beam measurements require the use of a target whose effective reflecting surface is small compared to an acoustic wavelength, causing little of the transmitted acoustic energy to be returned to the transducer.

Both limitations of the direct measurement system can be removed by the use of a heterodyne receiver. If the received echo is mixed with a reference signal, it is possible to filter the resulting signal to obtain only the information contained in a single frequency component of the received echo. If the reference signal and the transmitted signal are of the same frequency, the resulting signal, after filtering, will be

$$A(x,y;z)\ \cos[\phi(x,y;z)] \qquad (6)$$

The use of a heterodyne system allows selection of a single received frequency component even though the transmitted signal is pulse modulated. Furthermore, this type of system provides signal-to-noise ratio enhancement proportional to the band compression of the receiver, the ratio of the output bandwidth to the received bandwidth. Although this receiving system overcomes the most serious limitations of direct envelope measurement, it introduces its own unique problem. As seen in the above expression (6), the desired amplitude function $A(x,y;z)$ is multiplied by an unknown phase factor which is extremely sensitive to the path length between the target and transducer. The presence of this phase factor makes interpretation of the output from this type of system extremely difficult.

Figure 9 displays the block diagram of one of the systems we have developed to measure acoustic beam intensity. The operation of this system is as follows. A master oscillator produces a signal of the form $\cos(\omega_o t)$ which is pulse

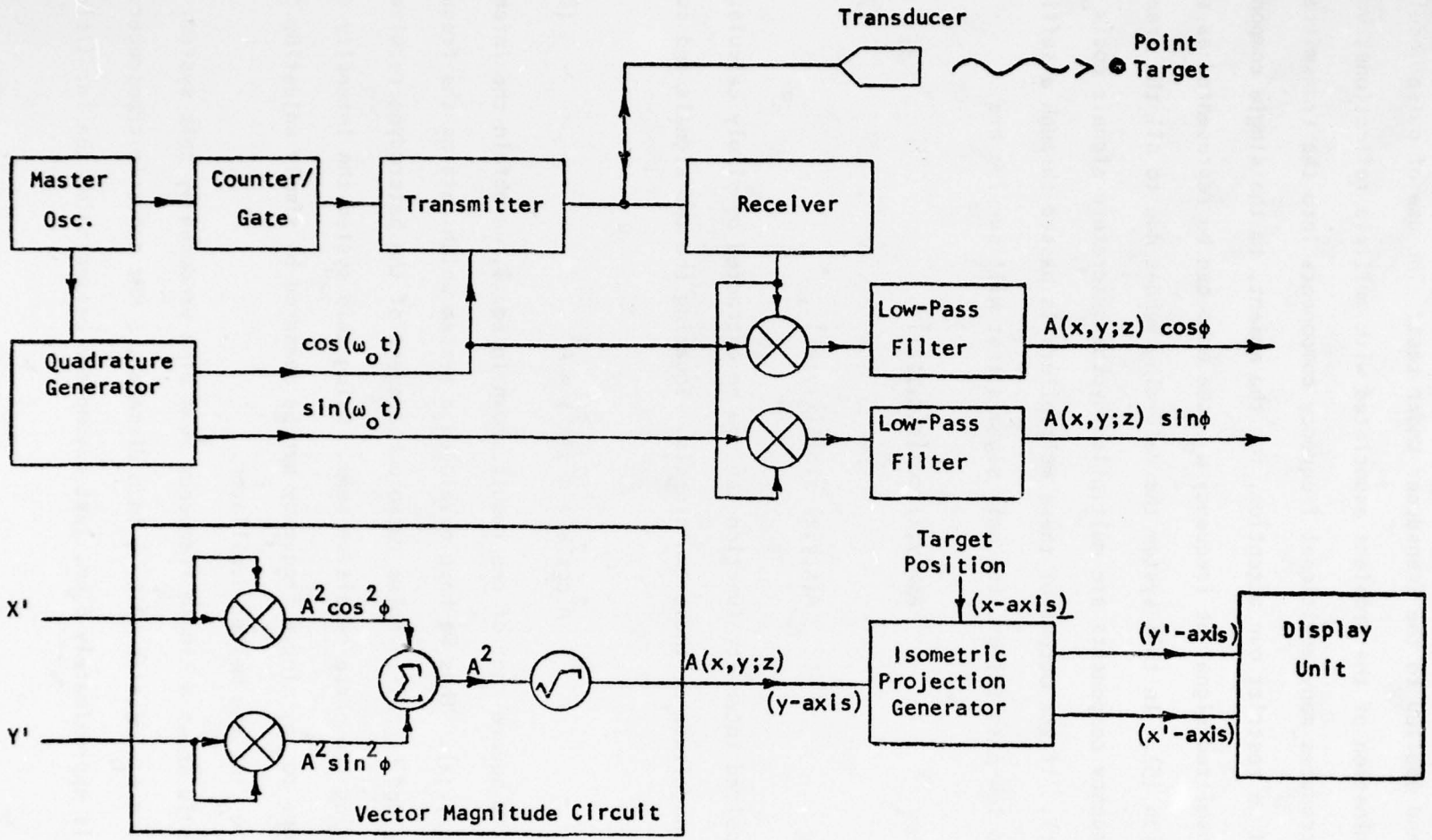

Figure 9. Block Diagram of Narrow Band Acoustic Beam Plotting System.

modulated and applied to the transducer under test. The use of pulse modulation allows elimination of the problems associated with multiple reflections, but it also introduces many additional frequency components into the transmitted signal. If we restrict our attention, for the moment, to the single component of the transmitted signal at frequency ω_o, the echo can be represented as shown in expression (5). In this system the returning echoes due to all the transmitted frequency components are multiplied by the quadrature signals $\cos(\omega_o t)$ and $\sin(\omega_o t)$. If the output of these multipliers is passed through a sufficiently narrow band low-pass filter, the only signals that will survive are

$$A(x,y;z)\ \cos[\phi(x,y;z)]$$

and (7)

$$A(x,y;z)\ \sin[\phi(x,y;z)]$$

The desired intensity function can now be extracted by simply calculating the vector magnitude of these two signals. Squaring the two signals and summing, we obtain

$$A^2\cos^2\phi + A^2\sin^2\phi = A^2 \qquad (8)$$

By taking the square root of the result shown in Eq. 8, we obtain the intensity function $A(x,y;z)$. Thus we have developed a system which retains the frequency selectivity and signal-to-noise ratio enhancement of the heterodyne receiver while removing the phase sensitive term. Using this system the intensity distribution due to any single frequency can be measured by simply adjusting the frequency, ω_o, of the master oscillator.

Figure 10 shows a single frequency beam plot produced by this system. The plot is for a Panametrics V310, ½ inch diameter, 5 MHz acoustic transducer. The range is approximately 6 cm, just beyond the beginning of the far field

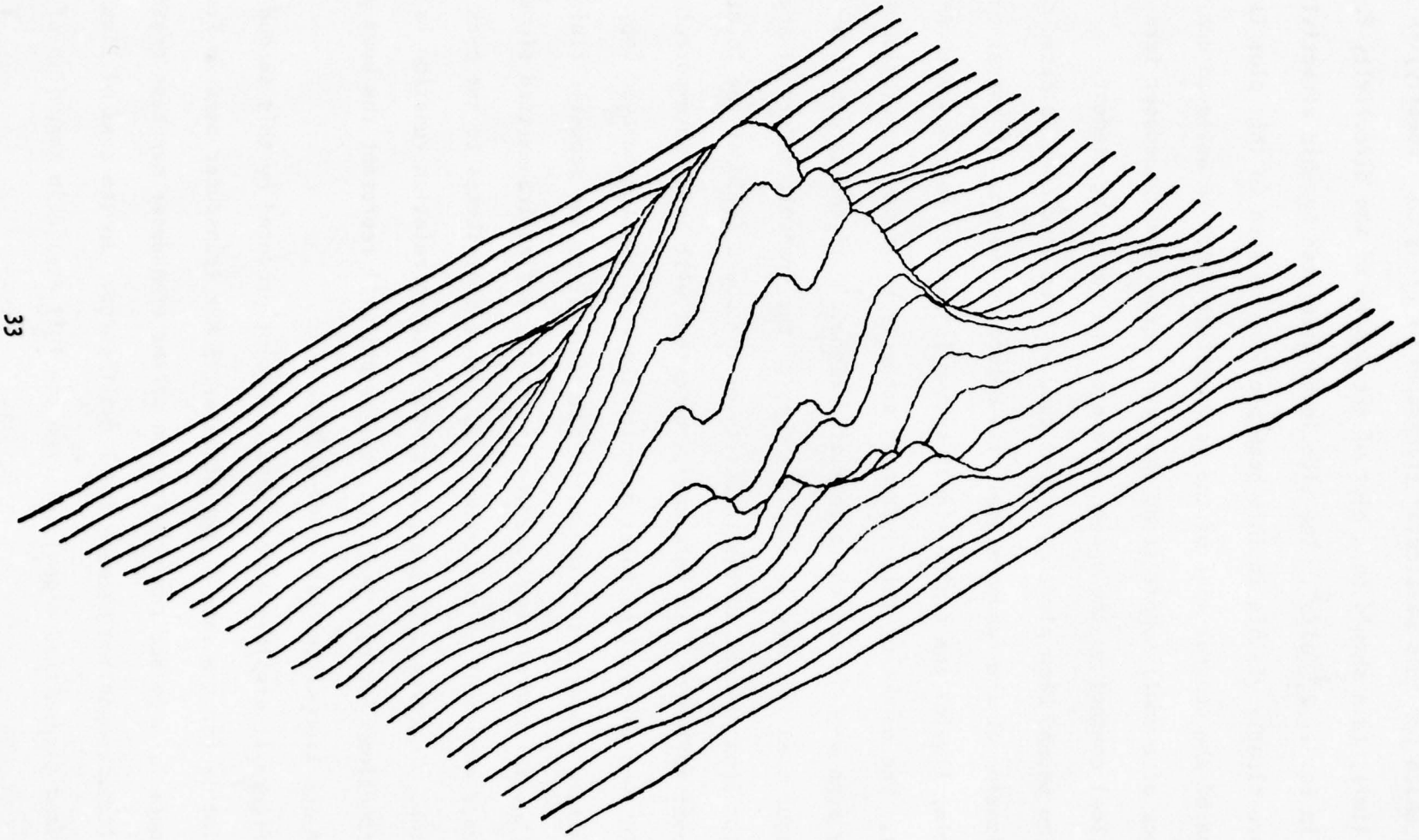

Figure 10. Single Frequency Beam Pattern of 1/4 inch Diameter, 5 MHz Acoustic Transducer. Range Approximately 6 cm (Far Field).

region which for this particular transducer is at 3½ cm. Ideally, in the far field limit, this should be a plot of the square of the directivity function given in Eq. 1, $J_1^2(\rho)/\rho^2$. The side lobes predicted by this directivity function are clearly visible in this beam plot. Also seen in this plot is a distortion of the central lobe of the beam pattern which is believed due to the presence of a small copper strap that runs across the transducer face to make electrical contact to the upper surface of the radiating element.

The second beam plotting system that we have developed is based on a modification of the random signal flaw detection system. In normal operation, the delay line of the random signal system is scanned to produce an A-scan type output. The output of this system is actually the cross-correlation function of the echo signals and the transmitted signal.[1] If the target is a point reflector then the echo is simply a copy of the transmitted signal scaled by a factor proportional to the intensity of the sound field at the location of the point reflector.[4] In this case, the output will be an auto-correlation function whose peak (the point at which the echo and the delayed copy of the transmitted signal are in phase) is proportional to the acoustic field intensity. Since the auto-correlation function is for the entire transmitted signal, every frequency component of the transmitted signal contributes to the peak of the function. Therefore, if the peak of the auto-correlation function is tracked as a function of target position, the output will represent the beam pattern due to the transmitted broadband signal.

Figure 11 displays a broadband beam plot produced by this second system. The plot is for the same ¼ inch diameter, 5 MHz transducer used in Figure 10. The range is 6 cm and the orientation of the transducer has been preserved to facilitate comparison between these two figures. In the case of Figure 11, the broadband transmitted signal utilized the full available bandwidth of the

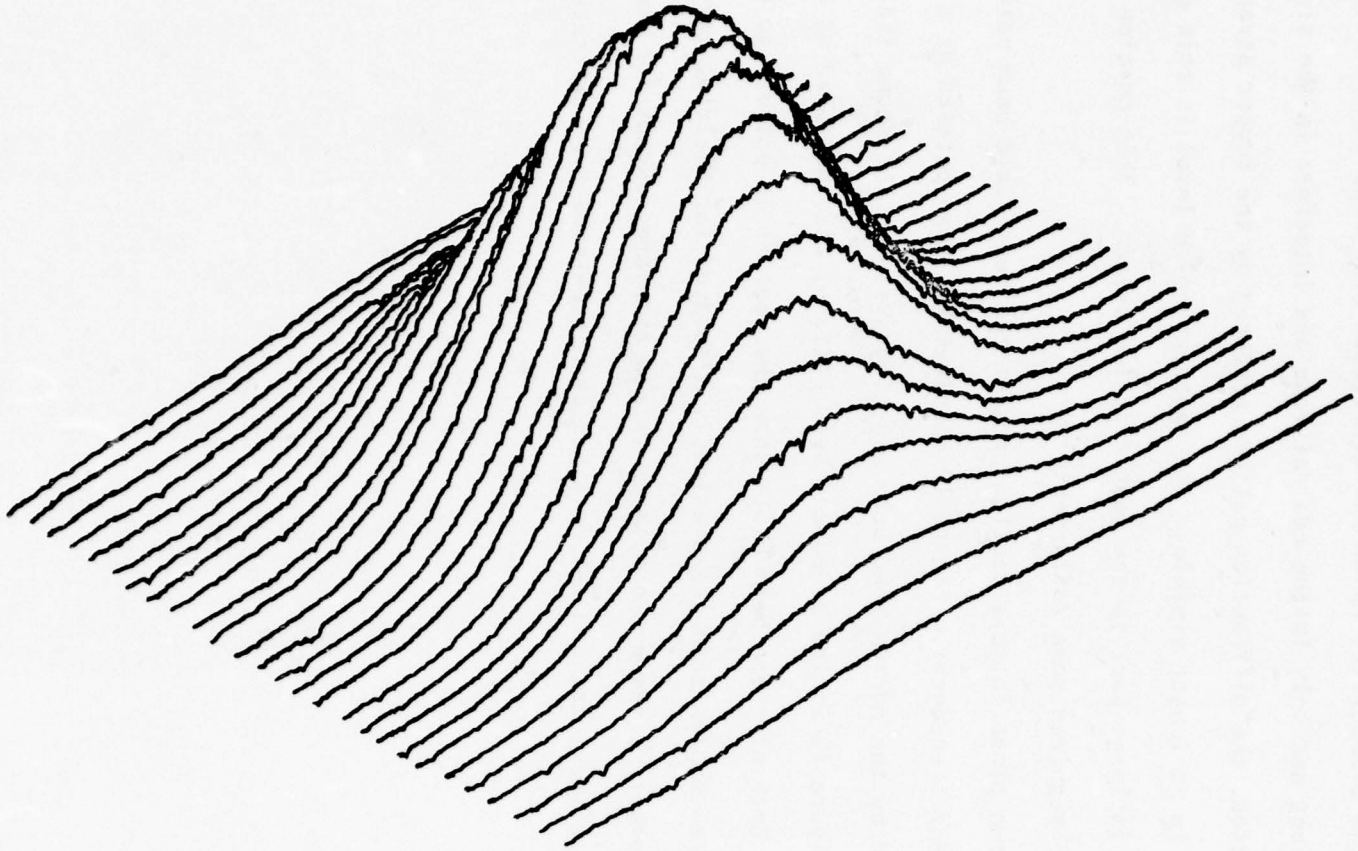

Figure 11. Broadband Beam Pattern of a 1/4 inch Diameter, 5 MHz Acoustic Transducer. Range Approximately 6 cm (Far Field).

ultrasonic transducer under test. As expected, the side lobes are no longer present, since the directivity functions associated with each transmitted frequency component add only in the central lobe and interfere in the side lobes. In addition, the diffraction pattern produced by the copper strap mentioned above is no longer visible. The apparent noise level in this output plot is due in large part to the peak tracking system. This portion of the system still requires some refinement.

The final two plots in this section present the near field beam pattern for the same 5 MHz transducer. Figure 12 displays the beam pattern at a range of 2 cm produced by the narrow band beam plotting system. The sound field plot shown in Figure 13 is the broadband beam pattern, also measured at a range of 2 cm. Both of these beam plots show the near field pattern to be considerably more complex than the previously displayed far field patterns.

The development of these two systems is now complete, except for some possible minor refinements, and the work has been submitted for publication.

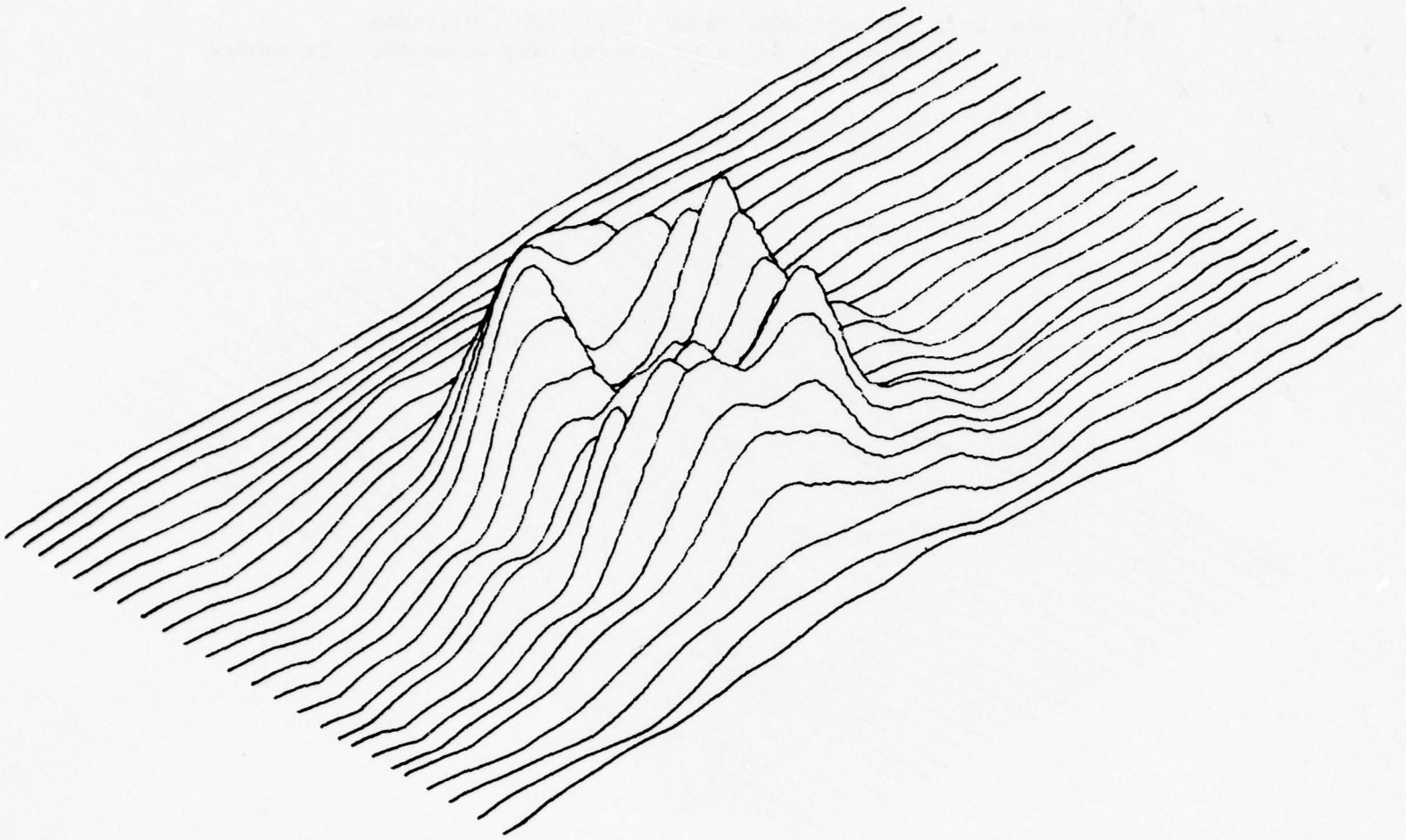

Figure 12. Single Frequency Beam Pattern of a 1/4 inch Diameter, 5 MHz Acoustic Transducer. Range approximately 2 cm (Near Field).

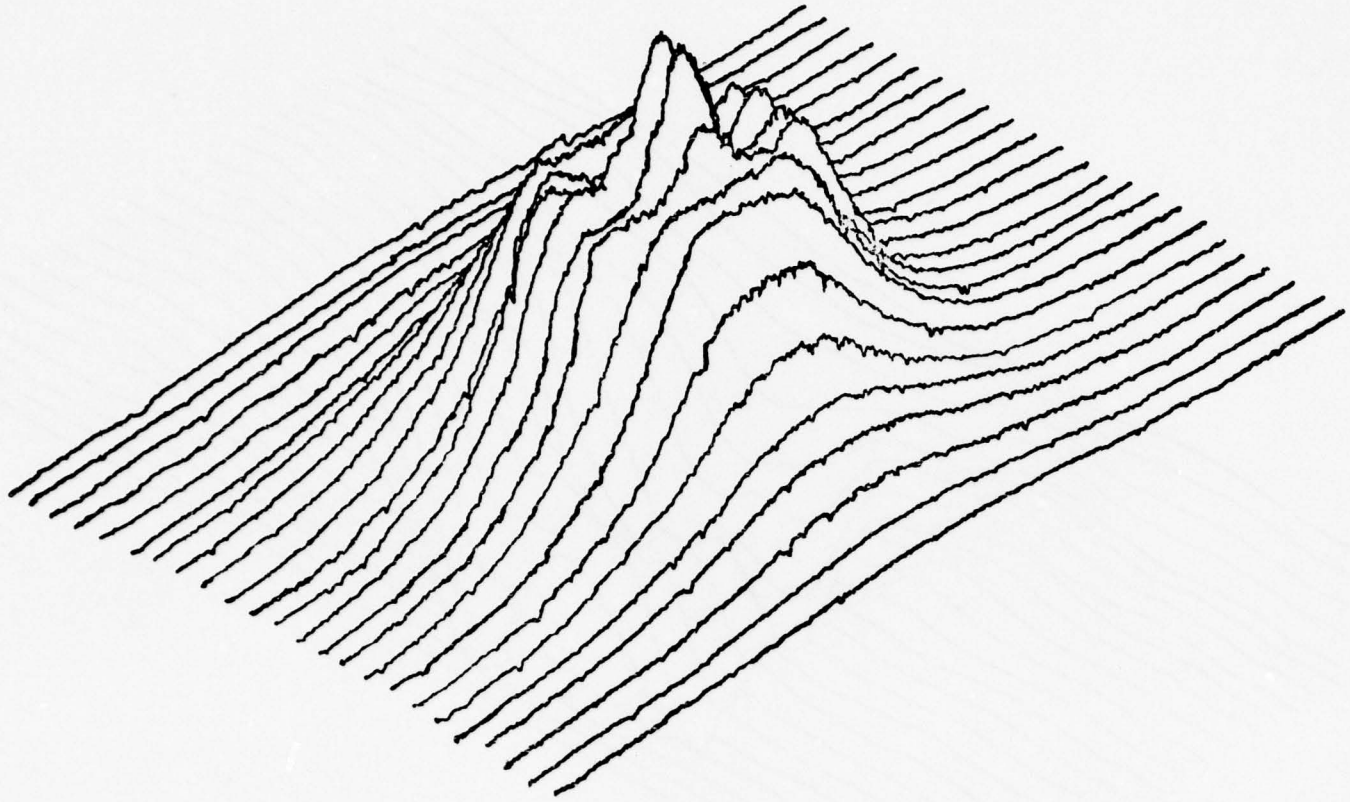

Figure 13. Broadband Beam Pattern of a 1/4 inch Diameter, 5 MHz Acoustic Transducer. Range approximately 2 cm (Near Field).

SECTION VI

DECONVOLUTION OF FLAW ECHOES

The ultimate resolution of all ultrasonic flaw detection systems is limited by transducer response. Although the system output actually contains detailed information about the target structure, these details are masked by the system characteristics. Since all test instruments interact with the object under test and therefore, to some extent, tend to alter or distort the quantities being measured, this type of problem is universal. However, the problem is particularly severe in the case of ultrasonic flaw detection systems due to the limited bandwidth of the acoustic transducer.

For any general linear measurement system the output can be shown to be the convolution of the signal which is to be measured and the impulse response of the measurement system. In an ultrasonic flaw detection system the flaw echoes are masked by convolution with an impulse response of the system that is almost entirely determined by the frequency response of the transducer. In principle, it should be possible to reverse the convolution process to remove the system response and extract the true target response. Unfortunately, it is found that in practice the presence of even relatively small amounts of noise makes the deconvolution process impossible. If, however, the flaw detection system has an extremely high output signal-to-noise ratio it is possible to use estimation techniques in the deconvolution process to achieve a good approximation to the actual target response.

1. THEORY OF THE INVERSION PROBLEM

In general for any linear measurement system, if we let $x(t)$ be the function representing the quantity to be measured and let $h(t)$ be the function representing the response of the measuring instrument, then the actual experimental data $y(t)$ can be expressed as the convolution of $x(t)$ and $h(t)$,

$$y(t) = x(t) * h(t) = \int_{-\infty}^{\infty} x(\tau)h(t - \tau)d\tau \qquad (9)$$

Over the years workers in many fields ranging from radiography to picture processing have considered the problem of extracting the function that was to be measured $x(t)$ from the actual measured data $y(t)$. The mathematical formalism for the process required to perform this operation is called 'deconvolution' and has been known for many years.[11] If the response of the measuring instrument $h(t)$ is known or can be measured, then the deconvolution process can be applied to recover the desired function $x(t)$ from the experimental data. The process begins by taking the Fourier transform of the expression representing the measured experimental data

$$F\{y(t)\} = F\{x(t)*h(t)\} = F\{x(t)\} \cdot F\{h(t)\} \qquad (10)$$

or

$$Y(\omega) = X(\omega) \cdot H(\omega) \qquad (11)$$

Dividing this equation by the Fourier transform of the impulse response of the instrument $H(\omega)$ yields

$$X(\omega) = Y(\omega)/H(\omega) \qquad (12)$$

In principle, all that is now required to obtain the desired function $x(t)$ is to take the inverse Fourier transform of this ratio

$$x(t) = F^{-1}\{Y(\omega)/H(\omega)\} \qquad (13)$$

With high speed mini-computers, accurate analog-to-digital converters, and Fast Fourier Transform routines in common use it should be relatively easy to implement the elementary mathematical operations required for deconvolution.

Unfortunately, there are two significant problems associated with the use of the deconvolution process. First, the response of the test instrument h(t) must be accurately known. In some cases this response can be measured directly while in other cases the response can only be estimated or predicted theoretically. In either case, the uncertainty in the impulse response of the test instrument can cause serious errors in the deconvolved signal. The second problem is universal and much more severe. The above analysis of the deconvolution process has ignored the effects caused by noise which is ever present in experimental data.

The result of taking the presence of noise into account in the above development of the deconvolution expression is that a unique solution to the deconvolution problem no longer exists.[12] Many workers have demonstrated that the presence of even relatively small amounts of noise in their experimental data leads to wildly oscillating solutions when deconvolution is attempted. As a result, several estimation techniques have been proposed to deal with the presence of noise in the measured signal. These techniques generally require some restrictions on either (or both) the response of the measuring system of the set of acceptable deconvolved signals. In addition these techniques all require that the measured signal have a high signal-to-noise ratio if the result is to be a good approximation to the actual desired signal.

To examine the influence of noise in the deconvolution process, consider the case of real experimental data contaminated with noise. In this case the quantity that is actually measured is a corrupted version of the system output

$\hat{y}(t)$ due to the presence of noise $n(t)$. Consequently, the experimentally measurable signal can be represented as

$$\hat{y}(t) = x(t) * h(t) + n(t) \tag{14}$$

If the straight forward deconvolution process described above is applied to this contaminated output signal, we obtain the following estimate of the signal being measured

$$\hat{x}(t) = F^{-1}\{Y(\omega)/H(\omega) + N(\omega)/H(\omega)\} \tag{15}$$

The first term in this expression is the desired signal while the second term is the contribution due to the noise present in the experimental measurement. Since the functions $N(\omega)$ and $H(\omega)$ are unrelated, their zeros can not in general coincide. Thus it is usually the case that at some frequency $H(\omega)$ becomes very small or zero while $N(\omega)$ remains relatively constant causing the second term to blow-up. As a result, the noise term will dominate, completely obscuring the desired component of the deconvolved signal. This result clearly demonstrates that it is essential to have the signal-to-noise ratio of the experimental data be as large as possible if deconvolution processing is to be applied.

The straightforward application of deconvolution to experimentally measured signals has been shown to lead to noise dominated solutions. In fact, it can easily be shown that the desired function to be measured $x(t)$ can never be exactly recovered once it has been corrupted by noise.[12] Thus we are forced to rephrase the original deconvolution problem as follows: Given a measurement system output

$$\hat{y}(t) = x(t) * h(t) + n(t) \tag{16}$$

contaminated by noise, obtain the best estimate (in some sense) of the quantity to be measured $x(t)$ using the least possible a priori information about $x(t)$.

In an actual system, the noise n(t) is an unknown random function of time. Thus examination of Eq. 15 reveals that straightforward deconvolution actually generates an entire set S of possible solutions, in which each of the infinitely many possible noise functions yields a different approximation $\hat{x}(t)$. In the vast majority of functions comprising the set S of possible solutions the noise contribution dominates. Thus these solutions yield virtually no information about the unknown function x(t). The objective of the deconvolution procedure reduces to the selection of a solution from the set S which best approximates (in some sense) the desired unknown function x(t).

For measurement systems which possess a high signal-to-noise ratio, the following estimation technique can be used to advantage. In all physical systems, we know that the noise is bounded in amplitude and exists only for a finite time interval. Hence the noise energy in the experimental measurement satisfies the following inequality

$$\int_{-\infty}^{\infty} n^2(t)\,dt \leq \epsilon^2 \tag{17}$$

We can select a particular solution $\hat{x}_s(t)$ from the set S of all possible solutions such that[11,12]

$$\int_{-\infty}^{\infty} [c(t) * \hat{x}_s(t)]^2\,dt = \min_{\hat{x}\epsilon S} \left\{ \int_{-\infty}^{\infty} [c(t) * \hat{x}(t)]^2\,dt \right\} \tag{18}$$

where c(t) is a constraint operator which forces the particular solution $\hat{x}_s(t)$ to meet predetermined criteria for smoothness. The original applications of this estimation technique to the deconvolution problem were in the field of radiography.[13] In this application it was assumed that the unknown functions x(t) should be represented by a very smooth response. Thus they employed the second difference

operator $\delta''(t)$ to select the solution which has the smallest squared second derivative. For this particular case, Eq. 18 becomes[13]

$$\int_{-\infty}^{\infty} [c(t) * \hat{x}_s(t)]^2 dt = \int_{-\infty}^{\infty} [\hat{x}_s''(t)]^2 dt = \min_{\hat{x} \epsilon S} \left\{ \int_{-\infty}^{\infty} \hat{x}''(t)]^2 dt \right\} \qquad (19)$$

To implement these operations on a digital computer, we must translate the above integral expressions to discrete form. Phillips and Twomey have shown that the constraint given by Eq. 18 is, for the case of discrete functions, equivalent to

$$\frac{\partial}{\partial \hat{x}_k} \{ |H\hat{x} - \hat{y}|^2 + \gamma \hat{x}^* C \hat{x} \} = 0 \qquad (k = 1,2,....N) \quad (20)$$

where H and C are the matrices that represent the system response and the constraint respectively and γ is a Lagrangian multiplier. Hunt demonstrated that the solution of Eq. 18 can be represented in terms of discrete Fourier transforms as

$$X(k) = \frac{\hat{Y}(k) H^*(k)}{|H(k)|^2 + \gamma |C(k)|^2} \qquad (k = 1,2,...N) \quad (21)$$

where the Lagrangian multiplier is chosen to satisfy the following condition on noise energy calculated from Eq. 17

$$\sum_{k=1}^{N} \frac{|\hat{Y}(k)|^2}{\left[\frac{|H(k)|^2}{\gamma |C(k)|^2} + 1 \right]^2} \cong \frac{\epsilon^2}{N} \qquad (22)$$

The following sections show how we have adapted this general deconvolution procedure for use with our random signal flaw detection system. Experimental results are also presented which demonstrate that the signal-to-noise ratio enhancement provided by the random signal correlation system permits this

technique to be used in ultrasonic flaw detection to provide a significant improvement in resolution. The possibility of extracting target orientation is also discussed.

2. EXPERIMENTAL APPLICATIONS

The extremely high signal-to-noise ratio provided by the random signal system makes deconvolution processing a practical method of enhancing the resolving power of this flaw detection system. A linear model of the essential components of the random signal system is shown in Figure 14. In this figure each element of the system is represented by its impulse response. From this block diagram it can be seen that the system output $y(t)$ due to a flaw which is represented by $g(t)$ is

$$y(t) = g(t) * m_r(t) * R_f(t) \tag{23}$$

where

$$R_f(t) = \int_{-\infty}^{\infty} \lambda_{12}(\tau)\lambda_{34}(t + \tau)\, d\tau$$

and

$$\lambda_{ij}(t) = x(t) * h_i(t) * h_j(t)$$

It can be assumed that the four transducers shown in Figure 14 have similar impulse responses. If it can also be assumed that the signal source produces broadband noise $x(t)$, then the transducers determine the details of the transmitted spectrum. In this case, the function $R_f(t)$ is simply the auto-correlation function of the band limited noise signal. If we further assume that the material of which the test object is composed introduces only a propagation delay in the acoustic signal, then the system output is given by

$$y(t) = g(t) * R_f(t) \tag{24}$$

where $R_f(t)$ is now the auto-correlation function of the noise signal band limited by the acoustic transducers. Therefore, in this simplified analysis, the auto-correlation function $R_f(t)$ represents the overall response of the random signal system.

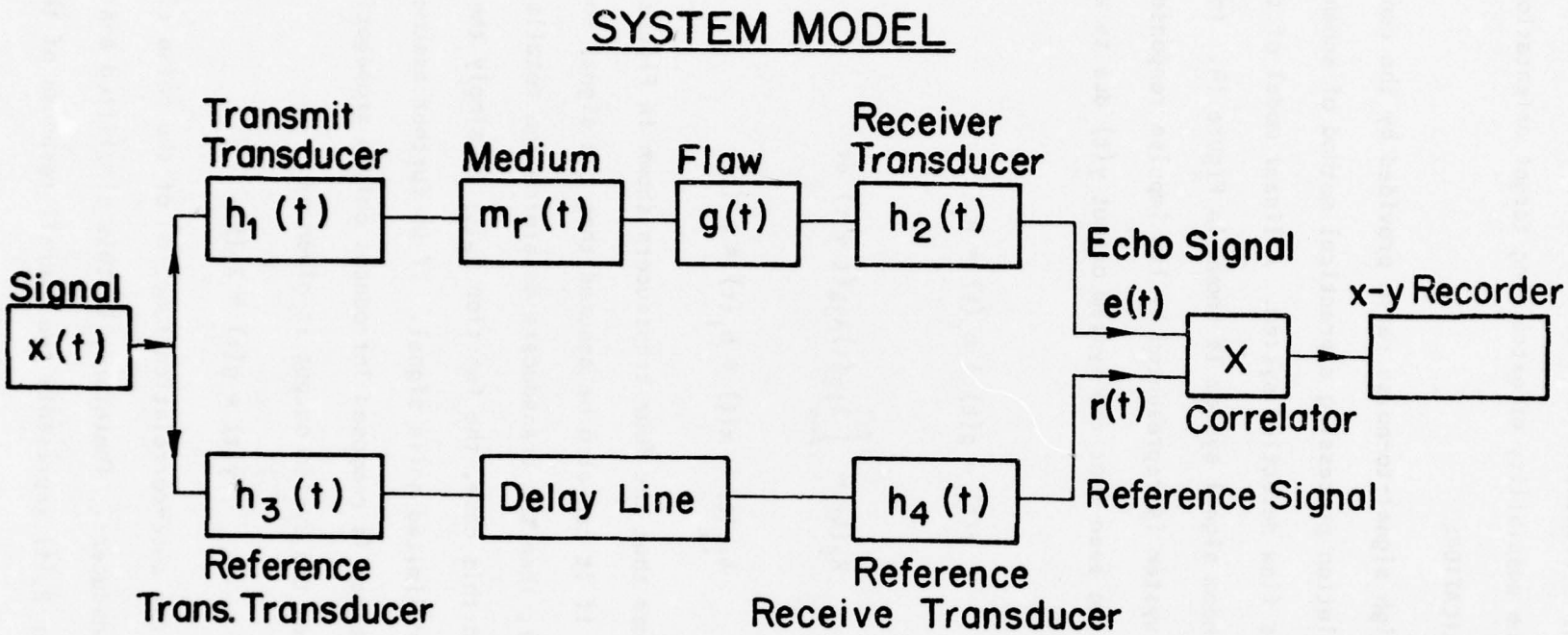

Figure 14, Linear Model of the Random Signal Flaw Detection System.

The function $R_f(t)$ can be determined experimentally by simply selecting a reference target whose response is an impulse (delta function). A single plane surface aligned parallel to the face of the transducer will be used to provide the required impulse response for the deconvolved signals presented below. The output expected from this type of reference target can be computed to be

$$y(t) = \delta(t) * R_f(t) = R_f(t) \tag{25}$$

the impulse response of the flaw detection system.

Figure 15 shows a computer simulation of the impulse response for the random signal flaw detection system corresponding to the output obtained from a plane reflector parallel to the face of the acoustic transducer. In this simulation, random noise (at a level comparable to that experienced in an actual experimental measurement) has been added to the signal to more accurately model actual experimental conditions. The impulse response has also been split in half and translated to the plot origin by the computer to eliminate phase information from this signal and prepare it for Fast Fourier Transforming.

The simulated output trace presented in Figure 16 corresponds to a target consisting of two plane surfaces separated by a distance less than the resolution limit of the detection system. It can be seen from this figure that random noise has also been added to this output signal. If straight forward deconvolution of this output signal is attempted using the impulse response displayed in the previous figure, the result is as shown in Figure 17. This figure clearly demonstrates the disastrous effect of even the relatively small amount of noise present in the simulated output signals. The high frequency oscillations

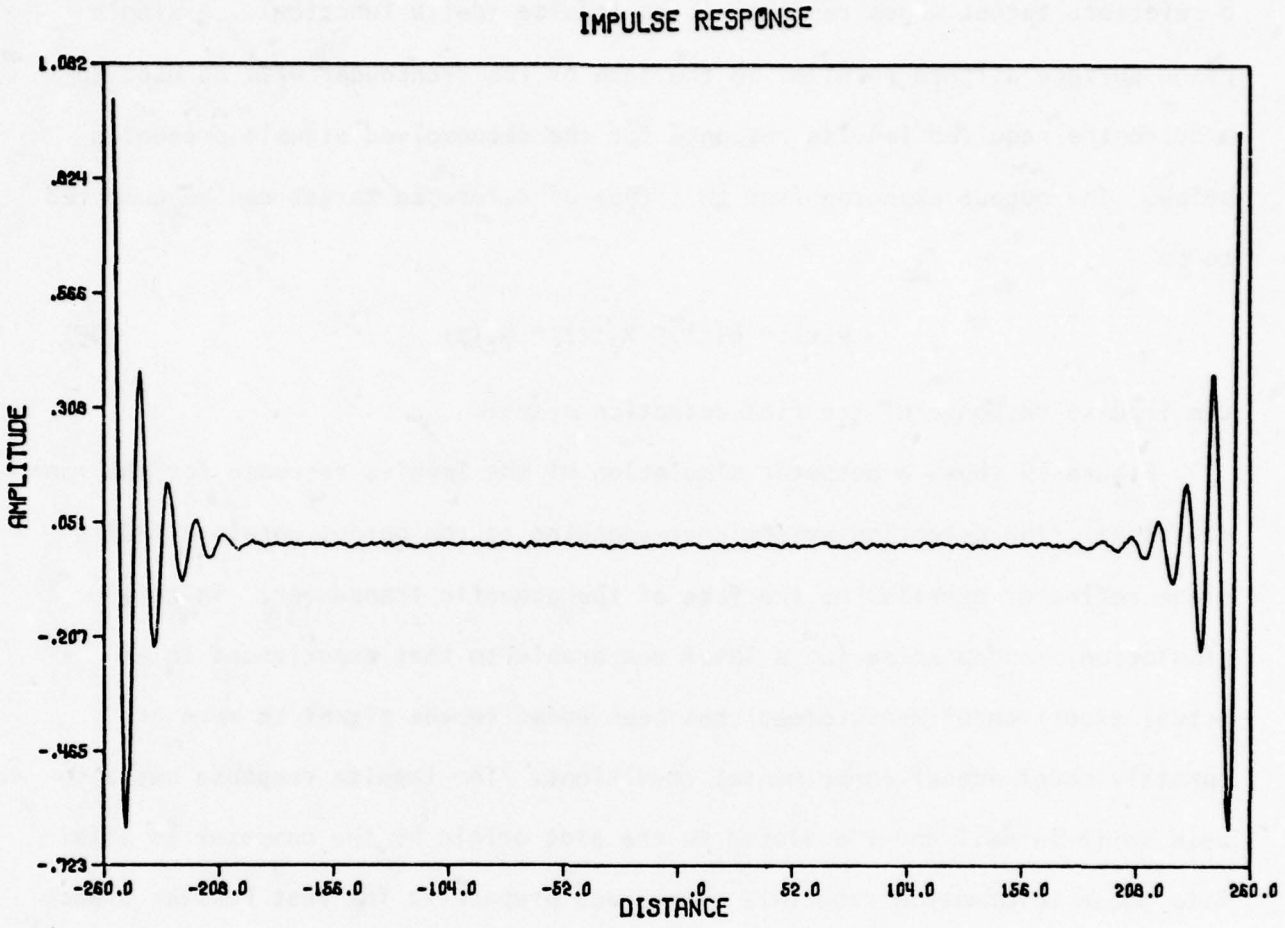

Figure 15. Simulated Impulse Response of a Plane Surface Retlector Superimposed with Uniform Density Noise 0.7% of the Maximum Value of the Impulse Response.

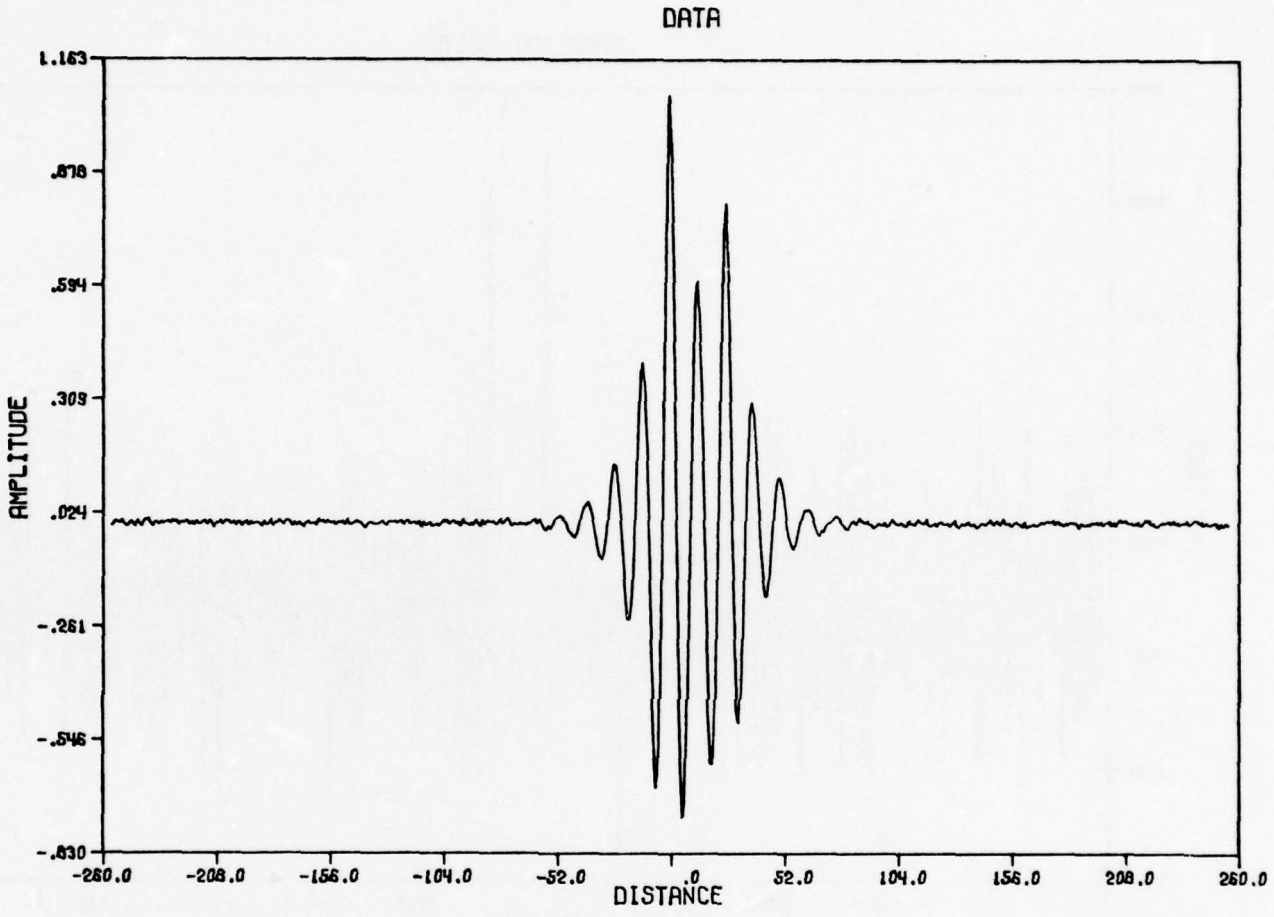

Figure 16. Simulated System Output Containing Two Parallel Plane Targets (Relative Amplitudes 1.0 and 0.7) Separated by 25 Points on a 512 Point Data Sample, Superimposed with Uniform Density Noise 0.7% of the Maximum Value of the Target Signal.

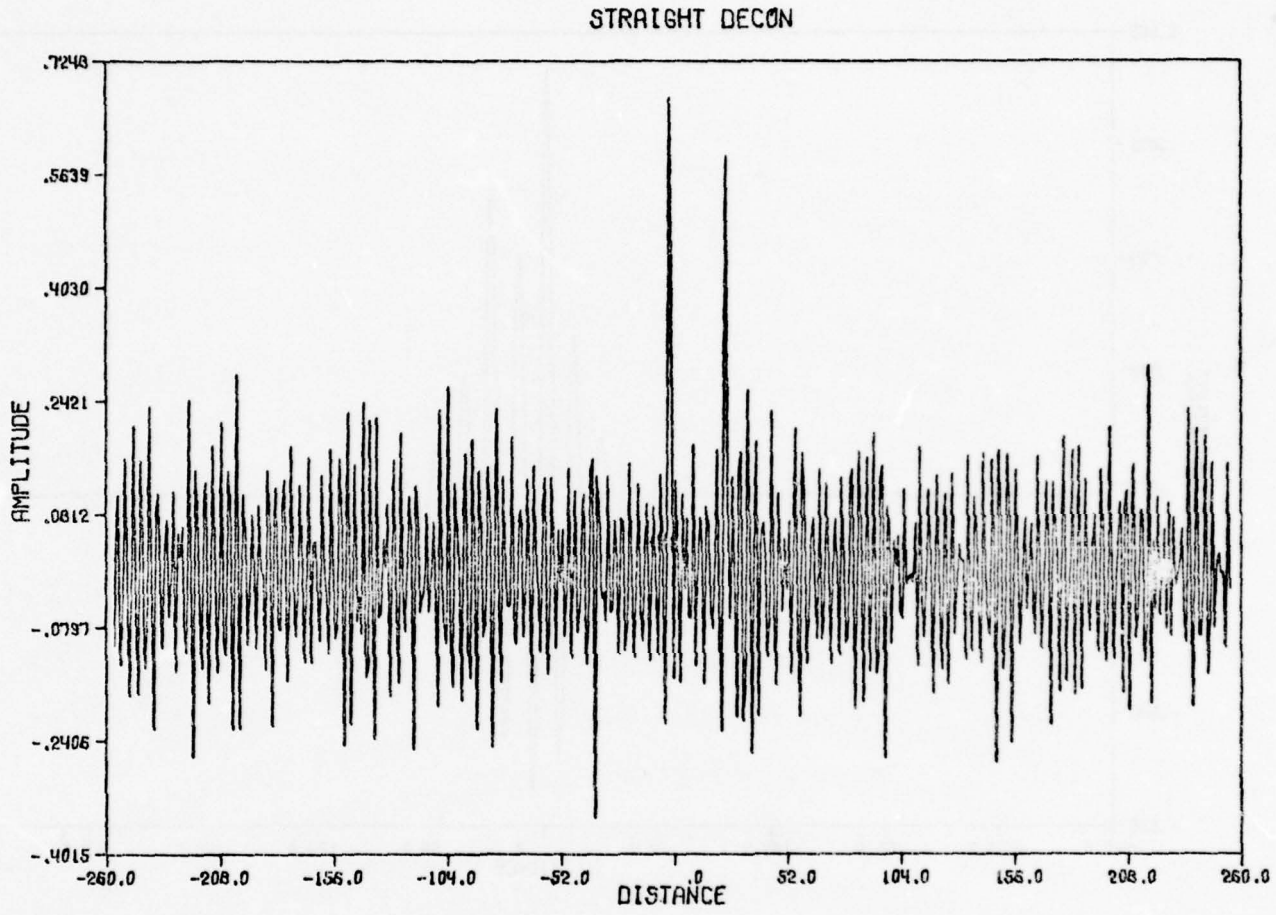

Figure 17. Deconvolution of Figure 16 by Straight Forward Division of Fourier Transforms Using the Impulse Response of Figure 15.

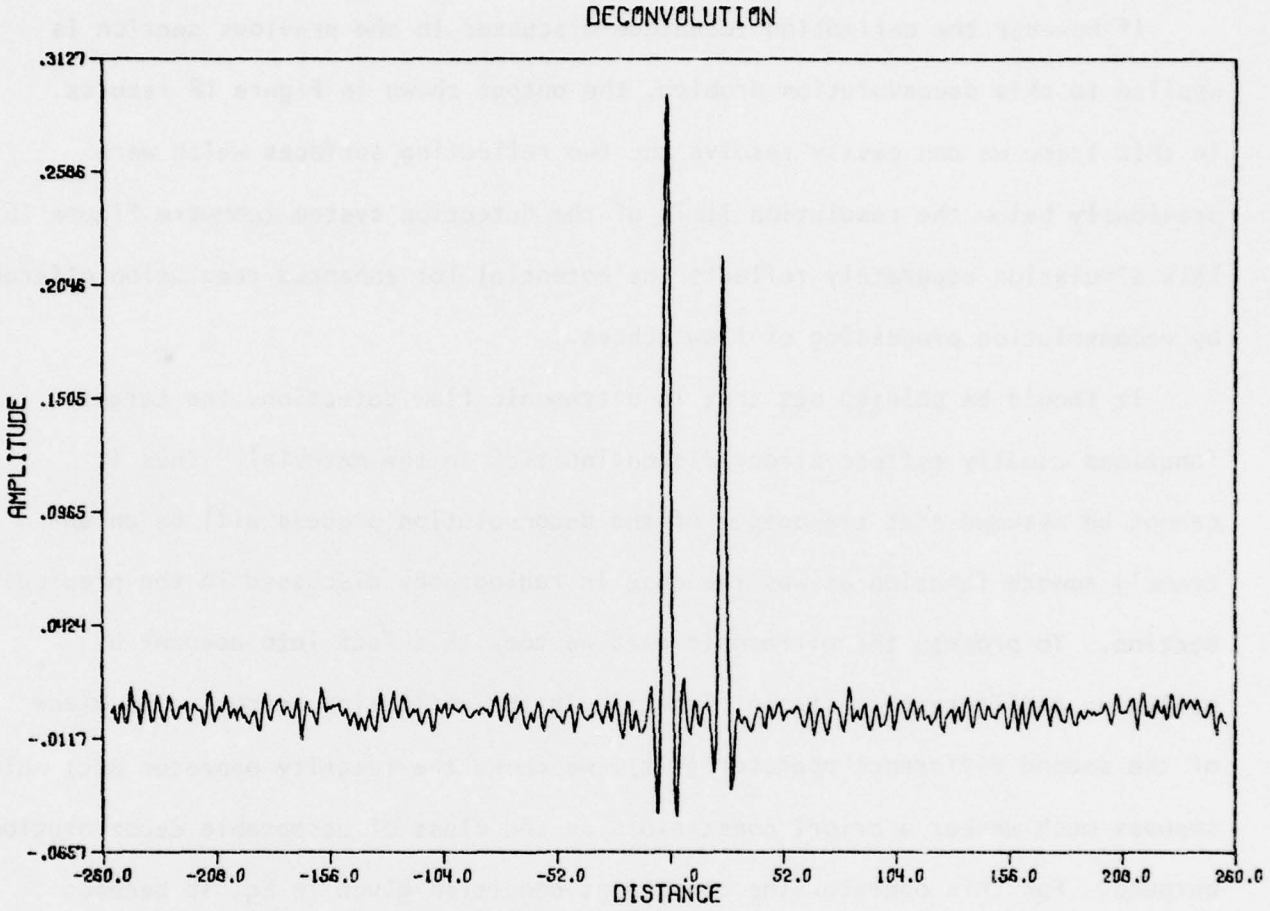

Figure 18. Constrained Deconvolution of Figure 16 by Optimization of Smoothing Function Using the Impulse Response of Figure 15.

present in the deconvolved output are typical of all attempts to apply straight forward deconvolution to real experimental measurements.

If however the estimation technique discussed in the previous section is applied to this deconvolution problem, the output shown in Figure 18 results. In this trace we can easily resolve the two reflecting surfaces which were previously below the resolution limit of the detection system (compare Figure 16). This simulation accurately reflects the potential for enhanced resolution offered by deconvolution processing of flaw echoes.

It should be pointed out that in ultrasonic flaw detection, the target functions usually reflect strong discontinuities in the material. Thus it cannot be assumed that the output of the deconvolution process will be an extremely smooth function as was the case in radiography discussed in the previous section. To process the ultrasonic data we took this fact into account by utilizing a different constraint function in the estimation process. In place of the second difference operator $\delta''(t)$, we chose the identity operator $\delta(t)$ which imposes much weaker a priori constraints on the class of acceptable deconvolution outputs. For this operator the constraint condition given in Eq. 18 becomes

$$\int_{-\infty}^{\infty} [c(t) * \hat{x}_s(t)]^2 dt = \int_{-\infty}^{\infty} \hat{x}_s^2(t) dt = \min_{\hat{x} \in S} \{ \int_{-\infty}^{\infty} \hat{x}^2(t) dt \} \qquad (26)$$

This constraint operator selects the output $\hat{x}_s(t)$ from the set S of all possible solutions which has the minimum energy instead of maximum smoothness in the sense of the second difference operator.

Figures 19 through 24 represent the application of this technique to experimental data obtained from a series of aluminum blocks containing steps of varying height. In the first of these plots, Figure 19, we see the actual output of the

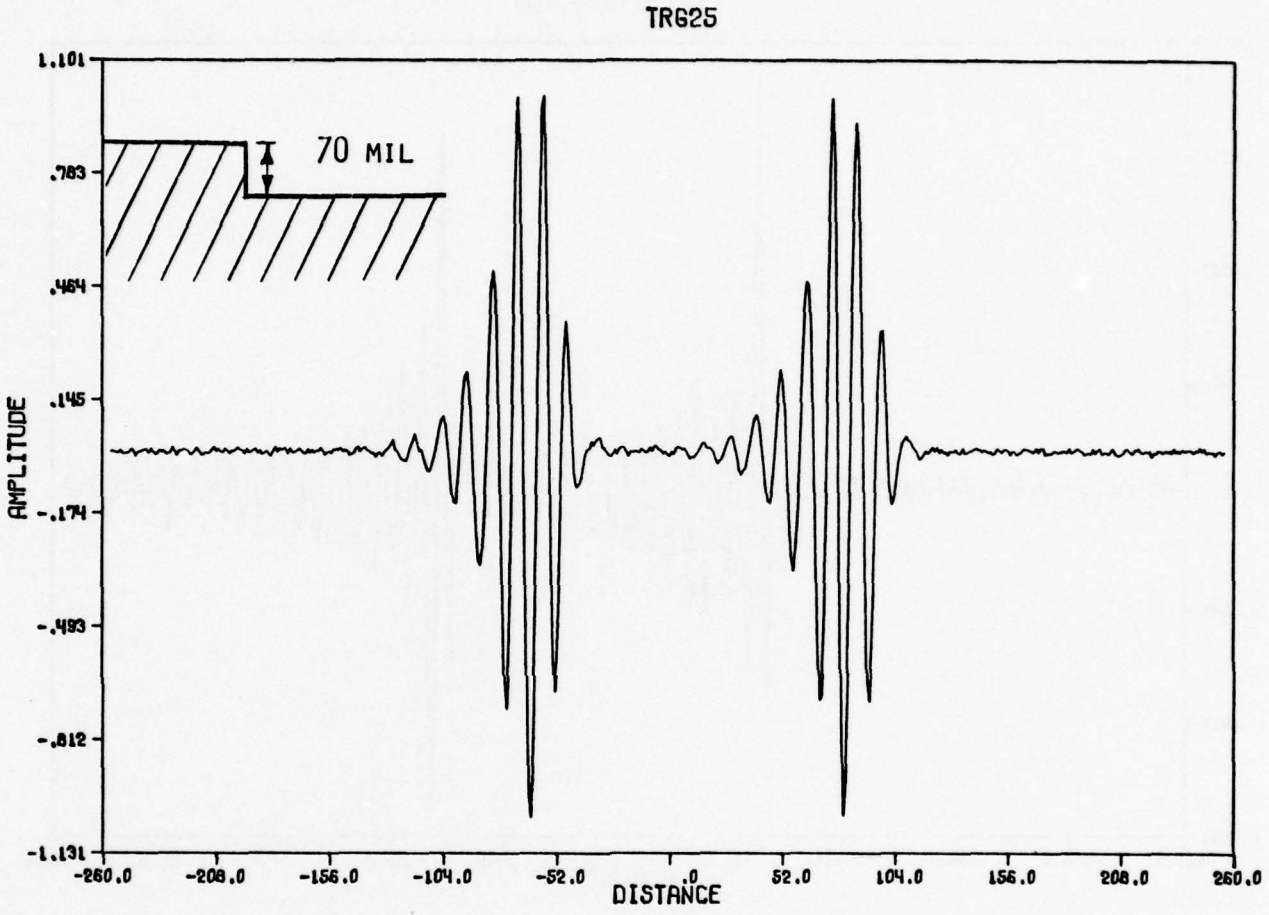

Figure 19. Actual System Output of a Plane Surface Aluminum Target Containing a 70 Mil Step and Assumed to be Parallel to the Face of the Transducer.

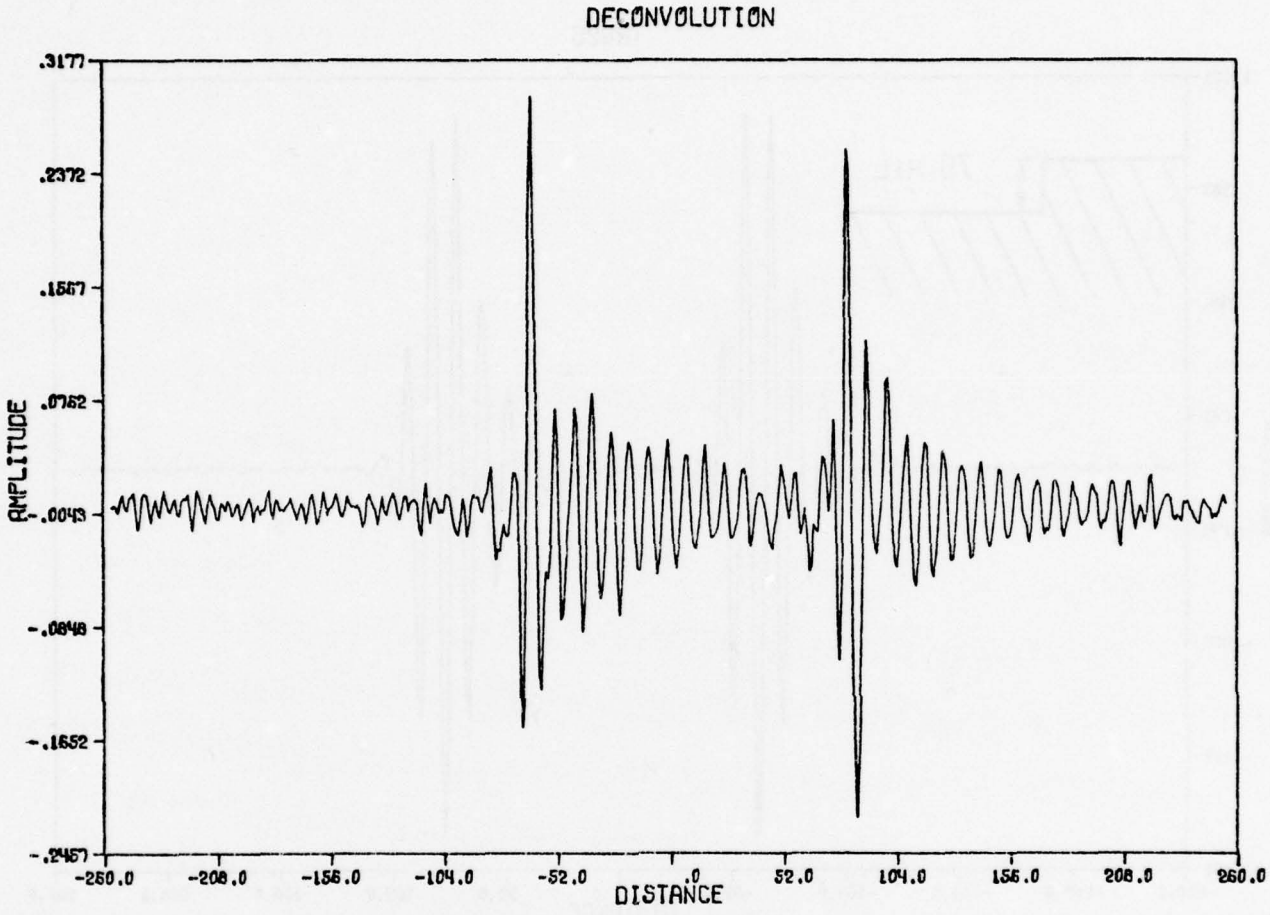

Figure 20. Constrained Deconvolution of Figure 19 Showing Locations of the Two Plane Reflectors. The Damped Oscillations Suggest that the Reference Target was at a Greater Angle to the Face of the Transducer than the Stepped Target.

random signal detection system produced by a 70 mil step. From this trace the location of the two reflecting surfaces can easily and accurately be determined. The constrained deconvolution of this output trace is displayed in Figure 20. Examining the deconvolved output we observe that the effective resolution of the system has been significantly increased. In addition, this plot also displays some unexpected oscillations about each of the deconvolved targets. As we will show later these oscillations provide information about the target orientation which could not possibly be deduced directly from the system output itself.

Figure 21 shows the system output obtained from a second aluminum block which contains a step whose height is much nearer the resolution limit of the flaw detection system. The constrained deconvolution of this output trace, displayed in Figure 22, again demonstrates the enhanced resolution offered by this processing technique.

Finally, Figure 23 presents the output due to a step whose height equals the resolution limit of the detection system. From this trace the height of the step cannot accurately be determined. However, after deconvolution processing, the locations of both reflectors are easily determined as shown in Figure 24.

The last two figures of this section are computer simulations of the system output that is expected when the orientation of the target is slightly altered. Note that in Figures 25 and 26 changing the orientation from a tilt angle of 2° to 3° causes a significant change in both the frequency and damping factor of the oscillations appearing around the deconvolved signal. We believe that this effect will allow us to extract orientation information about the target not available from the unprocessed system output in addition to the previously demonstrated increase in effective system resolution.

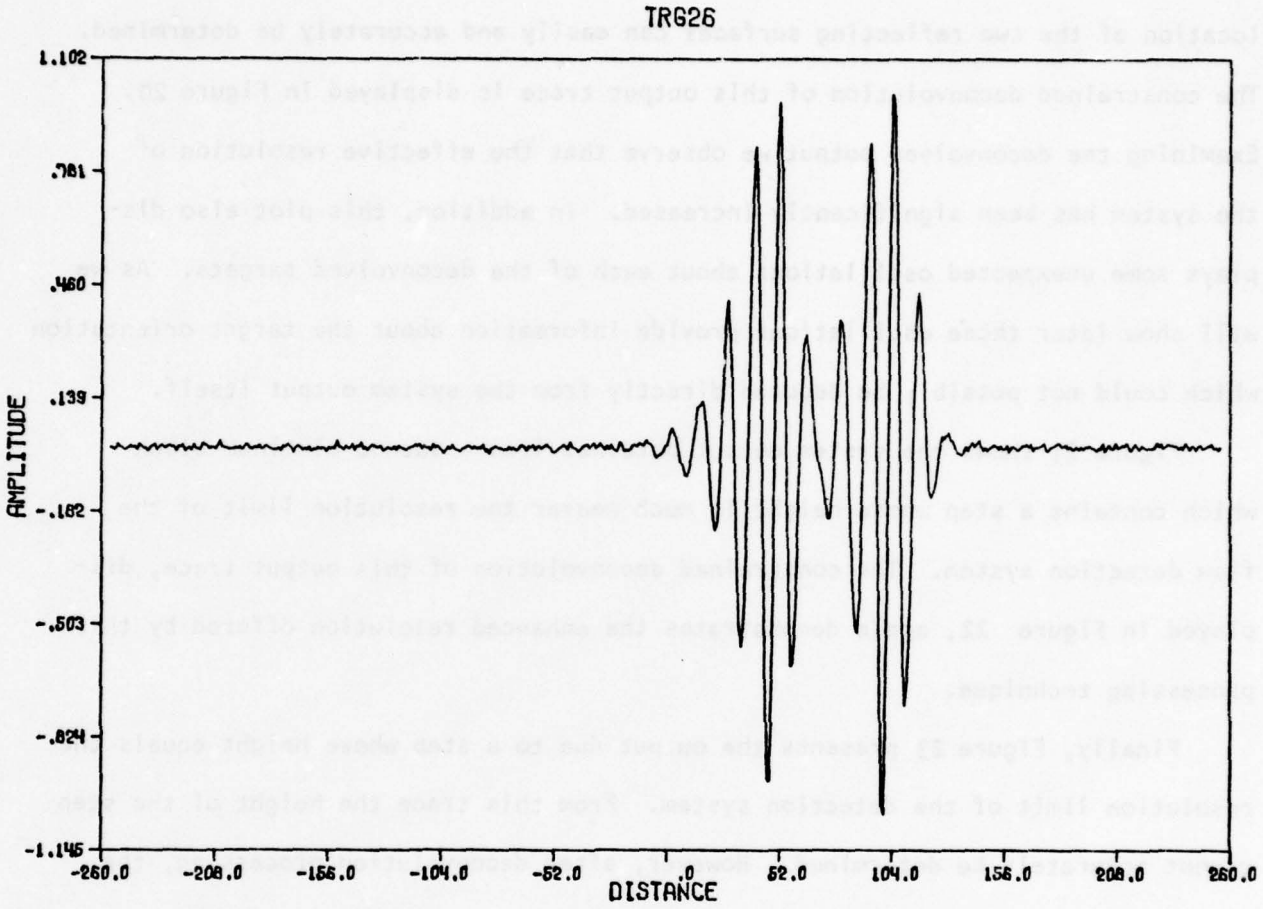

Figure 21. Actual System Output of a Plane Surface Aluminum Target, Containing a 24 Mil Step and Assumed to be Parallel to the Face of the Transducer.

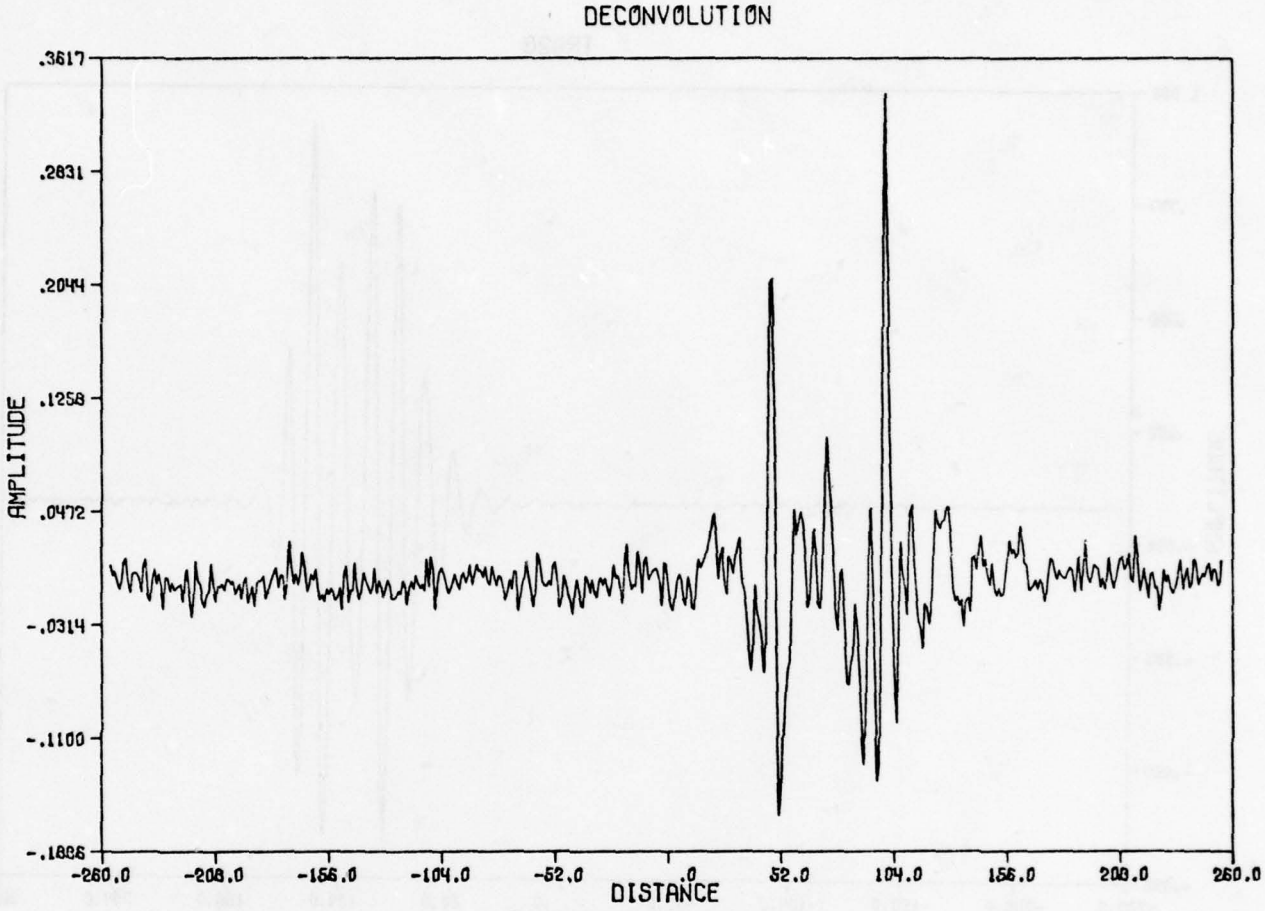

Figure 22. Constrained Deconvolution of Figure 21 Showing Locations of the Two Plane Reflectors and Suggesting that the Stepped Target and the Reference Target are at Approximately the Same Angle to the Face of the Transducer.

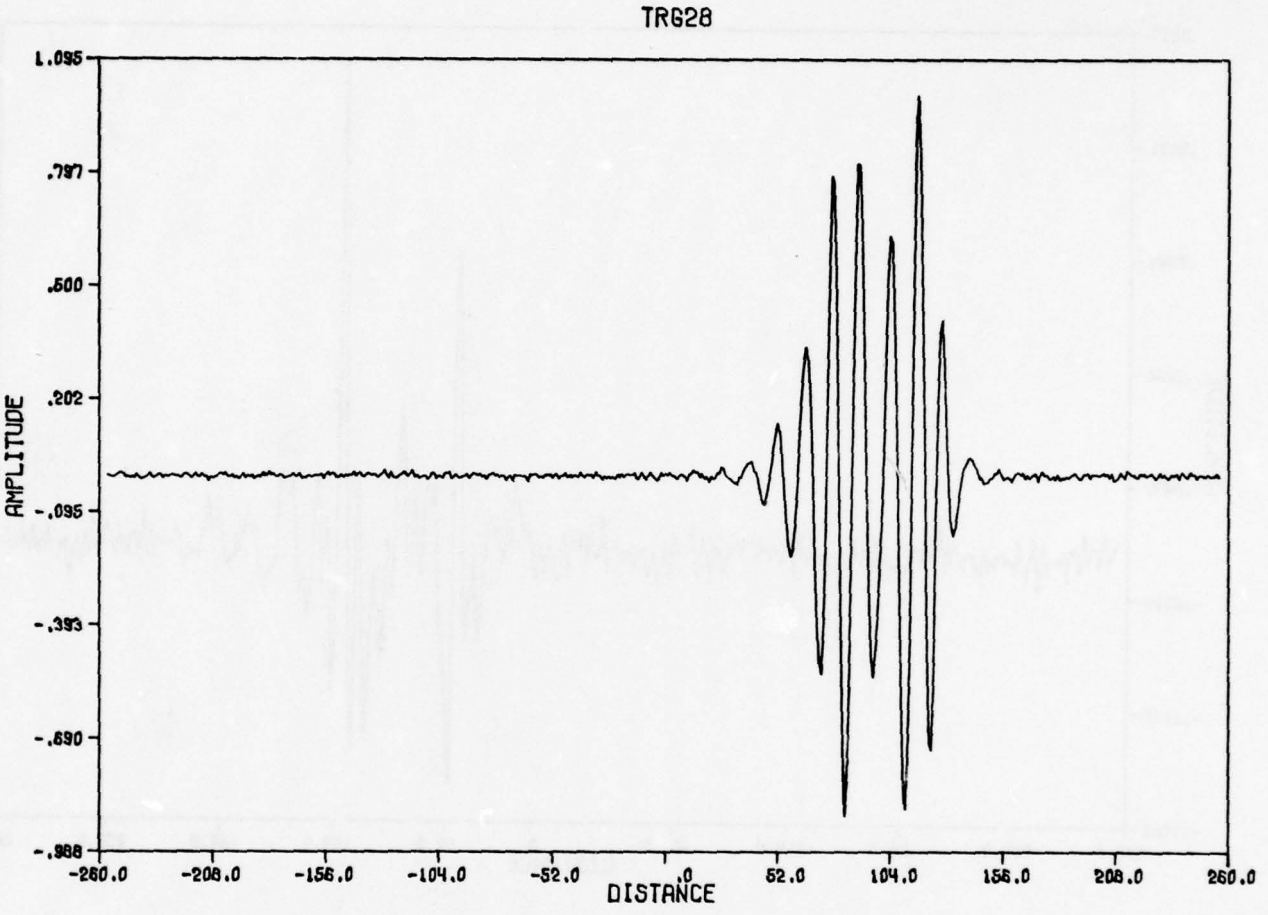

Figure 23. Actual System Output of a Plane Surface Aluminum Target Containing a 15 Mil Step and Assumed to be Parallel to the Face of the Transducer.

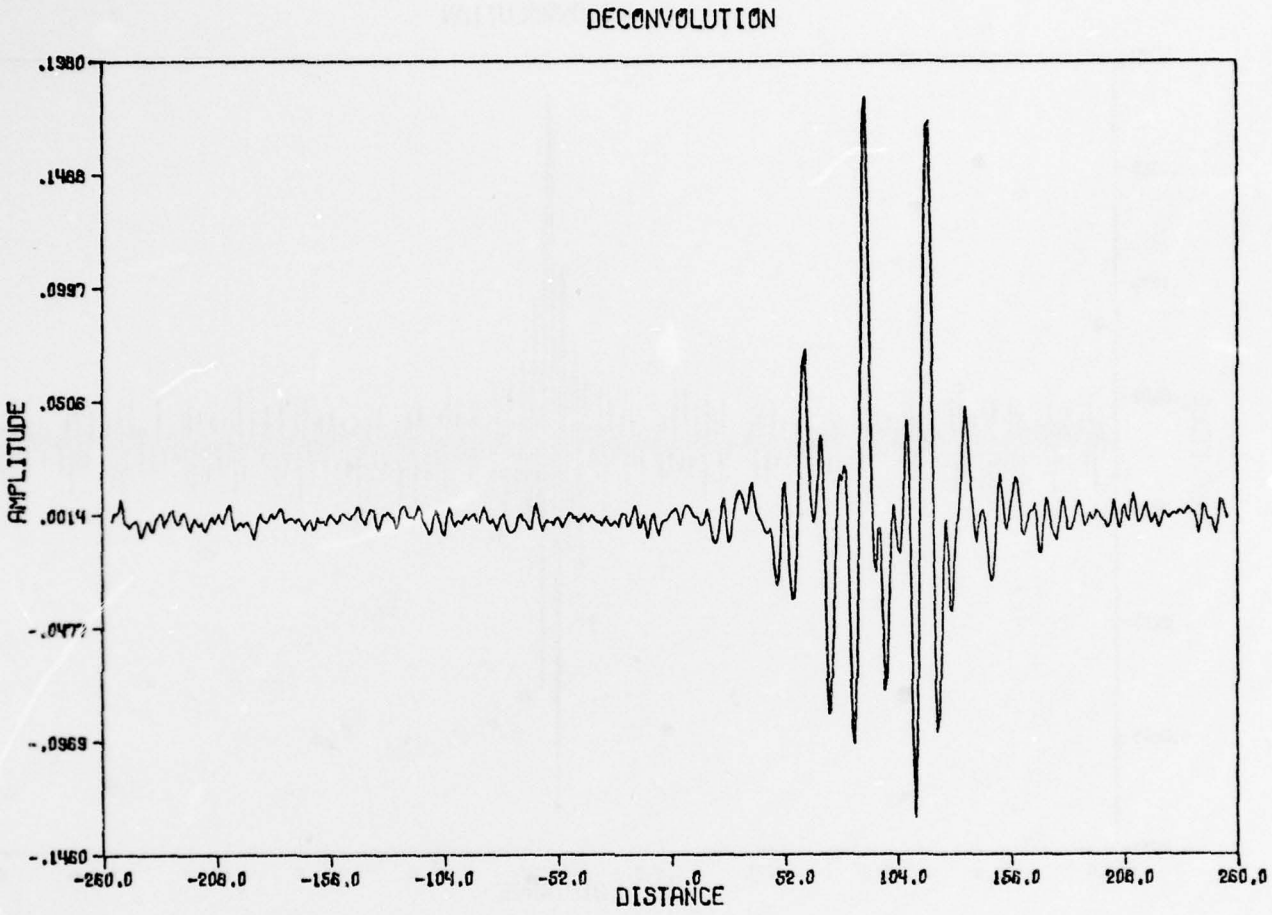

Figure 24. Constrained Deconvolution of Figure 23 Showing Locations of the Two Plane Reflectors and Indicating that the Stepped Target and the Reference Target are at Approximately the Same Angle.

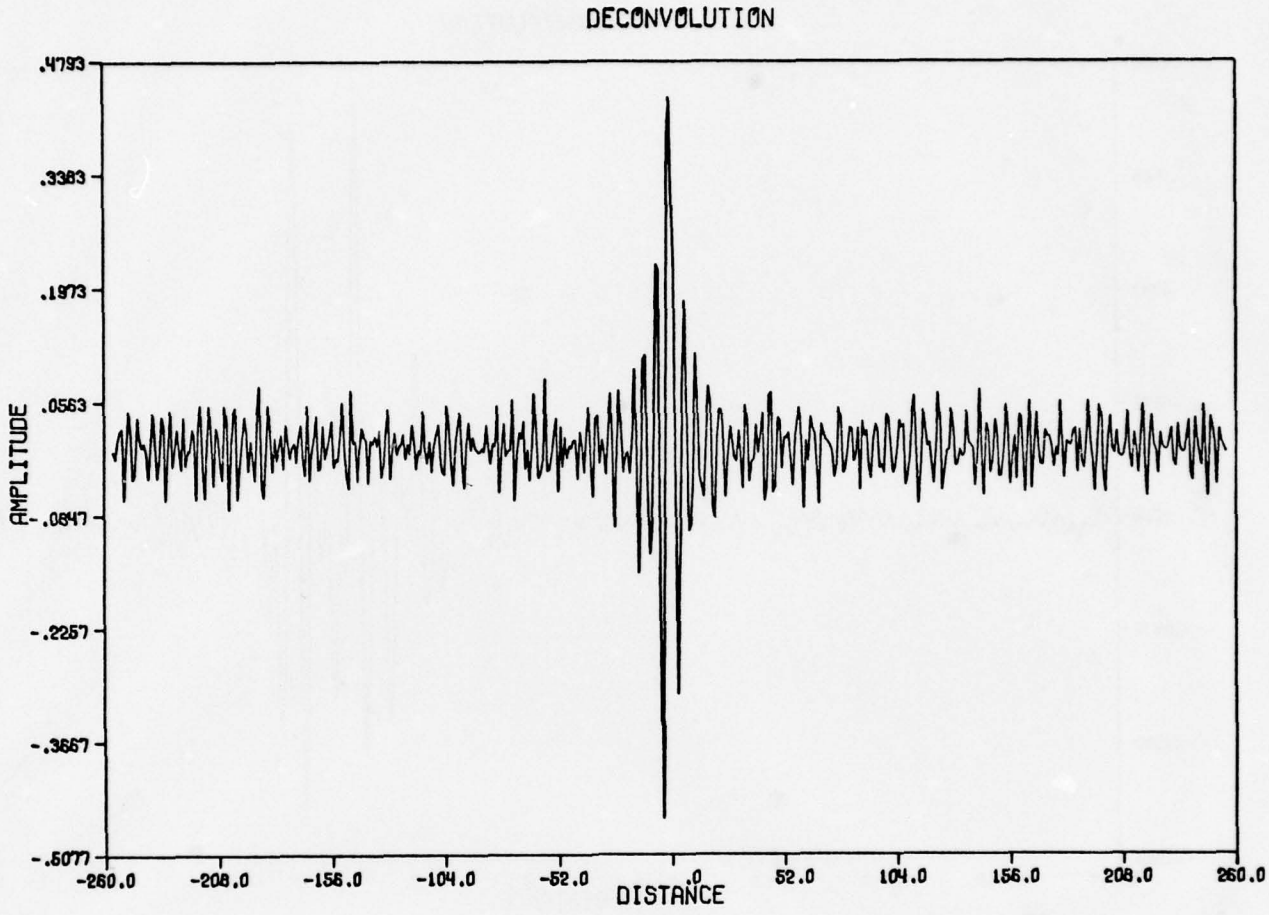

Figure 25. Constrained Deconvolution of a Simulated System Output From a Plane Target that is Parallel to the Face of the Transducer and Using an Impulse Response from a Plane Target That is Tilted 2° to the Face of the Transducer.

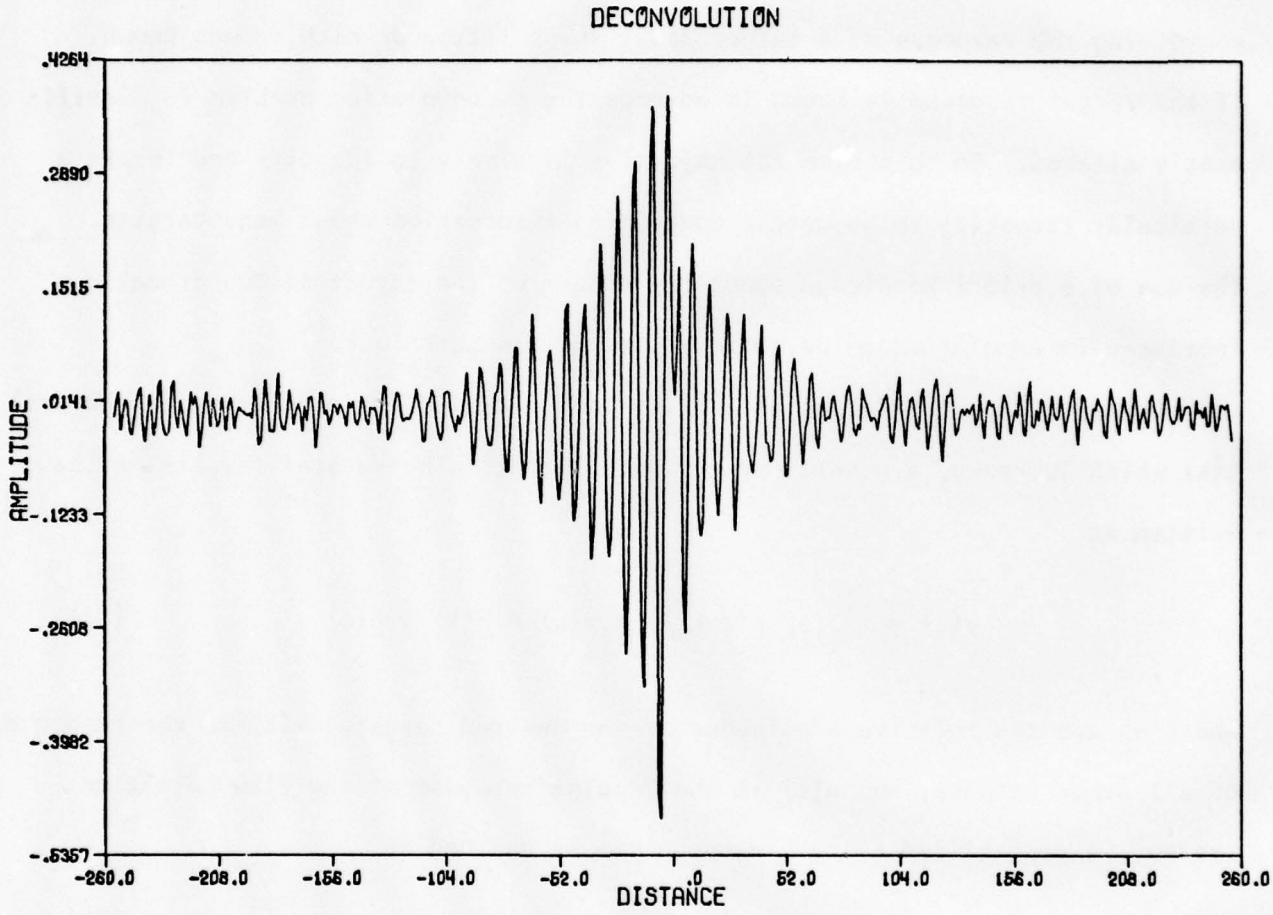

Figure 26. Constrained Deconvolution of a Simulated System Output Containing a Plane Target that is Parallel to the Face of the Transducer and Using an Impulse Response from a Plane Target That is Tilted 3° to the Face of the Transducer.

3. Flaw Signature Processing

The previous section presented a general approach to the problem of deconvolving the response of a target about which little or nothing was known. If the target response is known in advance the deconvolution problem is significantly altered. In this case the objective is simply to identify and locate a particular target(s) in an output containing information about many targets. The use of a priori knowledge about the nature of the target allows dramatic increases in resolution to be achieved using this technique.[14]

Assuming that the target of interest has a reflectivity function (signature) g(t) which is known, a general system output containing several targets may be written as

$$y(t) = \{[\sum_k \alpha_k\, g(t-t_k)] + x(t)\} * h(t) + n(t) \qquad (27)$$

where α_k are the relative amplitudes of the desired targets, x(t) is the response of all other targets, and h(t) is the impulse response of the flaw detection system. A generalized system response can be defined as

$$\tilde{h}(t) = g(t) * h(t) \qquad (28)$$

to combine the actual measurable system response h(t) and the response of the particular targets g(t) that we wish to locate. Thus all the information about the desired targets is now contained in the new function $\tilde{h}(t)$ which is also experimentally measurable. In terms of the generalized system response the output can be rewritten as

$$\hat{y}(t) = [\sum_k \alpha_k \delta(t-t_k)] * \tilde{h}(t) + [x(t) * h(t) + n(t)] \qquad (29)$$

Thus the deconvolution problem has been reduced to identifying delta functions in the output.

A processing method that we have used with some success begins as straight forward deconvolution by forming the following ratio of Fourier transforms

$$\frac{\hat{Y}(\omega)}{\tilde{H}(\omega)} = \sum_k \alpha_k e^{-j\omega t_k} + \frac{X(\omega)H(\omega) + N(\omega)}{\tilde{H}(\omega)} \qquad (30)$$

In this ratio each of the desired targets is represented by a complex exponential whose frequency is proportional to the location of the target. To identify the complex exponentials, the real and imaginary parts of this ratio are examined simultaneously using a pattern recognition routine to locate the cosine and sine terms corresponding to the complex exponentials. After the largest complex exponential terms have been identified, the function in Eq. 30 is altered in such a way that the exponential terms remain unaltered while the remaining terms in the expression are suppressed. Finally the function resulting from this nonlinear process is inverse transformed to yield the deconvolution output.

Figures 27 through 30 demonstrate the capability of this processing technique to enhance the effective resolution of a detection system. The first step in the application of this deconvolution scheme is to determine the generalized system response for the particular target of interest. Using the random signal flaw detection system, the response of a single plane aluminum surface was experimentally measured and is shown in Figure 27. Also shown in this figure is the Fourier transform, or amplitude spectrum, of the target.

The upper trace of Figure 28 shows the system output when the target is a 24 mil step in an aluminum block. The result of deconvolving this signal with the impulse response shown in the previous figure is displayed in the lower trace of Figure 28. The width of the peaks seen in the deconvolved output is approximately 0.5 mil. Since this linear version of the random signal detection system has previously been shown to have a resolution limit of approximately 15 mils,

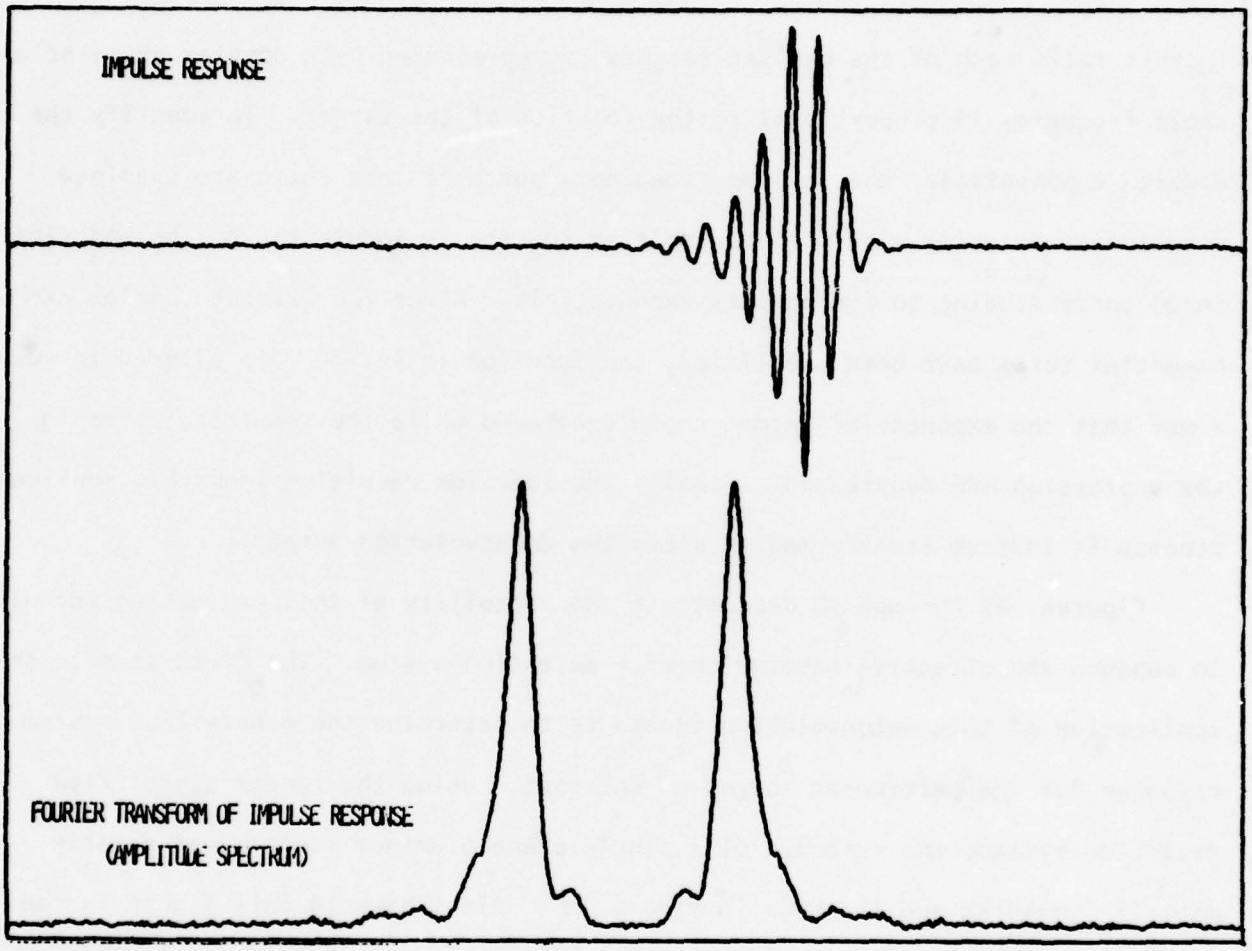

Figure 27. Actual System Impulse Response Taken from a Plane Surface Aluminum Target Showing the Amplitude Spectrum of the Fourier Transform.

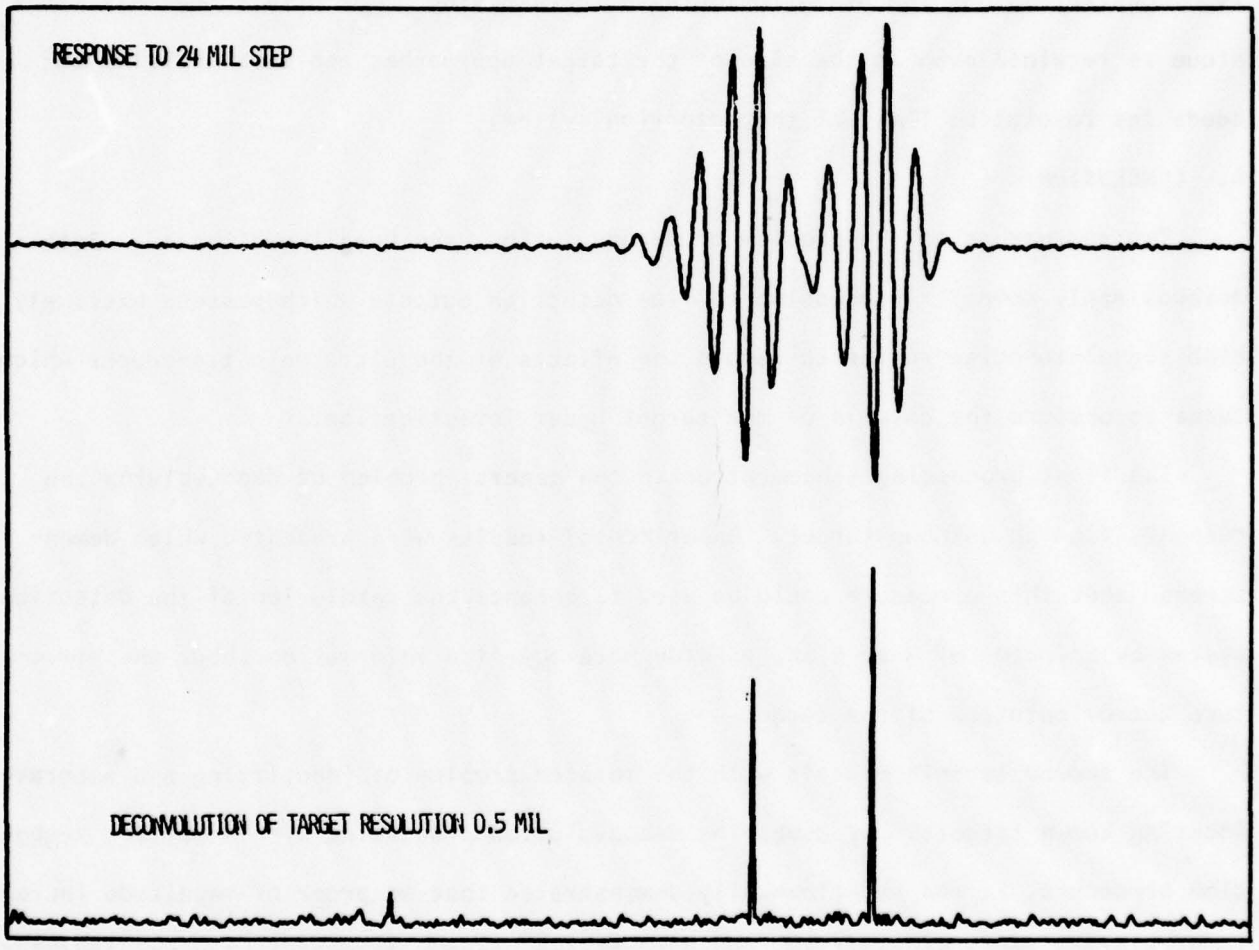

Figure 28. Actual System Output of a Plane Surface Aluminum Target Containing a 24 Mil Step Which is the Same as Figure 21 and Also Shows the Pattern Recognition Deconvolution of the Stepped Target Using the Impulse Response of Figure 27.

the deconvolution process has effectively increased the resolution of the system by at least an order of magnitude.

Figures 29 and 30 show the experimentally measured output corresponding to steps of height 15 mils and 5 mils respectively. The deconvolution of these outputs clearly demonstrates that the dramatic increase in resolving power offered by this technique is retained even as the size of the target approaches and substantially exceeds the resolution limit of the detection system.

4. CONCLUSION

Two approaches to the problem of deconvolution have been investigated. Both methods apply computer processing to flaw detection outputs which possess extremely high signal-to-noise ratios to remove the effects of the ultrasonic transducer which tends to obscure the details of the target under investigation.

The first processing scheme attacked the general problem of deconvolving the response from an unknown target. Experimental results were presented which demonstrated that this procedure could be used to enhance the resolution of the detection system by a factor of 3 to 5 and provide more detailed information about the structure and orientation of the target.

The second technique dealt with the related problem of identifying and accurately locating known targets. By combining deconvolution processing with a pattern recognition procedure, it was experimentally demonstrated that an order of magnitude increase in resolution could be realized. When examining unknown targets it may be possible to use the first technique to identify the target structure. This information can then be used with the second technique to provide optimum target resolution.

Another possible application of the pattern recognition deconvolution procedure is in conjunction with a library of flaw signatures. This should make it possible to characterize flaw type as well as enhance resolution. It should be stressed that both of the above deconvolution procedures are most effective when used on the outputs of a system providing considerable initial signal-to-noise ratio enhancement to the flaw echo signal, such as the random signal flaw detection system. The output signal-to-noise ratio will inevitably be worse than that of the input (see for instance Fig. 28 which a small spike in a region free of input echoes). Thus these techniques although capable of improving the resolution of two targets of similar size, are not suitable for improving the visibility of small targets which are very close to much stronger reflecting targets such as surfaces.

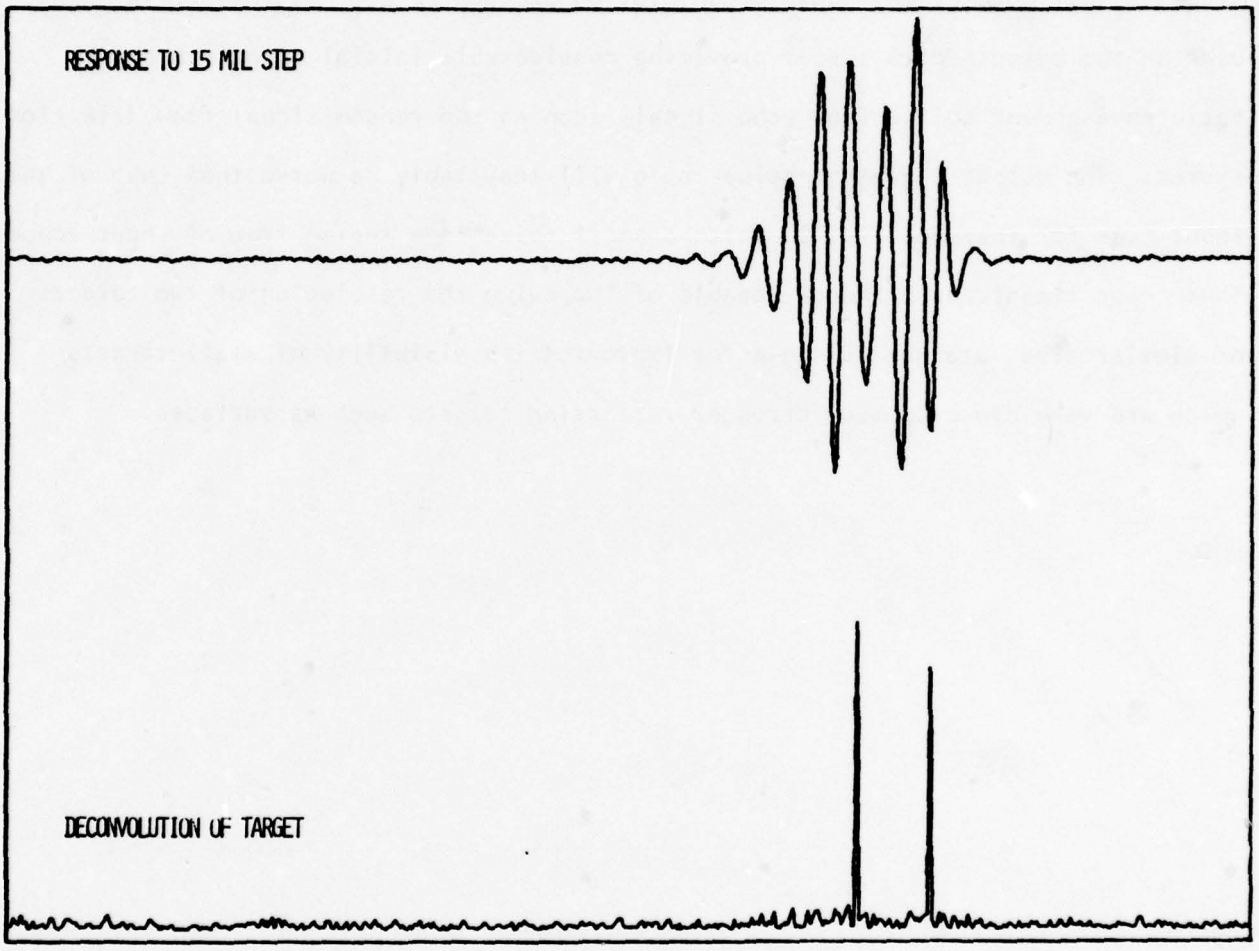

Figure 29. Actual System Output of a Plane Surface Aluminum Target Containing a 15 Mil Step, Which is the Same as Figure 23, and Also Shows the Pattern Recognition Deconvolution of the Stepped Target Using the Impulse Response of Figure 27.

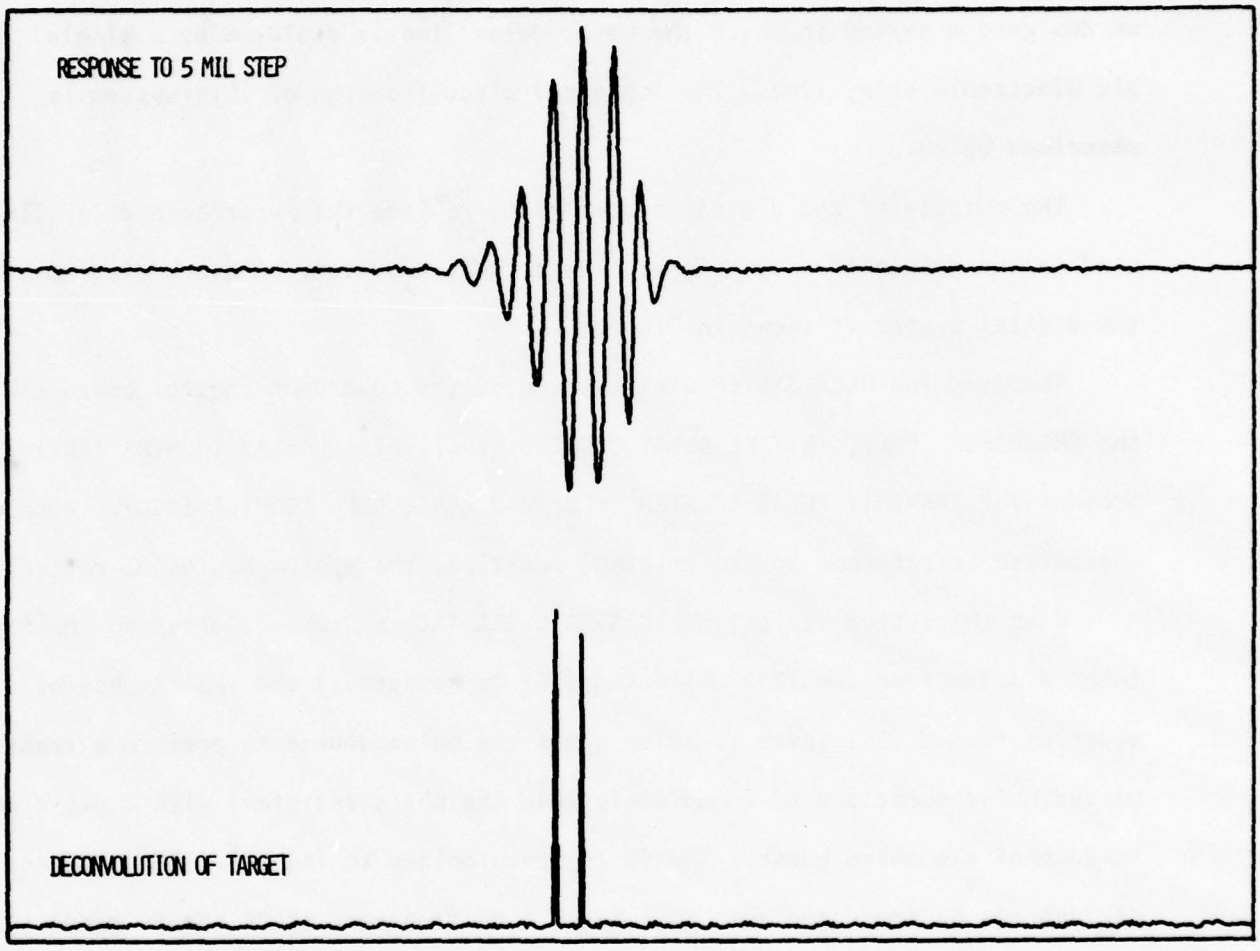

Figure 30. Actual System Output of a Plane Surface Aluminum Target Containing a 5 Mil Step and Also Shows the Pattern Recognition Deconvolution of the Stepped Target Using the Impulse Response of Figure 27.

SECTION VII

ELECTRONIC DELAY LINE SYSTEM

Our original random signal correlation system used a water delay line consisting of two transducers separated by a water path. As part of this project we designed a system in which the water delay line is replaced by a single bit electronic delay line. The logic and circuit design of this system is described below.

The purpose of the digital system is to replace the water-bath delay line used in the original random signal flaw detection system. A block diagram of the digital system is shown in Figure 31.

Throwing the USER SYSTEM START switch on the Load/dump control board clears the PRESCALER (PRE), INITIAL DELAY COUNTER (IDC), FINAL DELAY COUNTER (FDC) and presets the TRANSMIT PULSE COUNTER (TPC) and RANGE CELL COUNTER (RCC). When the switch is returned to its original position, the system begins operation.

When the system starts, the MASTER CLOCK (MC) pulses are gated to the PRE (when a pulse from the TRANSMIT CLOCK (TC) is detected,) and the PRE begins counting them. [This same TC pulse gates the noise source to produce a transmitted noise burst and to immediately load the shift registers with a digitized version of the noise burst. The TC is synchronized to the MC]. This counter divides the MC frequency down to 1 MHz. A MC frequency of 25 MHz is used, therefore, the PRE passes one out of every 25 MC pulses. The output of the PRE, the carry clock, provides the clock signal for the IDC at a frequency of 1 MHz. The IDC counts the PRE carry clock pulses until it counts NNN of them, where NNN is a user supplied number between 1 and 999 which constitutes the initial delay in microsecs. When the IDC has counted NNN pulses, or NNN μsecs after the original TC pulse, it produces a reset pulse which starts the FDC.

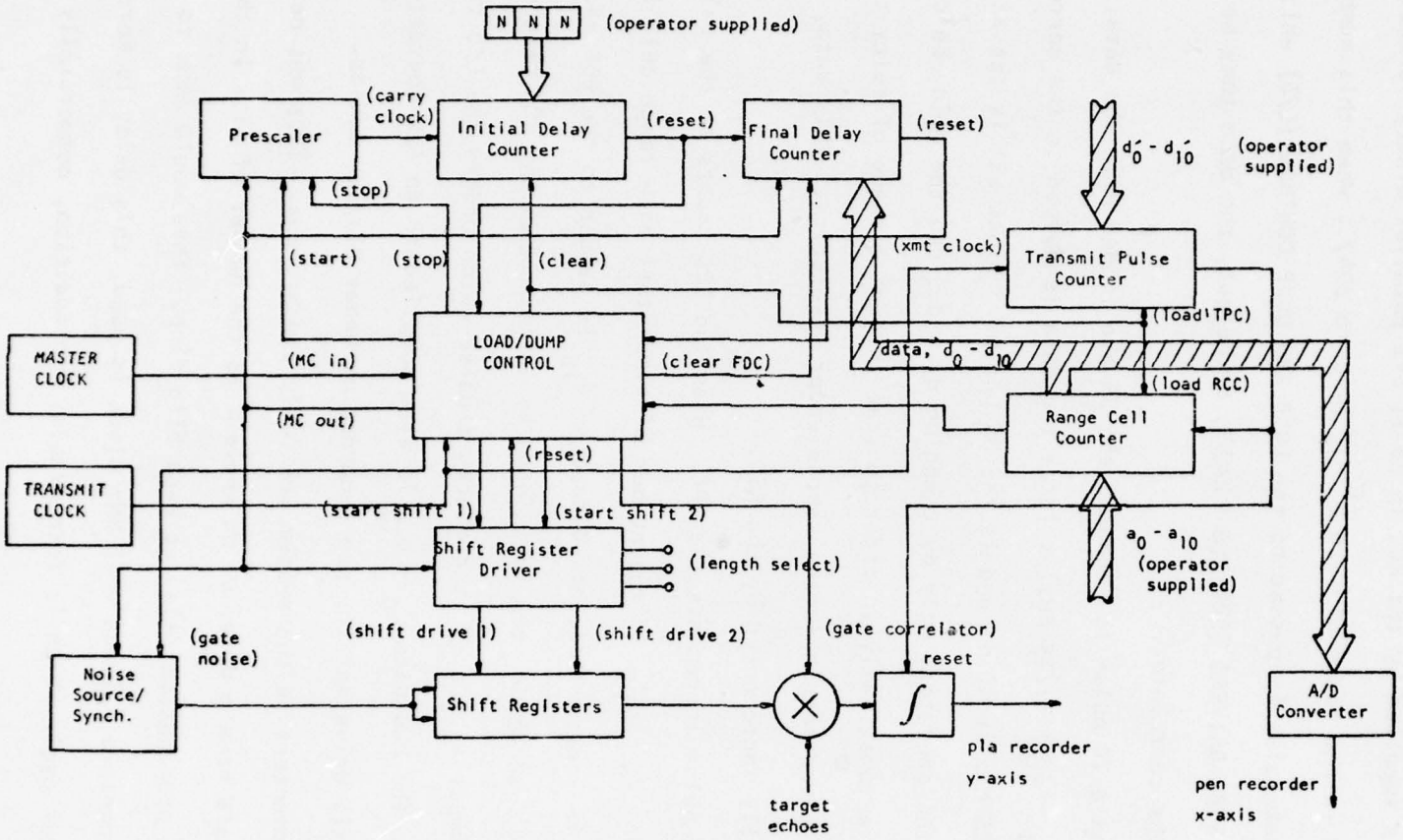

Figure 31. Electronic Delay Line System

The FDC begins to count MC pulses and counts until it reaches a certain number which is supplied by the RCC in an 11 bit parallel binary format. This number will be in the range of 1 to $2^{12}-1$, or 0 to 2047. When this number is reached, a reset pulse is passed to the LOAD AND DUMP CONTROL (L/D) which commands the SHIFT REGISTER DRIVERS (SRD) to "dump", or output, the data they have been holding into the correlator.

Thus, when a TC pulse is produced the SR are loaded with the data, and (NNN μs) + (d_0 - d_{10}) (1/25 MHz)μs later the data is dumped to the correlator. The factor 1/25 MHz is 40 ns and is the MC period. Since NNN is set at the beginning by the operator, only by changing d_0 - d_{10} can the delay be changed by the system automatically in order to scan through a range of relay times, or, in essence, a given length in the sample under inspection. This data, d_0 - d_{10}, is automatically incremented by the RCC.

Every TC pulse increments the TPC. When the TPC counts to the value programmed number, d_0' - d_{10}', is the number of times that each range cell is integrated. When the RCC is incremented, new data d_0 - d_{10} is passed to the FDC and the total delay from SR load to SR dump is changed by 40 ns. When the RCC reaches the preprogrammed number a_0 - a_{10}, it produces a pulse which orders the L/D to shut the system down. The RCC data d_0 - d_{10} is also supplied to an A/D converter to produce the x-axis drive for the pen recorder or other display device.

Three counters in the system are fully synchronous. This was necessary since ripple counters have a delay of nt where n is the number of bits in the counter and t is the propagation delay at each flip flop. This would come to 44 ns for the larger counters. Since a 25 MHz clock is used, this delay is more than a complete clock cycle which is intolerable. In addition, commercially packaged non-

synchronous counters operating at these frequencies (i.e., the 74S163) have a propagation delay on the order of 25 ns, which is also intolerable, being more than the width of a clock pulse. With the counters used, delay from clock to any Q output is that of one flip flop: about 4 ns for the 74S112 flip flops used. (All logic is Schottkey).

As noted earlier, the PRE is programmable, but it is normally programmed once the clock frequency is chosen and then never changed. Programming is done by entering the number N-1 in binary on the inputs of the 8-in NAND gate. N is the desired division ratio. A "one" is the Q output of the appropriate flip flop and a "zero" is ground. When the prescaler reaches count N-1, it presets to an all ones state rather than an all zeroes state, thus making up the additional count. This was easier to implement in the hardware.

Decoding of states in the IDC and FDC is done in the same manner. Each Q output is compared to its respective input with the X OR gates. When all Q outputs disagree with all the input data, the counter is cleared either with on board logic (IDC) or logic found in the LID (FDC). Obviously then, the counters are programmed with the ones complement of the desired data.

The TPC and RCC are located on the same board and utilize commercial non-synchronous standard TTL chip counters since they are operating at the TC frequency, typically a few KHz. These chips have built in preset capability which facilitates programming. The chips are actually programmed to the ones complement of the desired maximum count and then up-counted to an all ones state. The total number of pulses counted is then correct, but in the case of the RCC, where the outputs are needed elsewhere, (the FDC), the data is in ones complement. Fortunately, however, the FDC needs data in ones complement, thus inverters are not required. This method alleviated many hardware complexities. The RCC, as

a result, counts from maximum range to minimum range, which may at first seem "backward".

The SRD is a counter which can count in binary modulo-64, 128, 192, or 256, depending on the length select option chosen by the operator. It outputs the selected number of MC pulses to the shift registers at the proper time, as commanded by the L/D. There is a single reset out whether the driver is loading or dumping and whether it is operating on register one or two. The proper function is known in advance by the L/D.

The L/D contains master sequencing circuitry. Circuitry is included to prevent an attempt to load a pulse into the shift registers when they are already both full. A delay of four MC cycles after the TC pulse and before the load command to the shift registers is also included, so that the initial transient, identical for every burst, is not loaded into the registers.

The noise is digitized by the Schmidt trigger into a two level code and is then synchronized with the MC before being loaded into the shift registers. This done to satisfy the set-up time requirements of the shift register chips. The shift registers are simply 8 bit TTL chips (7491), 32 of them, strung together.

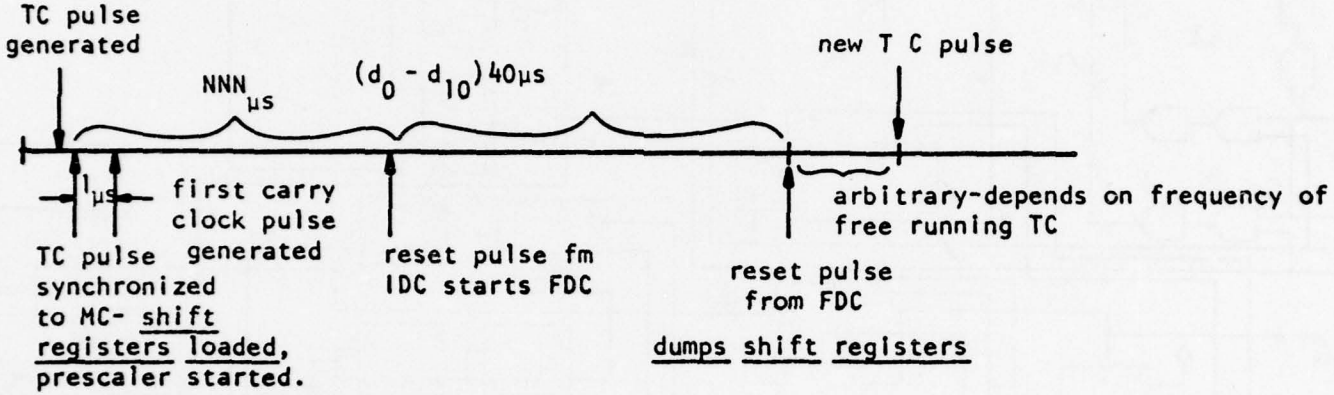

Figure 32. Signal Format

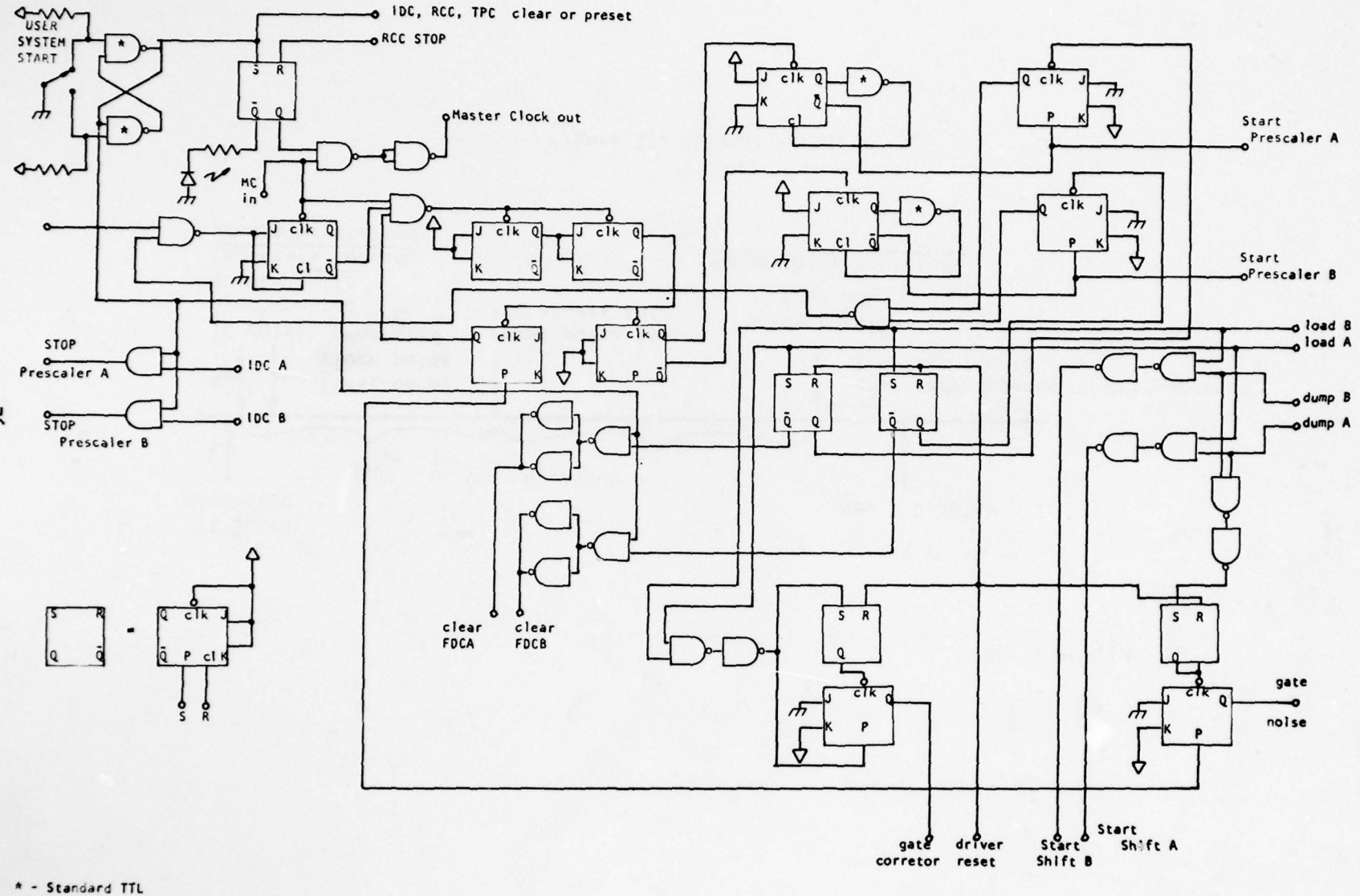

Figure 33. Load/Dump Control

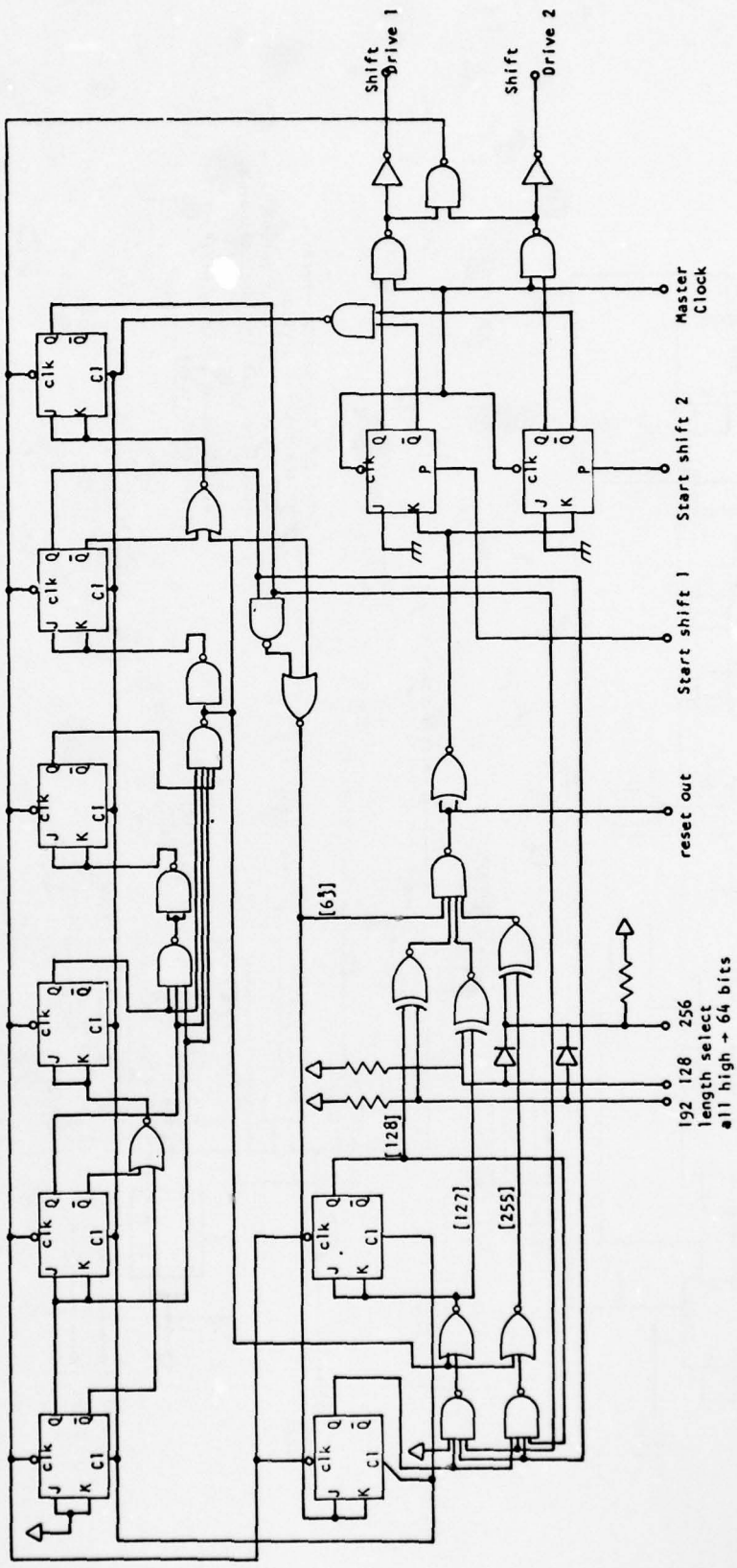

Figure 34. Shift Register Drivers

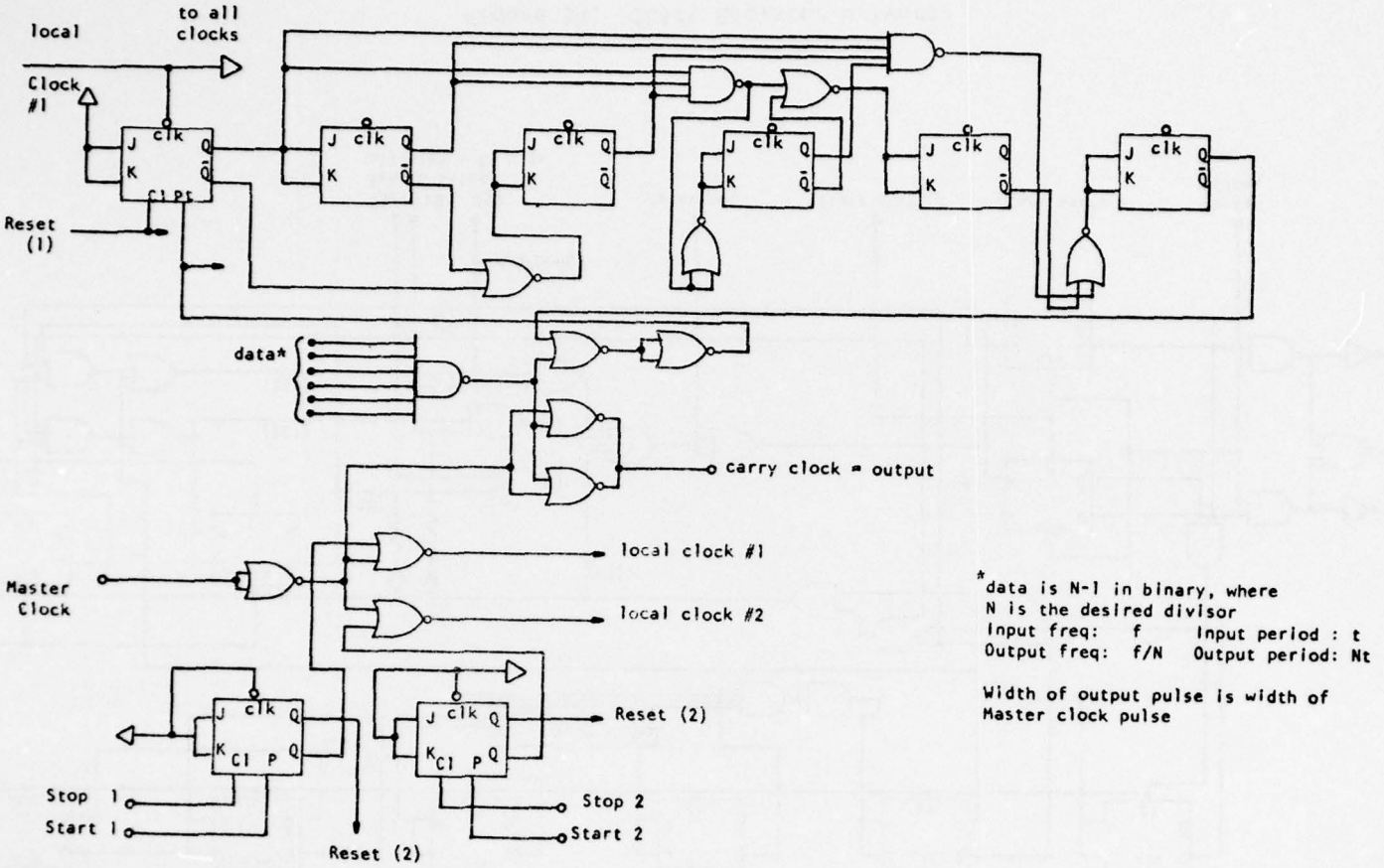

Figure 35. Prescaler

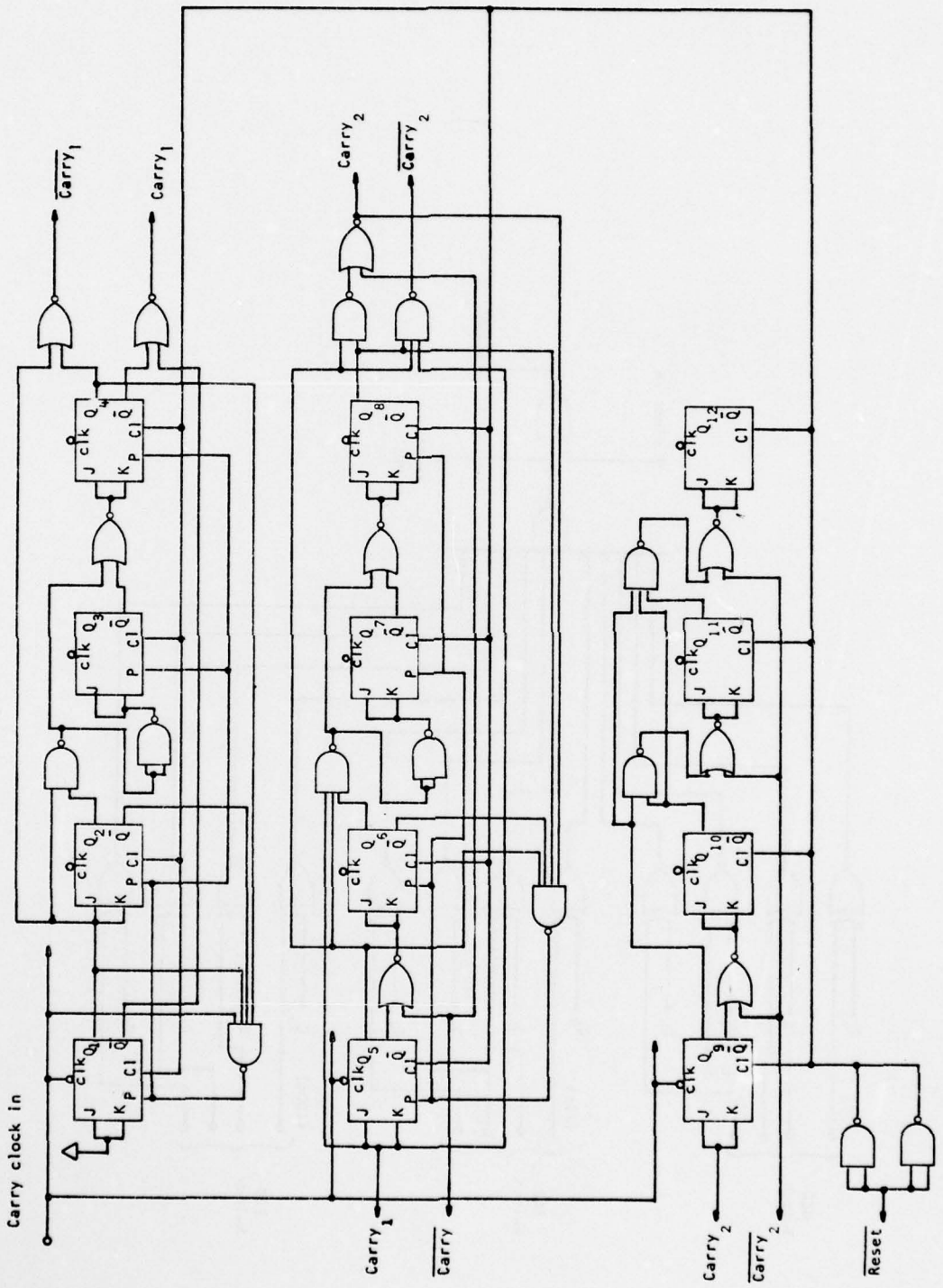

Figure 36. Initial Delay Counter -- 3 Decades

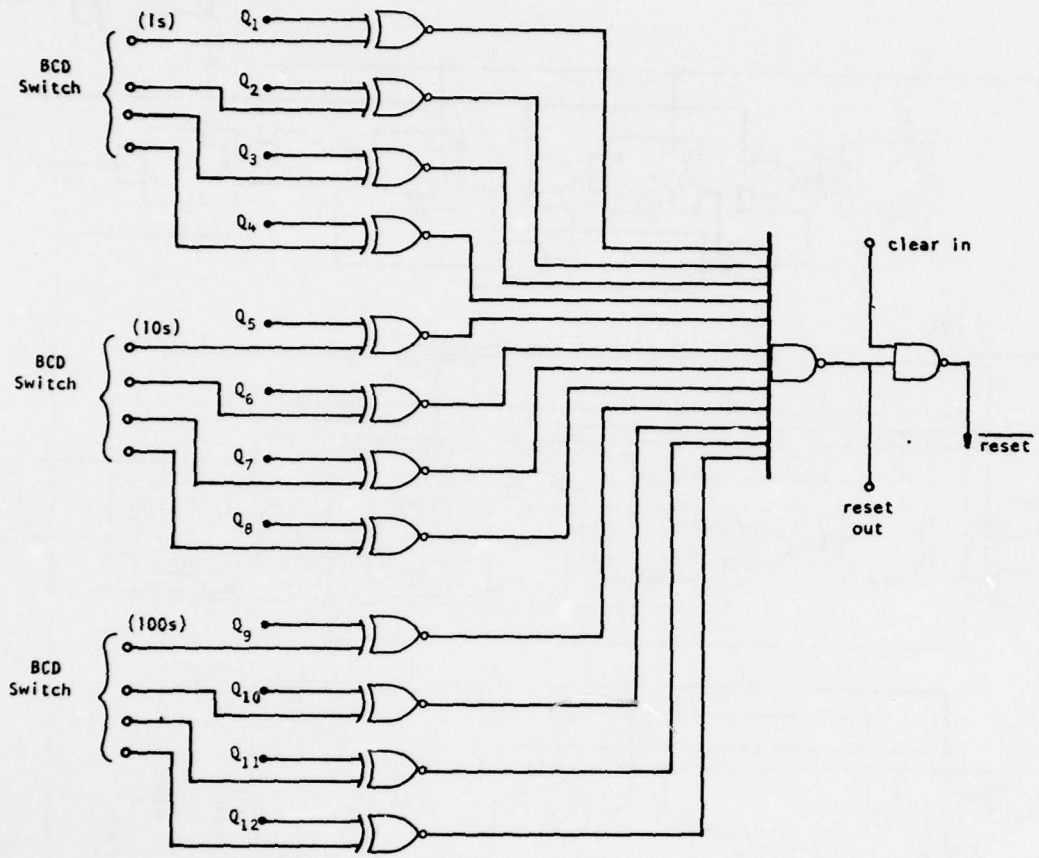

Figure 37. Initial Delay Counter (Continued)

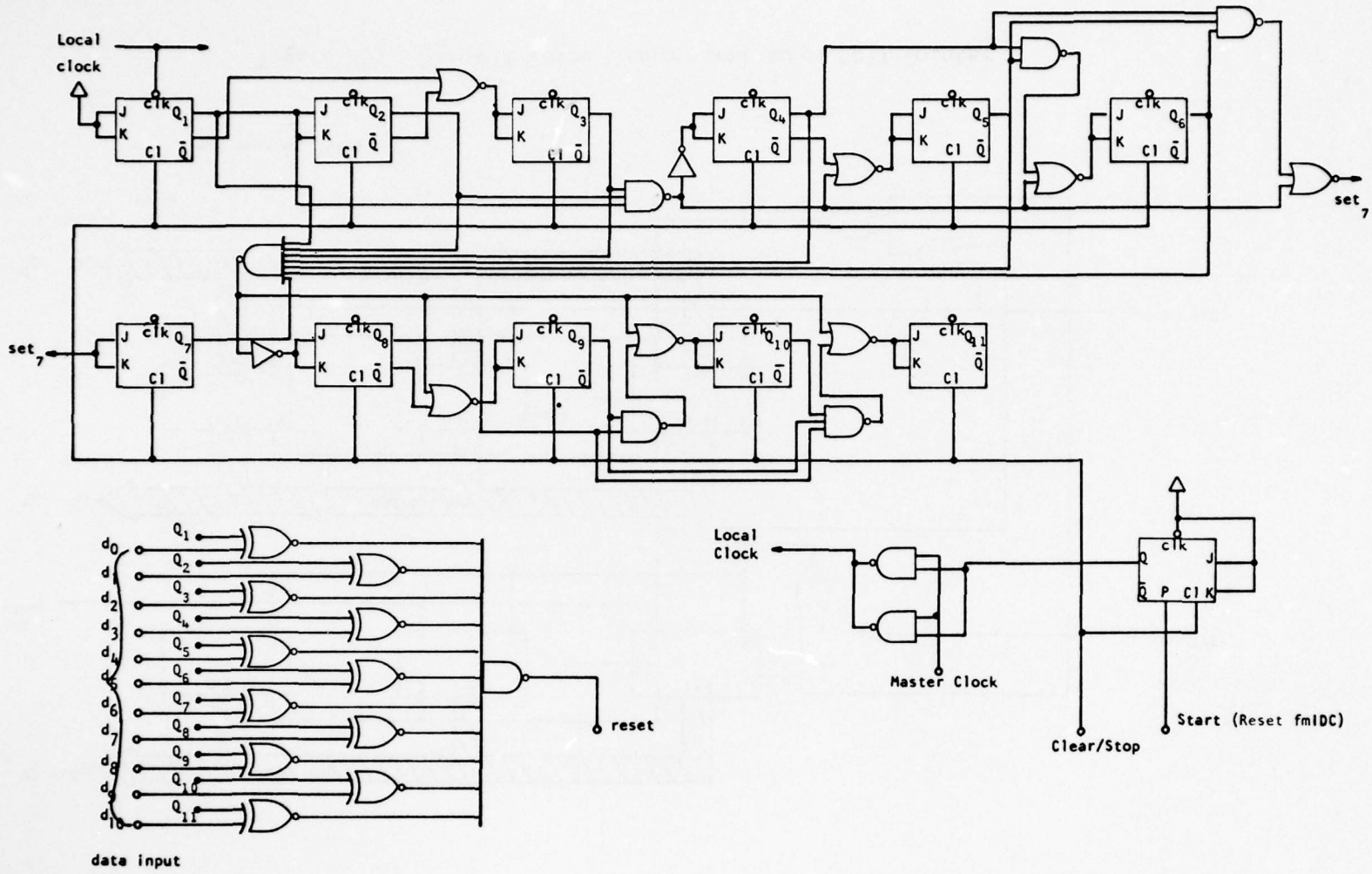

Figure 38. Final Delay Counter -- 11 Bits

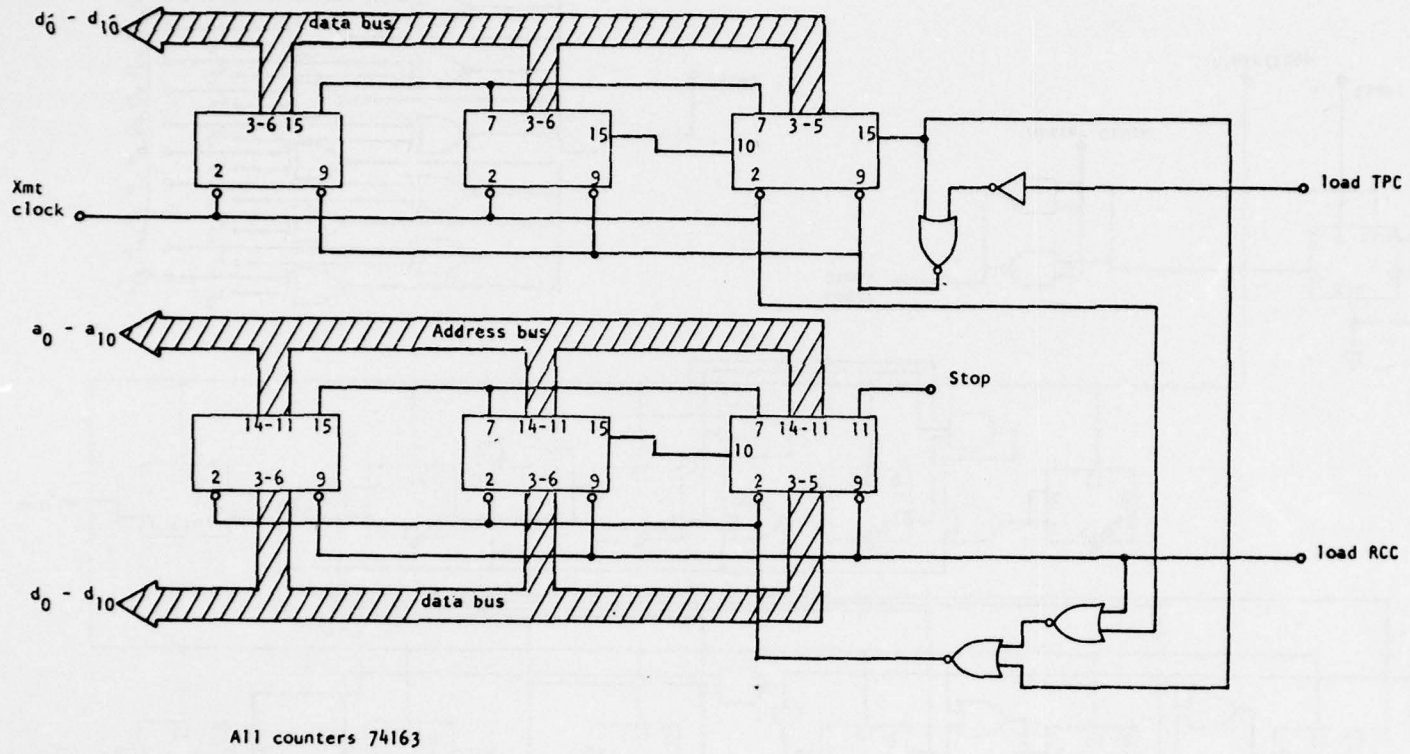

Figure 39. Transmit Pulse Counter and Range Cell Counter

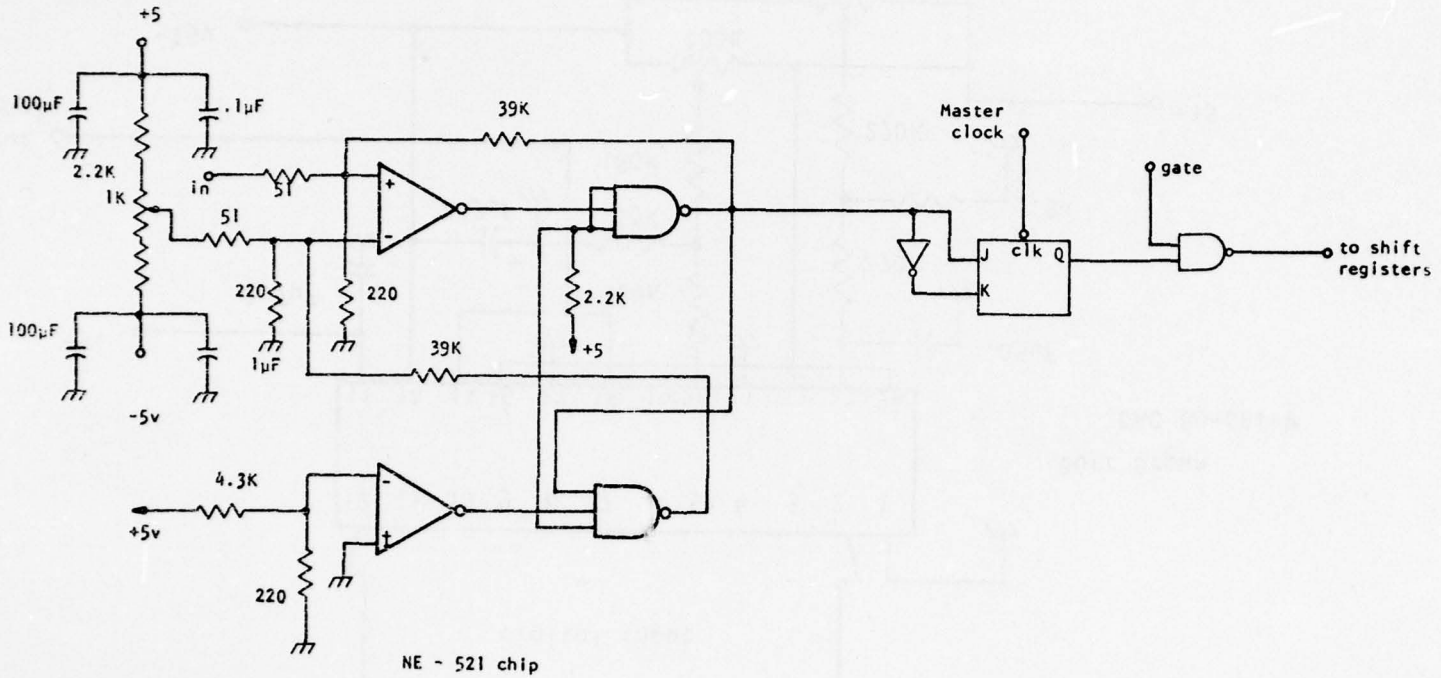

Figure 40. Schmidt Trigger and Data Synchronization

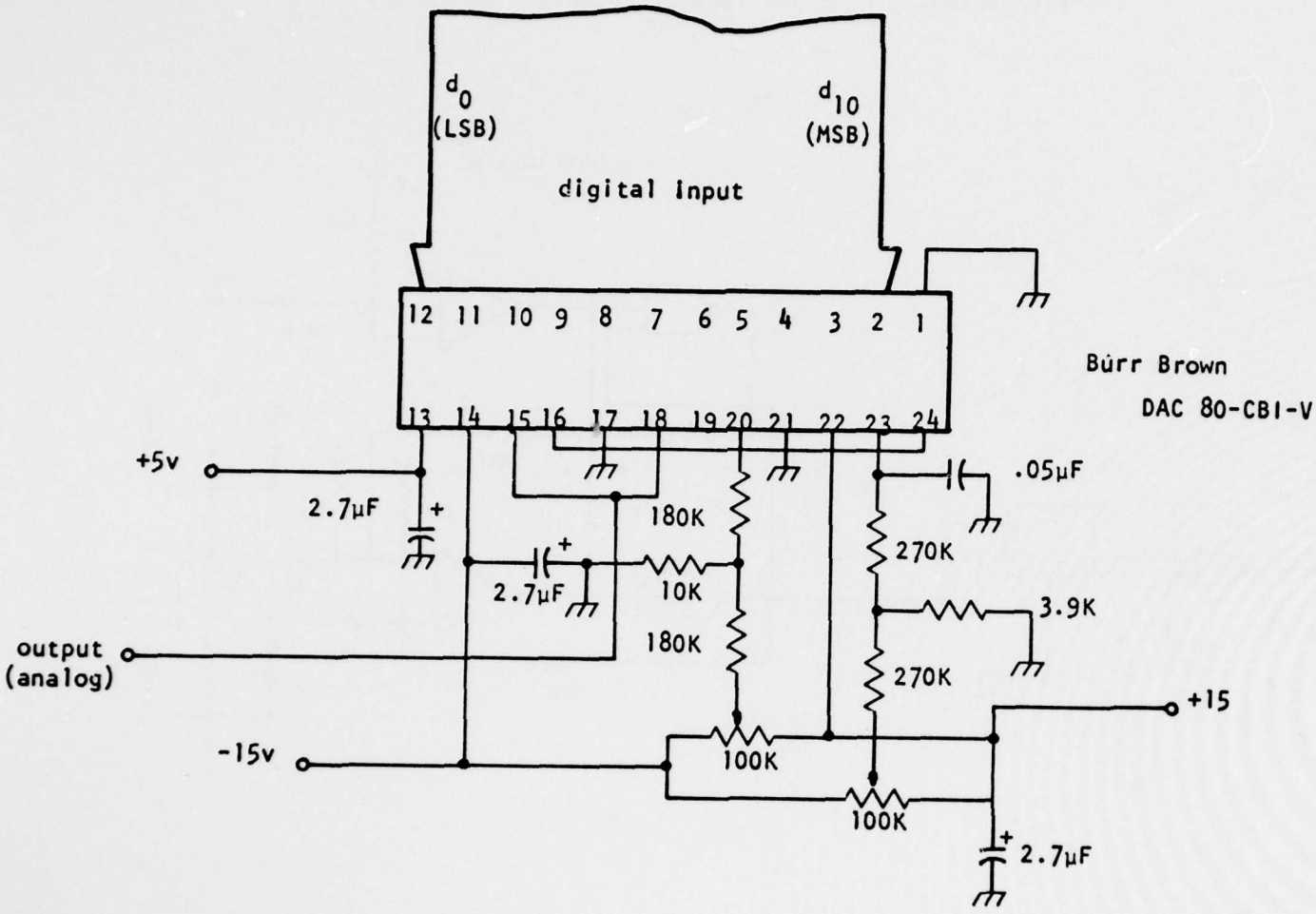

Figure 41. Digital to Analog Converter - 11 Bit

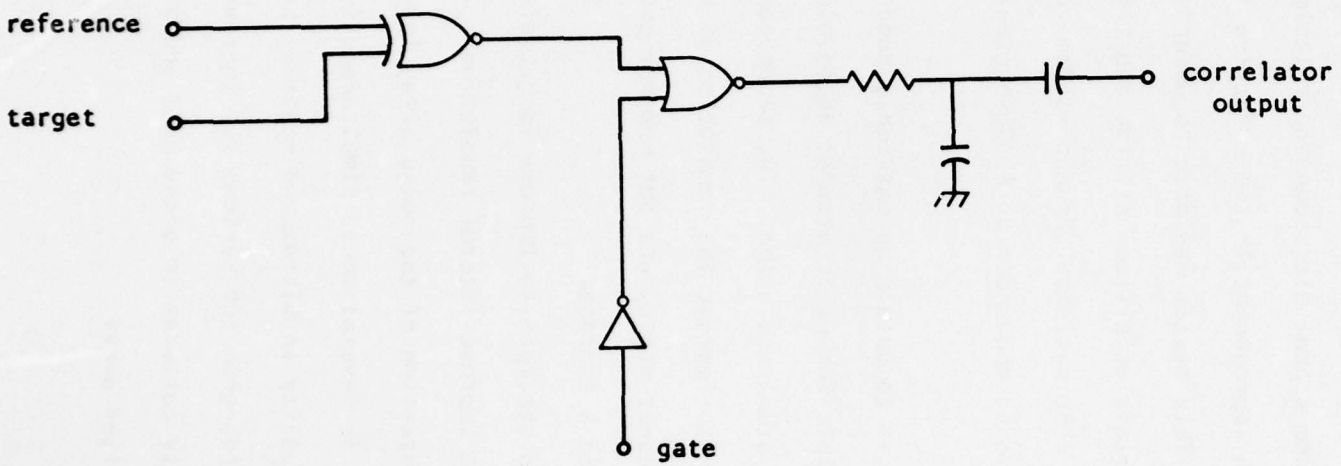

Figure 42. Digital Correlator

SECTION VIII

OVERALL CONCLUSIONS

The overall goal of this contract was the investigation of the use of transmitted random ultrasound signals in flaw detection. The first result of this research was a random signal ultrasound correlation A-scan system which provides the remarkably high improvement in the effective input signal to noise ratio of the order of 10^4. This system was able to detect smaller and deeper lying defects in such materials as silicon nitride and titanium than is possible for conventional pulse echo systems.[2] Pseudo-random code versions of this system are now being developed and under U. S. Government and French government sponsorship.

Having been able to obtain an extremely good output signal to noise ratio, it now became possible for us to attempt deconvolution procedures for improving the longitudinal system resolution. Two techniques are described in this report which are able to improve the resolution of surface features. The techniques in their present state, are not however good enough to detect a <u>small</u> defect very close to a surface.

In addition to attempts to improve longitudinal resolution research was performed on how to improve lateral resolution by the use of noise signals. This led to the conception of the noise array in which a single phased array is used to operate in several modes simultaneously. This technique promises to enhance image quality in ultrasound systems, but requires further development. As a part of this research two systems for improved characterization of transducer beam intensity patterns in broad band and narrow band operation, were developed as described above.

AD-A078 443 PURDUE UNIV LAFAYETTE IND DEPT OF ELECTRICAL ENGINEERING F/G 17/1
RANDOM SIGNAL FLAW DETECTION.(U)
JUN 79 V L NEWHOUSE , E S FURGASON F33615-75-C-5252
UNCLASSIFIED AFML-TR-79-4077 NL

2 OF 2
ADA 078443

END
DATE FILMED
1 -80
DDC

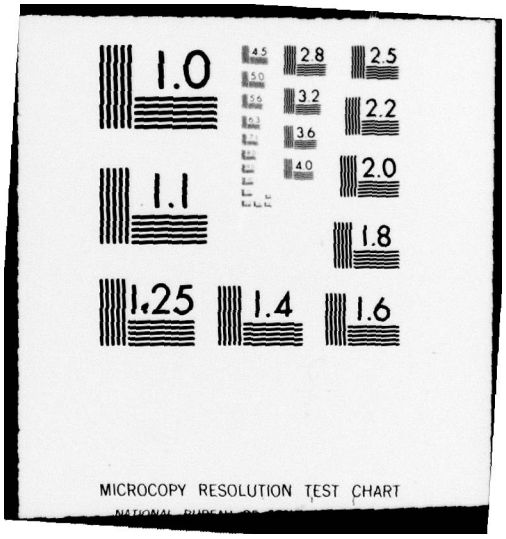
1.0
1.1
1.25
1.4
1.6
1.8
2.0
2.2
2.5
2.8
3.2
3.6
4.0
4.5
5.0
5.6
6.3
7.1
MICROCOPY RESOLUTION TEST CHART

Since a number of groups are developing pseudo-random code versions of our noise correlation system, we were requested to develop a system in which the water delay of our original system was replaced by an electronic delay line. It is hoped to evaluate this system and compare it to pseudo-random code versions in future work.

REFERENCES

1. E. S. Furgason, V. L. Newhouse, N. M. Bilgutay and G. R. Cooper, "Application of Random Signal Correlation Techniques to Ultrasonic Flaw Detection," Ultrasonics, Vol. 13, No. 1, pp. 11-17, 1975.

2. N. M. Bilgutay, E. S. Furgason and V. L. Newhouse, "Evaluation of a Random Signal Correlation System for Ultrasonic Flaw Detection," IEEE Trans. Sonics and Ultrasonics, Vol. SU-23, pp. 329-333, 1976.

3. V. L. Newhouse and E. S. Furgason, "Ultrasonic Correlation Techniques," in Research Techniques in Nondestructive Testing, Vol. III, R. S. Sharpe (Editor), Academic Press, London, 1977.

4. C. B. Burckhardt, P. A. Grandchamp and H. Hoffman, "Methods for Increasing the Lateral Resolution of B-Scan," Acoustic Holography, Vol. 5, (P. S. Green, ed.) pp. 391-413, Plenum, N. Y., 1973.

5. F. L. Thurstone and W. McKinney, "Focused Transducer Arrays in an Ultrasonic Scanning System for Biologic Tissue," in Diagnostic Ultrasound, (C. C. Grassman, et al. eds.) pp. 191-194, Plenum, N. Y., 1966.

6. F. R. Castella, "Application of One-Dimensional Holographic Techniques to a Mapping Sonar System," in Acoustical Holography, Vol. 3, (A. F. Metherell, ed.), pp. 247-271, Plenum, N. Y., 1971.

7. P. N. T. Wells, Physical Principles of Ultrasonic Diagnosis, Academic Press, London, N. Y., pp. 53-60, 1969.

8. J. H. McLeod, "The Axicon: A New Type of Optical Element," J. Opt. Soc. Amer., Vol. 44, pp. 592-597, 1954.

9. C. P. Jethwa, et al. "Blood Velocity Measurements by Ultrasonic Random Signal Processing and Dual Element Transducer," Proc. of San Diego Biomedical Symp., Vol. 13, Feb., 1974.

10. C. B. Burckhardt, P. B. Grandchamp and H. Hoffman, "Focusing Ultrasound over a Large Depth with an Annular Transducer," IEEE Trans. Sonics and Ultrasonics, Vol. SU-22, No. 1, pp. 11-15, 1975.

11. D. Phillips, "A Technique for the Numerical Solution of Certain Integral Equations for the First Kind," J. Assoc. Comput. Mach., Vol. 9, pp. 97-101, 1962.

12. S. Twomey, "The Application of Numerical Filtering to the Solution of Integral Equations Encountered in Indirect Sensing Measurements," J. Franklin Inst., No. 279, pp. 95-109, 1965.

13. B. Hunt, "The Inverse Problem of Radiography," Math. Biosci., Vol. 8, pp. 161-179, 1970.

14. E. S. Furgason, R. E. Twyman and V. L. Newhouse, "Deconvolution Processing for Flaw Signatures," Proc. 1977 ARPA/AFML Conf. on Non-Destructive Testing.

15. E. S. Furgason and V. L. Newhouse, "The Use of Noise Signals for Multi-Mode Operation of Phased Arrays," Proc. of 3rd International Symposium on Ultrasonic Imaging and Tissue Characterization, NBS, Gaithersburg, Md., June, 1978. INVITED

16. E. S. Furgason, G. F. Johnson, and B. B. Lee, "Beam Intensity Profiling Using Correlation Systems," Proc. 1978 ARPA/AFML Conference on Non-Destructive Testing, La Jolla, CA, 1978.

☆U.S.Government Printing Office: 1979 — 657-084/280